Programme for UKNC Conference, Cardiff

8th-9th January 2020

Institute for Compound Semiconductors

Sefydliad Lled-ddargludyddion Cyfansawdd

Wednesday 8th January

10.15-10.40: Arrival/Registration/Coffee

10.40-10.45: Opening remarks (Rachel Oliver / Philip Shields / David Wallis)

10.45 – 12.45: Session 1 – Defects and characterisation
Chairs: Matthew Halsall/Rachel Oliver

10.45-11.30: **The Humphreys Lecture**
Defects in Nitride semiconductors
Zlatko Sitar
North Carolina State University, Materials Science and Engineering, 911 Partners Way, Raleigh, NC, 27695-7907, USA.

11.30-11.45: *Defects introduction during sputter deposition on GaN semiconductor*
Xiaoyan Tang[1], Simon Hammersley[1], Vladimir Markevich[1], Ian Hawkins[1], Iain Crowe[1], Trevor Martin[2], Tony Peaker[1], Matthew Halsall[1]

[1] Photon Science Institute and School of Electrical & Electronic Engineering, The University of Manchester, Manchester, M13 9PL, UK
[2] IQE, Pascal Close, Cardiff, CF3 0LW, UK

11.45-12.00: *DLTS of Defects in GaN Produced by 6MeV Electron Irradiation*
Simon Hammersley[1], Xiaoyan Tang[1], Vladimir Markevich[1], Ian Hawkins[1], Iain Crowe[1], Trevor Martin[2], Tony Peaker[1], Matthew Halsall[1]

[1] Photon Science Institute and School of Electrical & Electronic Engineering, The University of Manchester, Manchester, M13 9PL, UK
[2] IQE, Pascal Close, Cardiff, CF3 0LW, UK

12.00-12.15 *Investigating the structural properties of AlN thin films grown on nano-patterned sapphire substrates in the scanning electron microscope*
C. Trager-Cowan[1], A. Alasamari[1], W. Avis[1], J. Bruckbauer[1], G. Ferenczi[1], B. Hourahine[1], G. Kusch[1*], R.W. Martin[1], R. McDermott[1], G. Naresh-Kumar[1], S. Hagedorn[2], S. Walde[2], M. Weyers[2], P.-M. Coulon[3], P. A. Shields[3] and A. Winkelmann[4]

[1] Department of Physics, SUPA, University of Strathclyde, Glasgow, G4 0NG, UK
[2] Ferdinand-Braun-Institut, Leibnitz-Institut für Höchstfrequenztechnik, 12489 Berlin, Germany
[3] Department of Electronic and Electrical Engineering, Centre of Nanoscience & Nanotechnology, University of Bath, Bath, BA2 7AY, UK
[4] Academic Centre for Materials and Nanotechnology, AGH University of Science and Technology, 30-059 Krakow, Poland *Now at Department of Materials Science and Metallurgy, University of Cambridge, Cambridge CB3 0FS, UK

12.15-12.30: *Temperature Dependent Cathodoluminescence of Closed-Packed Arrays of GaN Inverted Nanopyramids*

P. Bozinakis[1], P.M. Coulon[2], G. Kusch[3], J. Bruckbauer[1], P.R. Edwards[1], R.A. Oliver[3], P.A. Shields[2], R.W. Martin[1]

[1] Department of Physics, SUPA, University of Strathclyde, Glasgow, G4 0NG, UK
[2] Department of Electronic and Electrical Engineering, Centre of Nanoscience & Nanotechnology, University of Bath, Bath, BA2 7AY, UK
[3] Department of Materials Science and Metallurgy, University of Cambridge, Cambridge CB3 0FS, UK

12.30-12.45: *Three Posture Cathodoluminescence for Nanostructure Characterisation*

Douglas Cameron[1], Paul R. Edwards[1], Pierre-Marie Coulon[2], Phillip A. Sheilds[2], Robert W. Martin[1]

[1] Department of Physics, SUPA, University of Strathclyde, Glasgow, G4 0NG, UK
[2] Department of Electronic and Electrical Engineering, Centre of Nanoscience & Nanotechnology, University of Bath, Bath, BA2 7AY, UK

12.45-13.45: Lunch

Defects introduction during sputter deposition on GaN semiconductor

Xiaoyan Tang[1], Simon Hammersley[1], Vladimir Markevich[1], Ian Hawkins[1], Iain Crowe[1], Trevor Martin[2], Tony Peaker[1], Matthew Halsall[1]

1. *Photon Science Institute and School of Electrical & Electronic Engineering, The University of Manchester, Manchester, M13 9PL, United Kingdom*
2. *IQE, Pascal Close, Cardiff, CF3 0LW, United Kingdom*

xiaoyan.tang@manchester.ac.uk

Gallium nitride (GaN) based semiconductor materials have many applications in optical and electrical devices, due to their wide bandgap, high electron mobility and good thermal stability. However, deep-level defects are known to degrade device performance since defects can assist in carrier diffusion process, act as non-radiative recombination centres, trap carriers causing current collapse in high electron mobility transistors and increase leakage. In this study, we demonstrate how sputter metal deposition degrades the performance of a GaN diode, by comparing the IV and CV characteristics of Schottky diodes made using thermal evaporation and samples with varying thicknesses of sputtered material followed by an evaporated layer of the same material such that the total thickness of deposited metal is nominally identical in all samples. For sputtering Argon gas was used for plasma generation under the pressure of 1×10^{-3} mbar and voltage of 178 V respectively. All samples consisted of a 300 nm thick Gold Schottky diode, of which the sputtered samples contained between 5 and 300 nm of sputtered material prior to evaporation.

Current – voltage (IV) measurement shows that sputtering increases the diode leakage current significantly, with the leakage current of the diode with only 5 nm of sputtered gold being approximately ten times larger than the fully evaporated diode (Figure 1). This leakage was found to greatly increase as the sputter thickness was increased. For samples with a sputtered thickness of more than 20 nm, the diodes were found to be no longer rectifying. Carrier concentration profiles were derived from capacitance - voltage (CV) measurement on the evaporated sample and the sample with 5 nm of sputtered material. The sputtered diode was found to have a larger carrier concentration and the depletion region is closer to the sample surface. These results suggest that sputter deposition introduced a large number of donor like defects, which result in an increase of carrier concentration and leakage current.

To investigate the defects introduced into the sample during sputtering, samples were then characterized using deep-level transient spectroscopy (DLTS). Two peaks were observed in the sputtered sample: one is a positive peak at 150 K and the other is a negative peak at 260 K, corresponding to an electron and a hole trap respectively. Compared to the fully evaporated diode, DLTS amplitude of the sputtered diode is about a hundred times larger for all peaks, indicating a much higher defect concentration (Figure 2). The energy of electron trap is 0.26 ± 0.01 eV below the conduction band, while the energy of hole trap is 0.62 ± 0.04 eV above the valence band (Figure 3). The 0.26 eV defect could be attributed to V_N [1], a V_NO_N complex [2], or a dislocations related defects [3] [4]. The source of the hole trap is not yet known but it has also been reported by Polyakov *et al* [5].

The concentration profile of the electron trap was obtained by measuring DLTS with different reverse bias and fill pulse voltages, as a result, traps at different depth can be filled and emptied with carriers selectively, and the corresponding DLTS peak intensity used to measure the density of traps within the excited volume. The density of the electron trap was found to reduce from $2\times10^{15}cm^{-3}$ to $4\times10^{14}cm^{-3}$ when increasing the probing depth from 57 nm to 81 nm from the sample surface (Figure 4).

In conclusion, sputter deposition has been found to degrade the GaN device performance by introducing additional defects near to the sample surface. Compared with evaporated diodes, the sputtered diodes have a larger leakage current, higher carrier concentration near the sample surface

and higher defect density. DLTS measurement also indicates that at least two defects have been introduced into the sputtered sample, one 0.26 eV from the conduction band, and one 0.62 eV from the valence band. The density of electron trap was found to be the highest close to the sample surface, rapidly decreasing at increasing the probing depth. This defect density distribution further indicates the defect was introduced by sputter metal deposition. The defect introduction by sputtering leads to significant performance degradation of diodes and as such will be relevant to other device structures which use sputtering for the deposition of electrical contacts.

Reference

[1]. Fang, Z. Q., *et al*, *Appl. Phys. Lett.*, **82**, 1562-1564 (2003)
[2]. Soh, C. B., *et al*, *J. Appl. Phys.*, **96**, 1341-1347 (2004)
[3]. Polyakov, Lee, *Materials Science and Engineering,* **94**,1-56 (2015)
[4]. Soh, C. B., *et al*, *J. Phys.: Condens. Matter*, **16**, 6305-6315 (2004)
[5]. Polyakov, *et al*, *Journal of Applied Physics*, **109**, 123701 (2011)

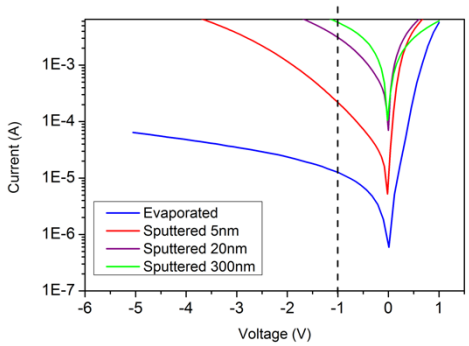

Figure 1 Current-voltage relationship of fully evaporated diode and sputtered diodes with different sputtered thickness.

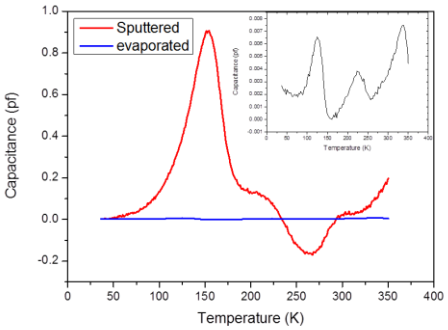

Figure 2 DLTS plot of the 5 nm sputtered diode, measured at rate window 20 s^{-1}, V_r = -1V, V_p = 0 V, and fill pulse width is 10 ms, the insert figure is the DLTS of fully evaporated diode, measured under the same condition.

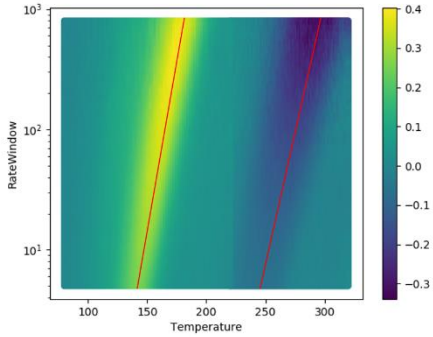

Figure 3 DLTS of sputtered sample of different rate windows. Red lines represent the trend of two peaks as increasing rate window.

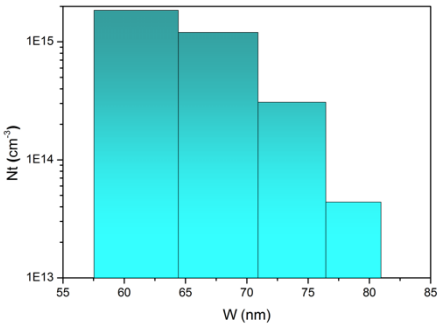

Figure 4 Trap concentration profile of defect P_1 in the 5 nm sputtered sample. Horizontal axis is the distance from the sample surface.

DLTS of Defects in GaN Produced by 6 MeV Electron Irradiation

Simon Hammersley[1], Xiaoyan Tang[1], Vladimir Markevich[1], Ian Hawkins[1], Iain Crowe[1], Trevor Martin[2], Tony Peaker[1], Matthew Halsall[1]

[1] Photon Science Institute and Department of Electrical and Electronic Engineering, School of Engineering, University of Manchester, Manchester, M13 9PL, UK. [2] IQE, Pascal close, Cardiff, CF3 0LW, UK.

Corresponding author: simon.hammersley@manchester.ac.uk

Group III-Ns are becoming increasingly indispensable for use in both optical and electrical devices. These devices have a key role to play in the reduction of carbon emissions worldwide, not only through their use in high quality high efficiency lighting applications, but also through their use in power conversion applications such as high efficiency switch mode power supplies and inverters.

While there has been a large amount of success with devices based on group III-Ns, the effect of defects in these devices is still far less understood than in other semiconductors such as Si and GaAs. One of the key techniques for investigating defects in semiconductors is deep level transient spectroscopy (DLTS) however when applied to GaN it has not been as successful. This is in part due to the wide band gap making investigation of traps near the mid gap more difficult but also that the peaks that do present in are often significantly broadened, making discrimination of traps with similar energies more difficult.

We will report on the DLTS study of two samples taken from the same wafer, one of which has been exposed to a 6MeV electron beam with an electron dose of 1.2×10^{17} cm^{-2}. Nominally identical Schottky diodes, consisting of a 0.5 mm diameter 300 nm thick Au Schottky contact and a large area 300nm thick Al Ohmic contact were then fabricated from the two samples.

DLTS measurements were then conducted on both samples. In the as grown sample, a weak DLTS signal was observed around 140K with a trap density of $\sim1.9\times10^{13}$ cm^{-3}. The activation energy of this trap was calculated from an Arrhenius plot of the DLTS peak position as a function of emission rate window to be 207±6 meV. In the sample exposed to the electron beam, the DLTS signal is observed to increase by a factor of 27 and now exhibits as a main peak around 90K, with a small shoulder on the high temperature side. The spectra were fitted to extract two peaks, one at 90K with a trap density of 2.6×10^{14} cm^{-3} and a smaller peak responsible for the shoulder that coincides with the peak observed in the as grown sample but with a trap density of 8.6×10^{13} cm^{-3}. The activation energies of these two peaks were again calculated from an Arrhenius plot, and found to be 123±4 and 198±9 meV for the larger and smaller peaks respectively.

The origin of these two peaks is still under some debate in the literature, with both peaks having been ascribed to the presence of the V_N defect [1-3], and the higher energy peak having been also been ascribed to dislocation clustering along screw dislocations [3] and the presence of the V_NO_N complex [4]. It is expected that the dominant vacancy species in n-type GaN during growth will be the V_{Ga} and that any V_N that do form will be highly mobile during growth, allowing them to form stable complexes [5]. For this reason it is not expected that V_N will be present in any great quantity in the as grown sample, but is expected to be introduced in considerable quantities when the sample is exposed to the electron beam irradiation. This would fit well with the attribution of the peak at 123±4 meV to the V_N, and the peak at 198-207 meV to the V_NO_N complex.

[1] ZQ Fang et al, Appl. Phys. Lett. 82, 1562 (2003)
[2] SJ Pearton et al. ECS J. Solid state Sci. and Tech., 5, q35-60 (2016)
[3] CB Soh et al, J. Phys.: Condens. Matter 16, 6305 (2004)
[4] CB Soh et al, J. Appl. Phys. 96, 1341 (2004)
[5] AY Polyakov Materials science and engineering R 94, 1-56 (2015)

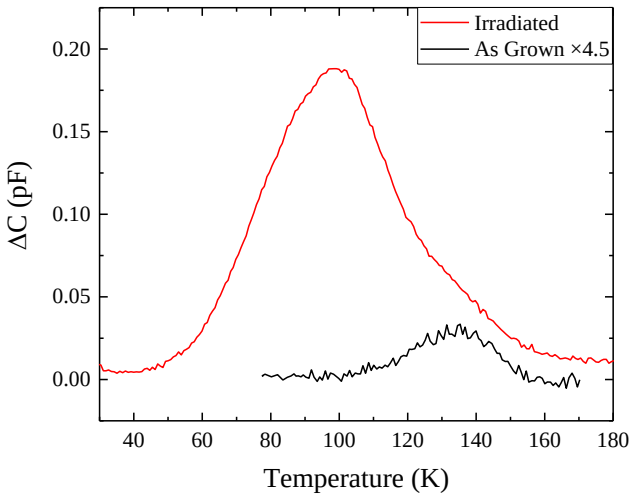

DLTS spectra of the as-grown material (black) and the material exposed to the electron beam (red) recorded at an emission rate window of 80 s^{-1}.

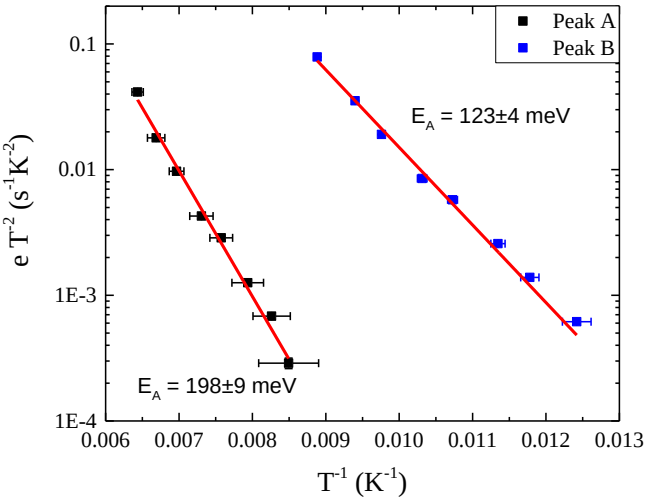

Arrhenius plot of the extracted peak positions for the sample exposed to electron irradiation as a function of emission rate window. Blue/Black points show the shift in the peak at 90/140 K in the DLTS spectra above. Red lines show the Arrhenius fits to the data points.

Investigating the structural properties of AlN thin films grown on nano-patterned sapphire substrates in the scanning electron microscope

C. Trager-Cowan[1]*, A. Alasamari[1], W. Avis[1], J. Bruckbauer[1], G. Ferenczi[1], B. Hourahine[1], G. Kusch[1†], R.W. Martin[1], R. McDermott[1], G. Naresh-Kumar[1], S. Hagedorn[2], S. Walde[2], M. Weyers[2], P.-M. Coulon[3], P. A. Shields[3] and A. Winkelmann[4]

[1]*Department of Physics, SUPA, University of Strathclyde, Glasgow, G4 0NG, UK*
[2]*Ferdinand-Braun-Institut, Leibnitz-Institut für Höchstfrequenztechnik, 12489 Berlin, Germany*
[3]*Department of Electronic and Electrical Engineering, Centre of Nanoscience & Nanotechnology, University of Bath, Bath, BA2 7AY, UK*
[4]*Academic Centre for Materials and Nanotechnology, AGH University of Science and Technology, 30-059 Krakow, Poland*
*c.trager-cowan@strath.ac.uk

AlN thin films exhibiting high structural quality are crucial for maximising the internal quantum efficiency (IQE) of AlGaN-based ultraviolet light emitting diodes (UV-LEDs). The production of high quality material requires the understanding and minimisation of structural defects such as threading dislocations. In our presentation we will describe the application of the scanning electron microscope (SEM) techniques of electron backscatter diffraction (EBSD) [1-2] and electron channelling contrast imaging (ECCI) [3-5] to image local lattice tilts and twists and threading dislocations in AlN thin films [6]. These techniques are non-destructive and have a spatial resolution of tens of nanometres.

The AlN thin films under study were overgrown by MOVPE on a nano-patterned sapphire substrate (nPSS).

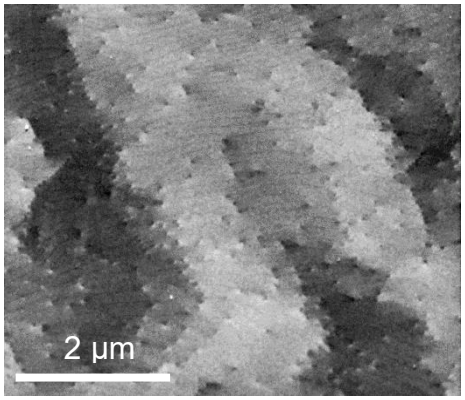

Fig. 1. Electron channelling micrograph from an AlN thin film grown on nPSS.

Hexagonal arrays of truncated cones were prepared on a 2 inch wafer by combining displacement Talbot lithography and lift-off to create metal nanodot masks, followed by chlorine-based dry etching [7]. AlN was subsequently overgrown on these sapphire nanopillars according to the growth process given in [8]. ECCI micrographs (see Fig. 1 for example) reveal the presence of sub-grains with a significant number of threading dislocations (TDs) located on the boundaries of the sub-grains. These TDs are identified as being predominantly threading a-type dislocations. The average TD density was determined to be $\approx 1.5 \times 10^9$ cm^{-2} where approximately 90% of the TDs were found to be edge-type TDs.

To obtain quantitative information on the relative misorientation of the sub-grains, EBSD maps were acquired. Fig. 2 (a) shows a grain reference orientation deviation (GROD) map (the deviation of orientation of the sub-grains relative to an average orientation [9]) derived from EBSD data using MTEX [10]. The first step of the analysis involved

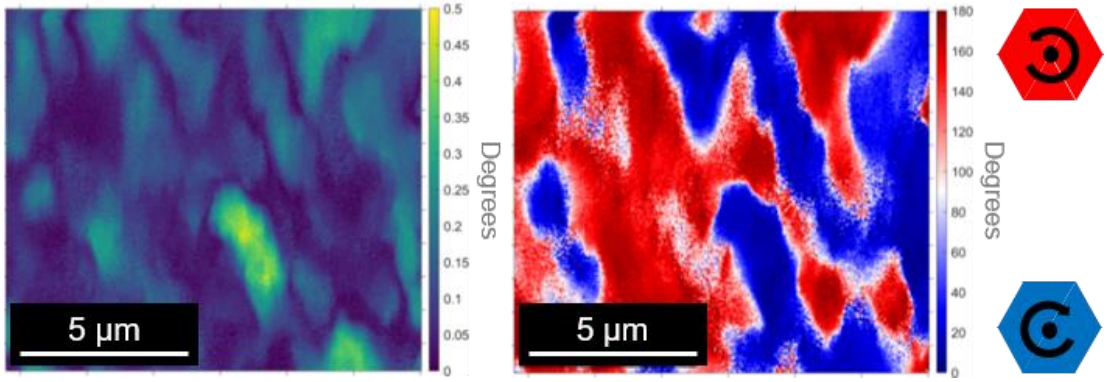

Fig. 2. Maps derived from EBSD data from the AlN/nPSS thin film (a) grain reference orientation deviation (GROD) map and (b) GROD axis map relative to the sample normal (c-axis, [0001] direction]) where the colours denote direction of in-plane rotation (i.e., around the c-axis). The red regions are rotated in the opposite direction to the blue regions as indicated.

---

†Now at Department of Materials Science and Metallurgy, University of Cambridge, Cambridge CB3 0FS, United Kingdom

comparison of each experimental EBSD pattern with dynamical simulations [11]. Figure 2(b) is a GROD angle map which shows the local misorientations relative to the normal to the sample, i.e., the *c*-axis ([0001] direction) and reveals that the local misorientations are predominantly rotations around the *c*-axis.

Work is ongoing to investigate AlN thin films overgrown on nano-patterned sapphire as a function of the sapphire off-cut and truncated cone diameters. Their impact on the surface morphology, sub-grain morphology and density of dislocations will be presented and discussed.

[1] A. J. Schwartz, M. Kumar, B. L. Adams and D. P. Field. Electron Backscatter Diffraction in Materials Science (Springer, 2009).
[2] A. J. Wilkinson and P. B. Hirsch, Micron, **28**, 279 (1997).
[3] G. Naresh-Kumar et al., Phys. Rev. Lett. **108**, 135503 (2012).
[4] Y. Picard et al., Micros. Today **20**, 12 (2012).
[5] G. Naresh-Kumar et al., Mater. Sci. Semicond. Process. **47**, 44 (2016).
[6] C. Trager-Cowan et al., Photonics Res. **7** B73 (2019).
[7] P. M. Coulon et al., Microsyst. Nanoeng. **5**, 52 (2019).
[8] S. Walde et al., J. Cryst. Growth. **13** 125343 (2019).
[9] S. I. Wright et al., Microsc. Microanal. **17**, 316 (2011).
[10] F. Bachmann et al., Solid State Phenom. **160**, 63 (2010).
[11] A. Winkelmann et al., Ultramicroscopy **107** 414 (2007).

Acknowledgements: Research was carried out with support of EPSRC grants: EP/J015792/1, EP/M015181/1 & EP/P015719/1.

Temperature Dependent Cathodoluminescence of Closed-Packed Arrays of GaN Inverted Nanopyramids

P. Bozinakis[1 *], P.M. Coulon[2], G. Kusch[3], J. Bruckbauer[1], P. R. Edwards[1], R.A. Oliver[3], P.A. Shields[2], R.W. Martin[1]

[1]*Dept. of Physics, SUPA, University of Strathclyde, G4 0NG, UK*
[2]*Dept. Electrical & Electronic Engineering, University of Bath, Bath, BA2 7AY, UK*
[3]*Dept. of Materials Science and Metallurgy, University of Cambridge, Cambridge, CB3 0FS, UK*
*pavlos.bozinakis@strath.ac.uk

The inherent polarization and piezoelectric fields in hexagonal gallium nitride (h-GaN) impair the radiative recombination of electron-hole pairs and limit the efficiency of GaN based optoelectronic devices such as light emitting diodes. These fields are reduced when h-GaN is grown in semi or non-polar orientations. Such orientations can be produced by selective growth of nanostructures, such as rods, tubes or pyramids. This paper reports on the characterization of GaN semi-polar nanostructured surfaces obtained by a combination of top-down etching and bottom-up regrowth using temperature dependent cathodoluminescence (CL) mapping, in the range 10 K to 320 K.

Displacement Talbot lithography was used to create a mask, in the form of a hexagonal array of SiN_x nanorings, on a GaN template [1]. Nanotubes were subsequently formed by chlorine based dry etching. Finally, GaN regrowth was performed by MOVPE on nanotubes, both with and without the SiN_x mask on the top *c*-plane. After complete coalescence two distinct nanostructured GaN surfaces were produced: first, isolated nanopyramids surrounded by a network of inclined nanowalls and second, a close-packed array of inverted GaN nanopyramids. Both the nanopyramids and the inverted nanopyramids are composed of six semi-polar $\{10\bar{1}1\}$ facets, while the nanowall network surrounding the nanopyramids is composed of mixed $\{10\bar{1}1\}$ and $\{11\bar{2}2\}$ semi-polar facets.

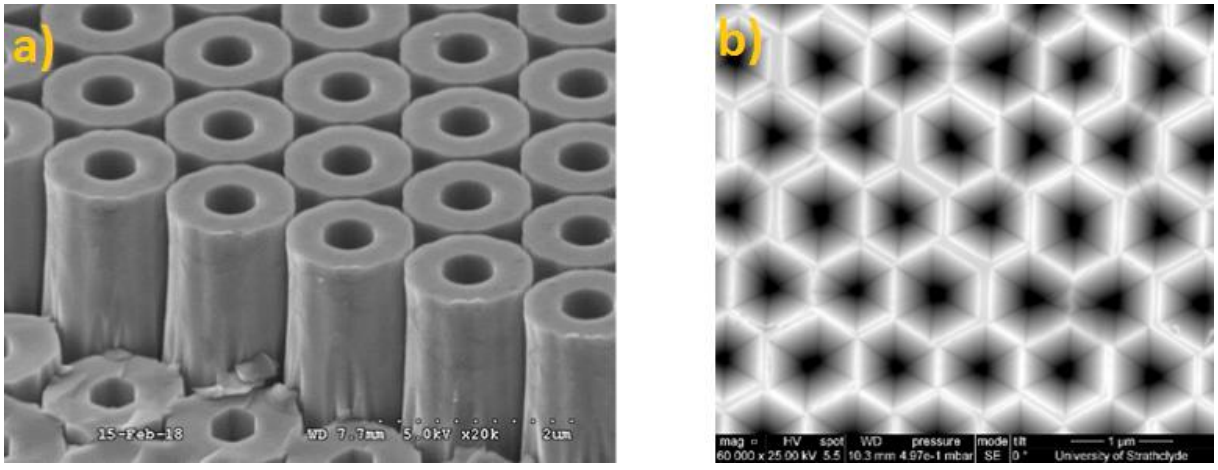

Figure 1: a) SE image showing the GaN nanotubes without the SiN_x mask at 45°, b) SE image showing a planar view of the inverted nanopyramids which are formed after GaN regrowth.

Two CL systems were used for the acquisition of CL hyperspectral images – one with the sample cooled using liquid helium and held at 90° to the incident beam and the other a room temperature (RT) system with the sample tilted at 45° to the beam. The tilted RT CL maps showed a bright peak centred near 376 nm (shown in Fig. 2b) from certain regions of both types of nanostructures along with the omnipresent emission near 365 nm. High spatial resolution CL hyperspectral images showed that the 376 nm light was emitted from some of

the $\{10\bar{1}1\}$ semi-polar facets. Coalescence boundaries were observed at these locations in the SE images of the same area of the CL hyperspectral images, as shown in Fig. 2a. We demonstrate a strong correlation between the presence of the coalescence boundaries and the 376 nm light emission. The temperature dependent CL helps to clarify the origin of this peak. Fig 3. shows a CL map at 10 K along with example spectra. The evolution of these peaks was followed as a function of temperature, up to room temperature.

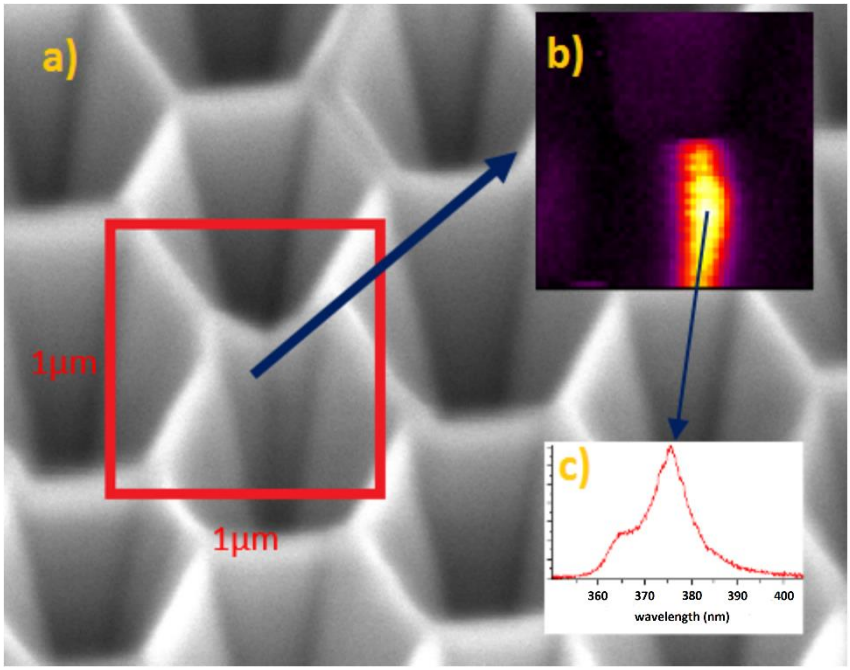

Figure 2: a) SE image of the inverted nanopyramids at 45°. The red square indicates the area where the CL was collected from, b) CL intensity map of the 376 nm peak, c) CL spectrum from the coalescence boundary.

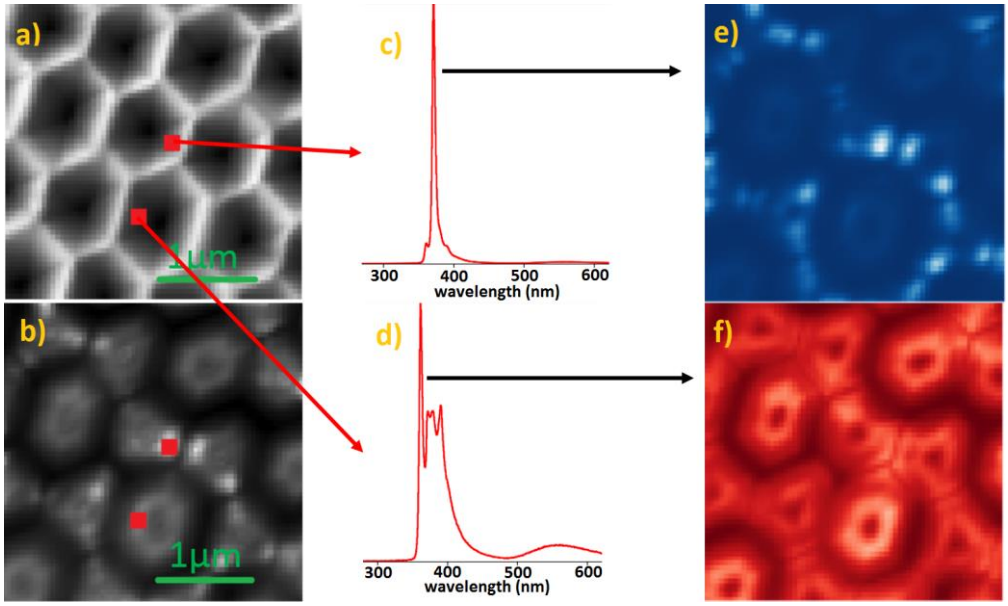

Figure 3: a) SE image of the area where CL was measured at 10K, b) Panchromatic CL map of the inverted nanopyramids, c) and d) example spectra taken from the red points of the panchromatic CL map, e) CL intensity map in the range 370-373 nm, f) CL intensity map in the range 359-362 nm.

[1] P-M. Coulon et al, "Optical properties and resonant cavity modes in axial InGaN/GaN nanotube microcavities", Opt. Express 25, 28246-28257 (2017)

Three Posture Cathodoluminescence for Nanostructure Characterisation

D. Cameron[1], P.R. Edwards[1], P.-M. Coulon[2], P.A. Shields[2], R.W. Martin[1]
[1]Department of Physics, SUPA, University of Strathclyde, Glasgow, G4 0NG, UK
[2]Dept. Electrical & Electronic Engineering, University of Bath, Bath, BA2 7AY, UK

Three dimensional nanostructures offer multiple potential advantages over planar counterparts, such as access to nonpolar facets and lower threading dislocation densities which will improve the performance of optoelectronic devices. Effective and accurate characterisation is critical to the successful development of such devices. We examine core-shell AlN/AlGaN nanorods for UV optoelectronics. The samples contain AlGaN quantum wells capped with the *p*-type AlGaN layer necessary for effective electrical pumping. Similar samples have previously been prepared and investigated, however they lacked the important *p*-layer [1]. Here, we investigate the effects of such a layer using cathodoluminescence hyperspectral imaging, with rods positioned in three distinct postures as seen in Fig. 1. Changing the angle of incidence of the exciting electrons allows for the true character of the nanorods to be explored whilst simultaneously combatting various intrinsic detrimental effects, such as charging and unrepresentative excitation volumes.

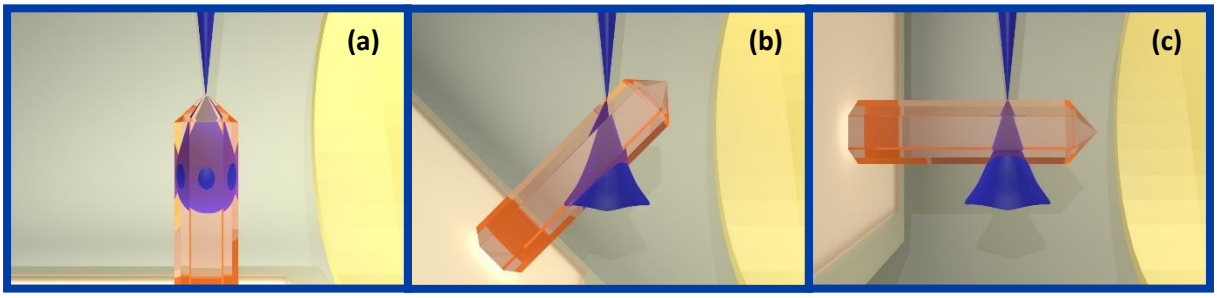

Figure 1: The three sample postures held for cathodoluminescence measurement represented in a triptych. The electron beam (blue) comes from the top and the collection optics are to the right for nanorods (a) parallel (b) tilted at 45° (c) orthogonal to the beam

For our cathodoluminescence system, a sample tilt of 45° relative to both e-beam and collection is standard procedure. In this geometry the small size of these structures (≈200nm diameter) — combined with the low levels of light emission — can muddy any spatial resolution. Using high acceleration voltages with rods mounted orthogonal to the beam, creates a transmission like mode of operation, preserving a significant level of spatial resolution. This configuration also allows for clearer access to the all-important sidewall regions and it was here that previously unseen behaviours were observed. Fig. 2 shows a linescan from tip to base along a rod. Region (a) shows emission from a series of localised GaN-rich clusters at the base of the pyramidal tip, whilst (b) and (c) show light from the AlGaN quantum well on the rod sidewalls. To complete the trio of measurements, the rods are held parallel to the beam to develop a 3D picture of the sample, and also to review any possible self-absorption effects.

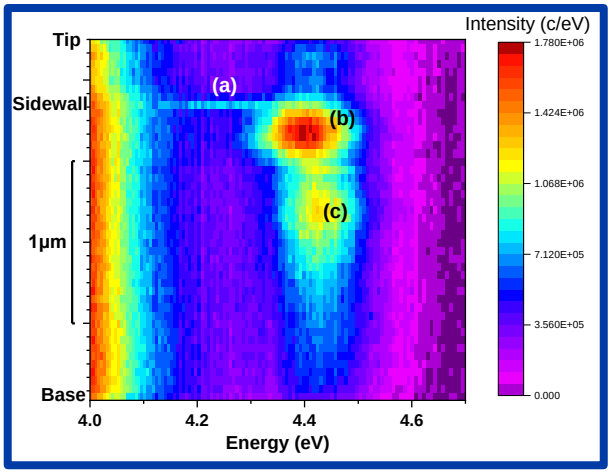

Figure 2: Hyperspectral linescan along rod, measured at 90° relative to the beam. This measurement reveals previously unseen intensity and energy fluctuations along rods.

We complement our luminescence measurements with compositional quantifiers such as wavelength dispersive X-ray analysis, to correlate defect luminescence and compositional fluctuations to our luminescence spectra. During this work we also utilized our nanomanipulation system to mechanically disperse and manipulate rods.

[1] P.-M. Coulon, G. Kusch, R.W. Martin and P.A. Shields, ACS Appl. Mater. Interfaces, 10, 39 (2018)

13.45-15.30: Session 2 – Novel and emerging materials
Chairs: Philip Shields

13.45-14.00 *Corundum α-Ga_2O_3 by atomic layer deposition: growth, detector application and prospects for bandgap engineering*

F. Massabuau[1,2], J. Moloney[2], A. Barthel[2], O. Tesh[2], B. Ding[2], J. Jarman[2], L. Lee[2], T. Huq[2], J. Brister[2], M. Napari[2], R. Oliver[2], M. Singh[3], S. Karboyan[3], M. Kuball[3], J. Gibbon[4], L. Jones[4], V. Dhanak[4], L. Phillips[4], J. Major[4], A. Kovacs[5], T. Sajavaara[6], J. Roberts[7], P. Chalker[7]

[1] Department of Physics, SUPA, University of Strathclyde, Glasgow G4 0NG, UK
[2] Department of Materials Science and Metallurgy, University of Cambridge, Cambridge CB3 0FS, UK
[3] School of Physics, HH Wills Physics Laboratory, University of Bristol, Bristol BS8 1TL, UK
[4] Stevenson Institute for Renewable Energy, The University of Liverpool, Liverpool L69 7ZF, UK
[5] Ernst Ruska-Centre for Microscopy and Spectroscopy with Electrons and Peter Grunberg Institute, Forschungszentrum Juelich GmbH, D-52425 Juelich, Germany
[6] Department of Physics, University of Jyvaskyla, FI-40014 Jyvaskyla, Finland
[7] School of Engineering, The University of Liverpool, Liverpool L69 3GH, UK

14.00-14.15: *Direct band-gap crossover in epitaxial monolayer boron nitride*

T.S. Cheng[1], A. Summerfield[1], C.J. Mellor[1], C. Elias[2], P. Valvin[2], T. Pelini[2], B. Gil[2], G. Cassabois[2], L. Eaves[1], C.T. Foxon[1], P.H. Beton[1], S.V. Novikov[1]

[1] School of Physics and Astronomy, University of Nottingham, Nottingham, UK
[2] Laboratoire Charles Coulomb, UMR5221 CNRS-Université de Montpellier, Montpellier, France

14.15-14.30: *Superconducting boron doped diamond on boron nitride ceramics*

Soumen Mandal[1], Henry Bland[1], Jerome A. Cuenca[1], Malcolm Snowball[2], Oliver A. Williams[1]

[1] School of Physics and Astronomy, Cardiff University, Cardiff, UK
[2] Ultra Biotecs Limited, Derby, UK

14.30-14.45: *High Piezoelectricity in Porous GaN*

Yonatan Calahorra, Adina Wineman, Bogdan Spiridon, Peter Griffin, Sohini Kar-Narayan, Rachel Oliver

Department of Materials Science and Metallurgy, University of Cambridge, Cambridge CB3 0FS, UK

14.45-15.00: *Stacking fault induced alloy segregation in Zincblende GaN heterostructure*
Boning Ding[1], Simon Fairclough[1], Martin Frentrup[1], Menno Kappers[1], Andras Kovács[2], Gunnar Kusch[1], David Wallis[1,3,4], Rachel Oliver[1]

[1] Department of Materials Science and Metallurgy, University of Cambridge, Cambridge CB3 0FS, UK
[2] Forschungszentrum Jülich
[3] Centre for High Frequency Engineering, University of Cardiff, 5 The Parade, Newport Road, CF24 3AA, Cardiff, UK
[4] Kubos Semiconductors Ltd

15.00-15.15: *Study of $Al_xGa_{1-x}N$ nucleation layers for the growth of cubic zincblende GaN*
Abhiram Gundimeda[1], Martin Frentrup[1], Simon M. Fairclough[1], Alexander Hinz[1], Huixin Xiu[1,2], Menno J. Kappers[1], David J. Wallis[1,3], Rachel A. Oliver[1]

[1] Department of Materials Science and Metallurgy, University of Cambridge, Cambridge CB3 0FS, UK
[2] School of Materials Science and Engineering, University of Shanghai for Science and Technology, 516 Jungong Road, Yangpu District, Shanghai, 200093, China
[3] Centre for High Frequency Engineering, University of Cardiff, 5 The Parade, Newport Road, CF24 3AA, Cardiff, UK

15.15-15.45: Tea

Corundum α-Ga_2O_3 by atomic layer deposition: growth, detector application and prospects for bandgap engineering

F. Massabuau[1,2], J. Moloney[2], A. Barthel[2], O. Tesh[2], B. Ding[2], J. Jarman[2], L. Lee[2], T. Huq[2], J. Brister[2], M. Napari[2], R. Oliver[2], M. Singh[3], S. Karboyan[3], M. Kuball[3], J. Gibbon[4], L. Jones[4], V. Dhanak[4], L. Phillips[4], J. Major[4], A. Kovacs[5], T. Sajavaara[6], J. Roberts[7], P. Chalker[7]

[1] *Department of Physics, SUPA, University of Strathclyde, Glasgow G4 0NG, UK*
[2] *Department of Materials Science and Metallurgy, University of Cambridge, Cambridge CB3 0FS, UK*
[3] *School of Physics, HH Wills Physics Laboratory, University of Bristol, Bristol BS8 1TL, UK*
[4] *Stevenson Institute for Renewable Energy, The University of Liverpool, Liverpool L69 7ZF, UK*
[5] *Ernst Ruska-Centre for Microscopy and Spectroscopy with Electrons and Peter Grunberg Institute, Forschungszentrum Juelich GmbH, D-52425 Juelich, Germany*
[6] *Department of Physics, University of Jyvaskyla, FI-40014 Jyvaskyla, Finland*
[7] *School of Engineering, The University of Liverpool, Liverpool L69 3GH, UK*

Corresponding author: f.massabuau@strath.ac.uk

Gallium oxide (Ga_2O_3) is a wide bandgap semiconductor of strong interest for future power electronics and ultraviolet (UV) optical applications [1]. This compound exists under several phases, with the corundum α phase variant (α-Ga_2O_3) displaying several indisputable assets: (i) it exhibits the largest bandgap (5.3 eV) amongst all phases, (ii) is isostructural with several other semiconducting group-III or transition metal sesquioxides (e.g. In_2O_3, Ti_2O_3) and (iii) with the cheap and widely available sapphire (α-Al_2O_3) substrate [2] (Figure 1).

In this study we demonstrated that α-Ga_2O_3 can be synthesized using plasma-enhanced atomic layer deposition (ALD) [3]. The deposition temperature has a critical impact on the film crystallinity, with deposition temperatures below 200°C resulting in amorphous material, while temperatures between 250 and 350°C result in mainly α phase material, and films of mixed α and ε phases are obtained for temperatures above 350°C [4].

The effect of post-growth annealing conditions (temperatures and ambient) on the deposited film quality was investigated. The annealing temperature was found to have a strong influence on the film crystallinity, with 400°C leading to the optimal crystal quality. These films were then processed into photodetectors and tested under 240 nm UV illumination and 10 V bias. All the films exhibited solar-blind photodetection behaviour, and a sharp 3-order of magnitude increase in device responsivity was obtained upon annealing (Figure 2) [5].

Finally, we demonstrated the potential for bandgap engineering of α-Ga_2O_3 films using Ti. Crystalline α-$(Ti_xGa_{1-x})_2O_3$ films can be produced with a composition up to x~5% (Figure 3), leading to a change of bandgap of ~ 200 meV [6].

These results highlight the potential of ALD for producing tunable UV optoelectronic devices based on α-Ga_2O_3 materials and alloys.

[1] Pearton *et al.*, Appl. Phys. Rev. **5**, 011301 (2018)
[2] Fujita *et al.*, Jap. J. Appl. Phys. **55**, 1202A3 (2016)
[3] Roberts *et al.*, J. Cryst. Growth. **487**, 23 (2018)
[4] Roberts *et al.*, J. Cryst. Growth. **528**, 125254 (2019)
[5] Moloney *et al.*, J. Phys. D: Appl. Phys. **52**, 475101 (2019)
[6] Barthel *et al.*, "Ti alloyed α -Ga2O3: route towards wide band gap engineering" (in preparation)

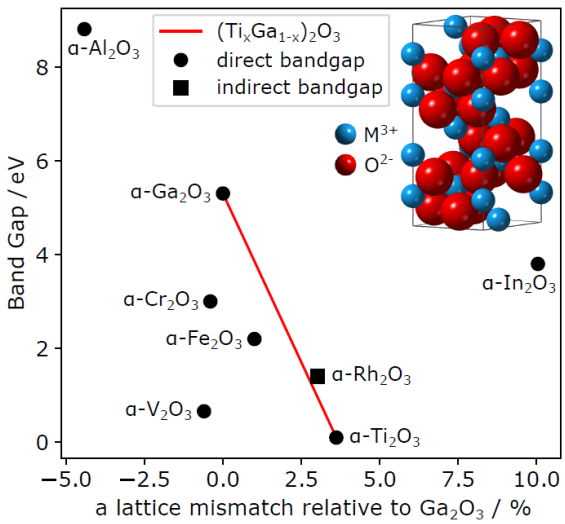

Figure 1. Corundum phase semiconducting sesquioxide design space, centered on α-Ga_2O_3.

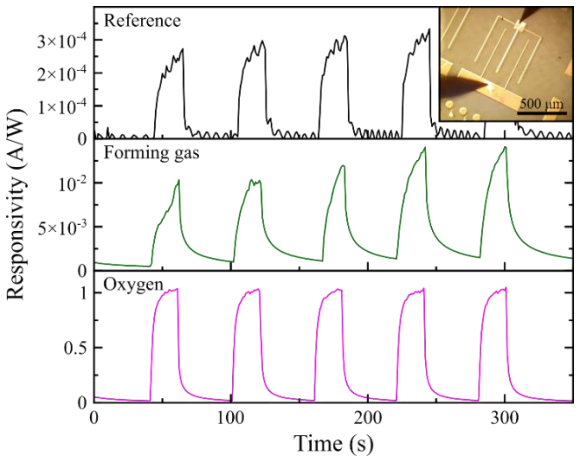

Figure 2. Responsivity of the photodetectors made from the as-grown material and the materials annealed at 400°C in oxygen and forming gas–tested under 240 nm illumination and 10 V bias.

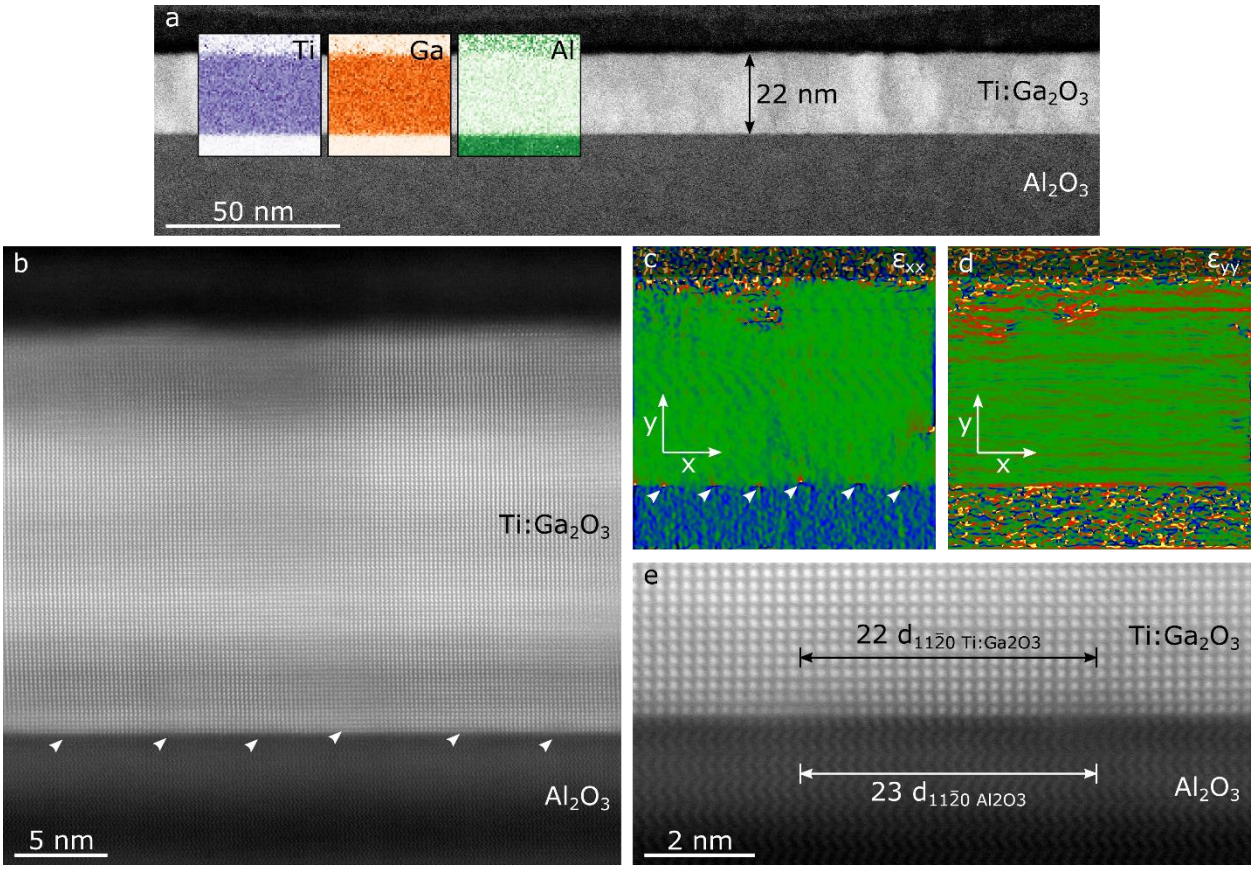

Figure 3. (a-b) HAADF-STEM images of a cross-section of $(Ti_{0.03}Ga_{0.97})_2O_3$ film and its interface with the sapphire substrate. EDS maps are overlaid in (a), showing a uniform distribution of Ti and Ga throughout the film. Strain in the film, perpendicular (c) and parallel (d) to growth direction, was obtained from geometrical phase analysis. Regularly spaced misfit dislocations are indicated by arrows in (b-c). (e) High resolution STEM image of film-substrate interface, clearly showing 2 misfit dislocations and their separation.

Direct band-gap crossover in epitaxial monolayer boron nitride.

T.S. Cheng[1], A. Summerfield[1], C.J. Mellor[1], C. Elias[2], P. Valvin[2], T. Pelini[2], B. Gil[2], G. Cassabois[2], L. Eaves[1], C.T. Foxon[1], P.H. Beton[1], S.V. Novikov[1,*]

[1]School of Physics and Astronomy, University of Nottingham, Nottingham, UK
[2]Laboratoire Charles Coulomb, UMR5221 CNRS-Université de Montpellier, Montpellier, France

Research studies on the growth and properties of hexagonal boron nitride (hBN) have recently attracted a lot of attention. First, the band gap of hBN is about 6eV and that has triggered the interest in hBN as a wide gap material for deep-ultraviolet device (DUV) applications. Secondly, the lattice parameter of hBN is very close to that of the recently discovered graphene. The surface of hBN is atomically flat and can provide an ideal chemically inert dielectric substrate for 2D-structures.

There are now attempts world-wide to develop a reproducible technology for the growth of large area hBN layers by chemical vapour deposition (CVD), metal-organic chemical vapour deposition (MOCVD) and molecular beam epitaxy (MBE).

We have developed a new MBE technology for the growth of graphene and hBN monolayers at extremely high growth temperatures up to 1850^{o}C. This high-temperature MBE approach offers new opportunities in the burgeoning fields of DUV materials, 2D materials and related van der Waals heterostructures. We have developed MBE growth of hBN at the temperatures from 1250^{o}C to 1700^{o}C. We have demonstrated that by growing hBN on highly oriented pyrolytic graphite (HOPG) substrates it is possible to produce monolayer and few-layer thick boron nitride with atomically flat hBN surfaces, which are essential for future 2D and DUV applications. The hBN coverage can be reproducibly controlled by the growth time, substrate temperature and boron to nitrogen flux ratios. We have achieved thicker hBN layers at higher B:N flux ratios. We have demonstrated an increase of the hBN layer thickness by decreasing the growth temperature. However, decreasing the epitaxy temperature below 1250^{o}C, rapidly degrades the optical properties of the hBN layers.

We have demonstrated the high-temperature MBE growth of hBN layers using a high-efficiency RF plasma source with high active nitrogen fluxes. Despite more than a three-fold increase in nitrogen flux with this new source, we observed no significant increase in the growth rates of the hBN layers, indicating that the growth rate of hBN layers is controlled by the boron arrival rate.

It has been demonstrated that bulk hBN is an indirect-gap semiconductor with a band-gap of 5.95eV. Recently we combined deep-ultraviolet photoluminescence and reflectance spectroscopy with atomic force microscopy to reveal the presence of a direct energy gap of 6.1eV in single atomic hBN layers, thus experimentally confirming a crossover to direct gap in the hBN monolayer limit. The closely lattice-matched graphite substrate enables synthesises of monolayer boron nitride by van der Waals epitaxy with an interface free from intermixing effects. With reflectance measurements on monolayer hBN showing a pronounced resonance at around 6.1eV, photoluminescence experiments now reveal emission at this energy. The absence of a Stokes-shift between reflectance and photoluminescence contrasts with multi-layer and bulk hexagonal boron nitride, thus providing the signature of a direct-gap in monolayer boron nitride.

Superconducting boron doped diamond on boron nitride ceramics

Soumen Mandal[1], Henry Bland,[1] Jerome A. Cuenca[1], Malcolm Snowball[2] and Oliver A. Williams[1]

[1] *School of Physics and Astronomy, Cardiff University, Cardiff, UK*
[2] *Ultra Biotecs Limited, Derby, UK*
Mandals2@cardiff.ac.uk, soumen.mandal@gmail.com

With the advancement in diamond growth technology it is possible to grow diamond on variety of non-diamond materials. The diamond films are polycrystalline in nature but retain all superlative properties such as superhardness[1], superconductivity[2], high thermal conductivity[3], high dielectric strength[4] seen in single crystal diamond. Another material with excellent dielectric property is boron nitride. It can be formed into synthetic material which is machinable, making it very attractive for variety of applications. Also known as white graphite, due to its graphite like structure, it is an excellent electrical insulator. In this work we have grown diamond on boron nitride ceramic to enhance the dielectric strength of machined parts. Apart from that, the machinable ceramic can from an excellent template for porous diamond film for supercapacitor application[5].

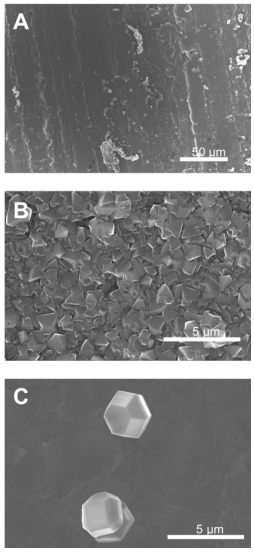

Fig. 1: SEM image of films grown on BN ceramic.

Here we test one of the superlative properties, namely superconductivity, of the diamond on the ceramics. We measured the zeta potential of the ceramics to select the diamond seeds. Diamond was then grown on the seeded ceramics using a microwave chemical vapour deposition system. Figure 1 shows the SEM images of diamond grown on the ceramics[6]. Panels A and B show the over view and zoomed image of the growth. Panel C shows the substrate exposed to growth plasma without any seeding. It is clear from the images that spontaneous growth on the ceramics is not possible even though the surfaces of the ceramics are extremely rough. Figure 2 shows the superconducting transition of the film shown in Figure 1A. The film has a transition temperature close to 3.5K[6]. It is clear from the results that it is possible to grow good quality diamond films on the boron nitride ceramics. Similar strategies can be applied for growth of diamond on other types of ceramics.

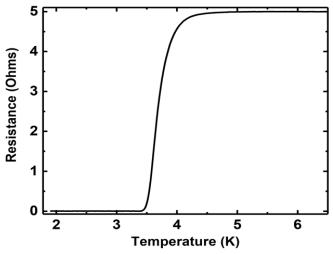

Fig. 2: R vs T curve for diamond grown on BN ceramic.

References

[1] O.A. Williams, Diam. Relat. Mater. **20**, 621 (2011).

[2] E.A. Ekimov, V.A. Sidorov, E.D. Bauer, N.N. Mel'nik, N.J. Curro, J.D. Thompson, and S.M. Stishov, Nature **428**, 542 (2004).

[3] T.R. Anthony, W.F. Banholzer, J.F. Fleischer, L. Wei, P.K. Kuo, R.L. Thomas, and R.W. Pryor, Phys. Rev. B **42**, 1104 (1990).

[4] E. Boettger, A. Bluhm, X. Jiang, L. Schäfer, and C. -P. Klages, J. Appl. Phys. **77**, 6332 (1995).

[5] S. Yu, N. Yang, H. Zhuang, S. Mandal, O.A. Williams, B. Yang, N. Huang, and X. Jiang, J. Mater. Chem. A **5**, 1778 (2017).

[6] S. Mandal, H.A. Bland, J.A. Cuenca, M. Snowball, and O.A. Williams, Nanoscale **11**, 10266 (2019).

High Piezoelectricity in Porous GaN

Yonatan Calahorra*, Adina Wineman, Bogdan Spiridon, Peter Griffin, Sohini Kar-Narayan and Rachel Oliver
Department of Materials Science & Metallurgy, University of Cambridge, Cambridge, UK.
* yc402@cam.ac.uk

Keywords: electromechanical properties, piezo-response-force-microscopy, porous GaN

Piezoelectricity, first discussed by the Curie brothers, is the linear interconversion of mechanical stress and electrical polarization [1]. It is a material property of non-centrosymmetric crystal structures. This electromechanical relation is beneficial for applications such as mechanical sensors and actuators. An interesting class of materials is piezoelectric semiconductors [2]. Particularly, polarization effects in III-Ns are inherent along the <0001> direction, and are exploited in high electron mobility transistors. Conversely, polarization fields are a limiting factor in GaN based light emitting diodes [3]. Nanostructuring of materials, may bring different physical properties into play, *e.g.* through increased surface area, or relaxation of bulk constraints [4]. Here we show that nanoscale porosification of a doped GaN layer (hence non-piezoelectric), results in measurable piezoelectricity, 2-3 times stronger than nominally undoped GaN.

Recently, researchers in the Cambridge Centre for GaN have developed an electrochemical process to etch pores in epitaxially grown GaN [5], and used this process to implement Bragg reflectors, improving the optical properties of GaN structures [6]. In the present work, the electromechanical properties of porous layer ware examined by piezoresponse force microscopy (PFM) and macro-scale device measurements.

PFM measurements show clear piezoelectricity in what previously was a conducting layer (Figure 1a). We attribute this mostly to effective depletion of the structure, brought about by enhanced surface area [7]. The piezoelectric strain coefficient measured, d_{33} ~ 8 pm/V, is about 3 times that of bulk GaN, probably due to softening/reduction of the bulk constraint. A capacitor structure formed by depositing a top contact on the porous layer (Fig. 1b) exhibited energy harvesting performance, by generating a current pulse on loading and unloading by a small weight (Figure 1c).

Overall, these results establish porosification as a handle to induce and control piezoelectricity in GaN, and encourage further studies, for example in integration of piezoelectric active layers within GaN devices.

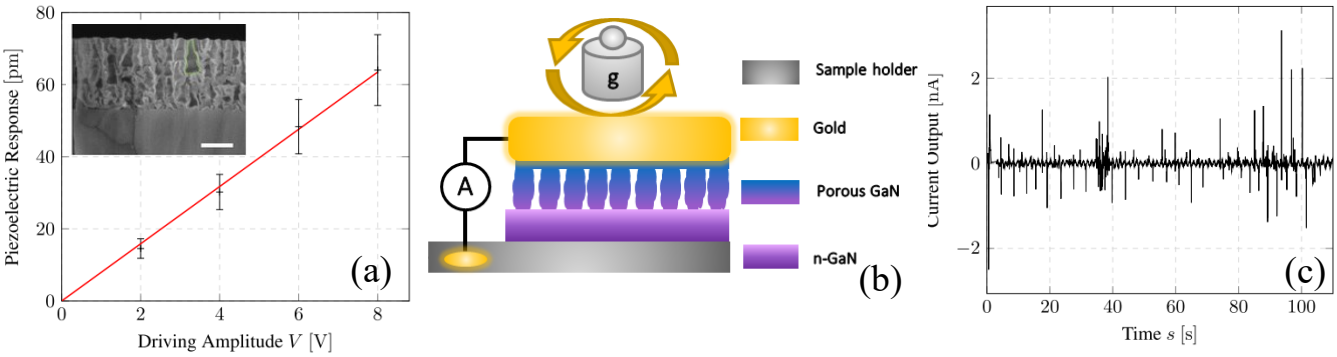

Fig. 1. (a) PFM response of porous GaN layer (inset, scale is 200 nm). Slope yields the piezoelectric coefficient ~8 pm/V; (b) Schematic of the two-terminal device used for macro-scale characterisation; (c) Short-circuit current measured from loading and unloading of the device by 10 g.

References

[1] J. Curie, P. Curie, *Bulletin de minéralogie* **3** (1880) 4.
[2] Y. Calahorra, C.L. Ou, C. Boughey, S. Kar-Narayan, *Nanowires for Energy Applications* **98** (2018) 445.
[3] C. Wood, D. Jena, SpringerLink (Online service), Polarization Effects in Semiconductors From Ab InitioTheory to Device Applications, Springer Science+Business Media, LLC,, Boston, MA (2008).
[4] M.H. Zhao, Z.L. Wang, S.X. Mao, *Nano Letters* **4** (2004) (4) 587.
[5] T.T. Zhu, Y.J. Liu, T. Ding, W.Y. Fu, J. Jarman, C.X. Ren, R.V. Kumar, R.A. Oliver, *Scientific Reports* **7** (2017).
[6] P. Griffin, T.T. Zhu, R. Oliver, *Materials* **11** (2018) (9).
[7] R. Calarco, T. Stoica, O. Brandt, L. Geelhaar, *Journal of Materials Research* **26** (2011) (17) 2157.

Stacking fault induced alloy segregation in Zincblende GaN heterostructure

B. Ding[1], S. M. Fairclough[1], M. Frentrup[1], M. J. Kappers[1], A. Kovács[2], G. Kusch[1], D. J. Wallis[1,3,4] and R. A. Oliver[1]

[1]Department of Materials Science and Metallurgy, University of Cambridge, 27 Charles Babbage Road, Cambridge CB3 0FS, United Kingdom

[2]Ernst Ruska-Centre for Microscopy and Spectroscopy with Electrons, Forschungszentrum Jülich, 52428, Germany

[3]Centre for High Frequency Engineering, University of Cardiff, Queen's Building, Cardiff, CF24 3AA, United Kingdom

[4]Kubos Semiconductors Ltd, Future Business Centre, Kings Hedge Road, Cambridge CB4 2HY

Despite the huge success of blue LEDs based on high quality wurtzite (0001) GaN crystals, green and amber LEDs lag behind in terms of performance. In this context, the alternative cubic zincblende crystal structure may offer a fundamental advantage over the hexagonal wurtzite phase: the absence of spontaneous and piezoelectric polarisation fields in the (001) growth direction, which reduce the internal quantum efficiency of conventional LEDs. The growth of phase pure zincblende GaN has recently been achieved by MOVPE on 3C-SiC/Si(001) substrates [1].

Two key elements of a typical GaN LED structure are the InGaN quantum wells (QWs) used to increase the radiative recombination rate in the active region and an AlGaN electron blocking layer (EBL) used to reduce electron leakage. We have used scanning transmission electron microscopy (STEM) and energy-dispersive X-ray spectroscopy (EDS) to investigate the microstructure and composition of these layers in zincblende blue light emitting heterostructures.

As the thermodynamically less favourable phase, epitaxial zincblende GaN films suffer from a high density of stacking faults (SFs) and SF bundles, i.e., planar violations of the ABC atomic stacking sequence [2]. From cross-sectional STEM, it is seen that these defects have a localised impact on the alloy composition of the InGaN QWs and AlGaN EBL. EDS reveals that in regions where SFs intersect these layers a local increase of the indium content of the QWs and an increase in the aluminium content of the EBLs occurs. However, the positions of the In and Al enriched regions relative to the SF are not the same. In QWs, the region with a higher indium content appears right next to the planar defects. In contrast, the region with a higher aluminium content seems to be coincident with the stacking fault in the EBL. It is speculated that stacking faults lead to a small strain variation having slightly smaller lattice spacing between planes compared to the surrounding material, and in consequence SFs are an energetically favourable site for small aluminium atoms but a less favourable site for large indium atoms, compared to gallium atoms. The mechanism of the composition changes and the difference between In and Al incorporation at stacking faults will be studied further in aberration-corrected STEM and Atom Probe Tomography (APT).

Reference:

[1] M. Frentrup, L. Y. Lee, S. L. Sahonta, M. J. Kappers, F. Massabuau, P. Gupta, R. A. Oliver, C. J. Humphreys and D. J. Wallis, *J. Phys. D. Appl. Phys.* **50** (2017) 433002

[2] L.Y. Lee, M. Frentrup, P. Vacek, M.J. Kappers, D.J. Wallis, and R.A. Oliver, *J. Appl. Phys.* **125** (2019) 105303

[3] S. Church, et al., *J. Appl. Phys.* **123** (2018) 185705

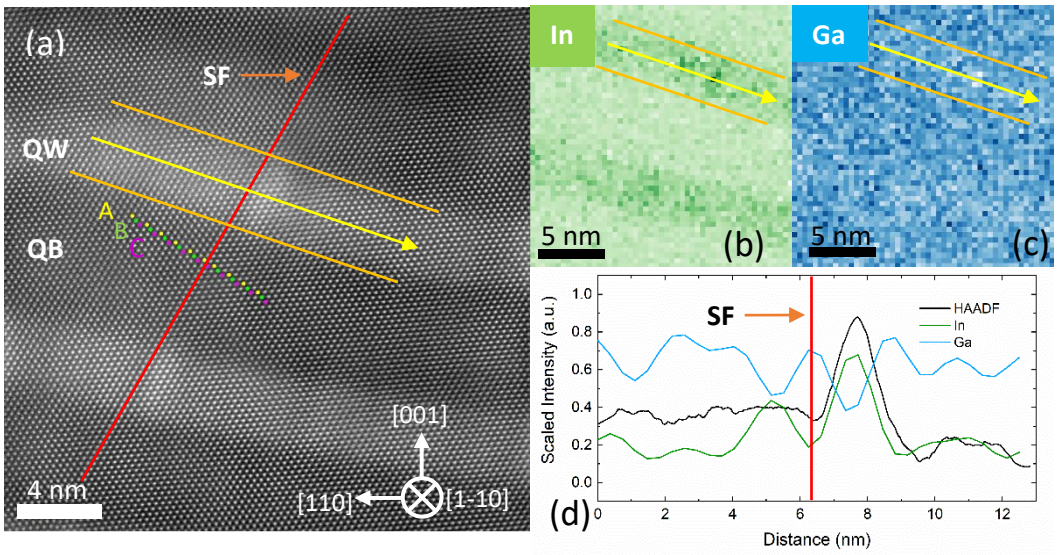

Fig. 1(a) shows the HRSTEM HAADF image of two InGaN QWs. The yellow, green and purple dots indicate the atomic columns with stacking type of -A-, -B- and -C- respectively. (b) is the In EDS signal map corresponding to (a), and (c) is the Ga EDS signal map corresponding to (a). The yellow arrows in (a), (b) and (c) mark a line scan taken on the top QW and the orange lines indicate the width of the line scan. (d) shows the resulting average profiles from the line scan on (a), (b) and (c). The red lines mark the position of an intrinsic SF.

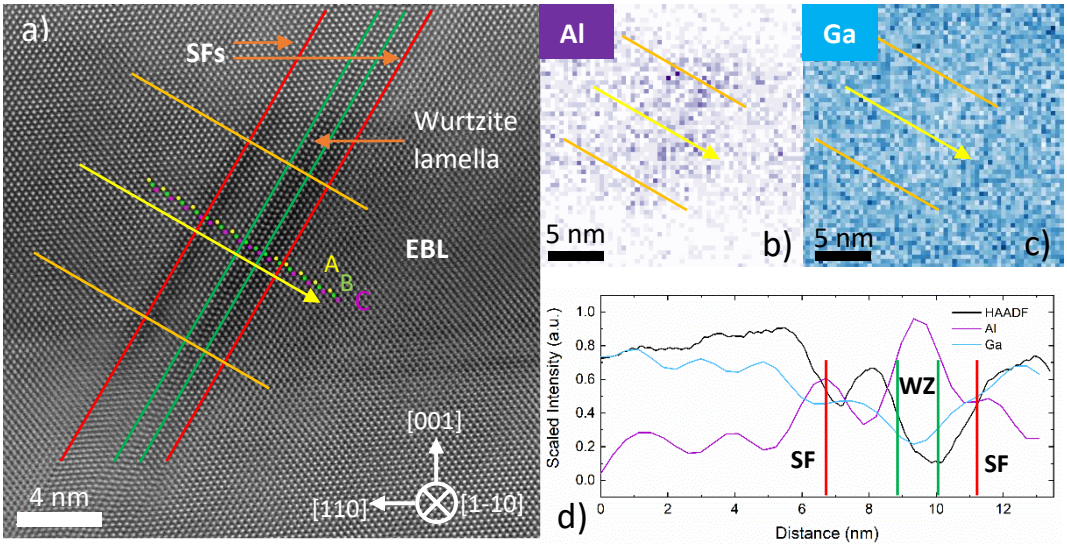

Fig. 2(a) shows the HRSTEM HAADF image of a EBL. The yellow, green and purple dots indicate the atomic columns with stacking type of -A-, -B- and -C- respectively. (b) is the Al EDS signal map corresponding to (a), and (c) is the Ga EDS signal map cooresponding to (a). The yellow arrows in (a), (b) and (c) mark a line scan taken on the EBL and the orange lines indicate the width of the line scan. (d) shows the resulting average profiles from the line scan on (a), (b) and (c). The red lines mark the position of two intrinsic SFs and the green lines enclose a wurtzite lamella.

Study of $Al_xGa_{1-x}N$ nucleation layers for the growth of cubic zincblende GaN

Abhiram Gundimeda[1,*], Martin Frentrup[1], Simon M. Fairclough[1], Alexander Hinz[1], Huixin Xiu[1, 2], Menno J. Kappers[1], David J. Wallis[1, 3], Rachel A. Oliver[1]

[1] *Department of Materials Science and Metallurgy, University of Cambridge, 27 Charles Babbage Rd, Cambridge, CB3 0FS, United Kingdom*

[2] *School of Materials Science and Engineering, University of Shanghai for Science and Technology, 516 Jungong Road, Yangpu District, Shanghai, 200093, China*

[3] *Centre for High Frequency Engineering, University of Cardiff, 5 The Parade, Newport*

**E-mail: ag2025@cam.ac.uk*

III-Nitride material systems have been extensively used for various optoelectronic applications. The conventionally used hexagonal wurtzite GaN suffers from the presence of piezoelectric and spontaneous polarisation fields when grown in the (0001) orientation, which reduce the device efficiencies. Cubic zincblende (zb-) (001) GaN has tremendous potential, due to the absence of such polarisation fields. However, growth of zb-GaN can be affected by the presence of high densities of stacking faults, wurtzite inclusions and misfit dislocations. To try to address these issues, we have explored the use of $Al_xGa_{1-x}N$ nucleation layers, which have an intermediate lattice constant that lies between zb-GaN and the 3C-SiC/Si template. Therefore, they should reduce the lattice mismatch of 3.4% for zb-GaN and could potentially improve the quality of the GaN layers grown over them.

In this study, we investigate the influence of $Al_xGa_{1-x}N$ nucleation layers with $0 < x < 1$ on the structural quality of the subsequent grown zb-GaN epilayer globally by X-ray diffraction (XRD) and locally by Transmission Electron Microscopy (TEM). XRD measurements revealed a high zincblende phase purity for zb-GaN grown on low Al content nucleation layers at gas phase compositions (x_{gas}) up to 25% AlN. With increasing x_{gas} from 37% to 62%, increased the formation of wurtzite inclusions was observed, and wurtzite is the only phase observed for $x_{gas} \geq 75\%$.

X-ray Photoelectron spectroscopy measurements revealed that the fraction of Al incorporated into the nucleation layers is around 20% lower than the gas phase compositions, which might be due to the parasitic pre-reactions in the reactor. Scanning TEM - energy dispersive X-ray spectroscopy measurements revealed a non-uniform distribution of Al across the nucleation layer, in both as-grown and annealed nucleation layers. The Al concentration is slightly lower close to the SiC interface and increases towards the top. This might be because of a slower decomposition of trimethylaluminum compared to trimethylgallium due to stronger bonds and a higher tendency for cluster formation in the gas phase before complete decomposition.

To observe the origin of wurtzite inclusions, cross-sectional high-resolution TEM (HRTEM) and Scanning Electron Diffraction (SED) measurements were performed on zb-GaN grown on AlGaN nucleation layer (x_{gas} = 50%). The SED phase maps revealed that the epilayer is predominantly zincblende phase with wurtzite inclusions starting within/from the nucleation layer. HRTEM measurements of the GaN/AlGaN/SiC region revealed that the wurtzite inclusions were originated from the GaN/AlGaN interface. Regions of both the zincblende phase and of mixed phases were also observed close to the GaN/AlGaN interface. However, the nucleation layer itself seems to be zincblende phase pure within the limitations of the TEM experiment with no wurtzite inclusions across the measured region. Hence, we suggest that wurtzite inclusions initiate from facets on the nucleation layers.

15.45-17.30 Session 3 – Nano and quantum
Chairs: Fabien Massabuau/Peter Parbrook

15.45-16.00: *Creation of an AlN topographical surface for the site-control of III-N quantum dots*

Robert Armstrong[1], Pierre-Marie Coulon[1], Pavlos Bozinakis[2], Robert Martin[2], Daniel Wolverson[3], Philip Shields[1]

[1] Department of Electrical and Electronic Engineering, University of Bath, Bath, UK
[2] Department of Physics, SUPA, University of Strathclyde, Glasgow, G4 0NG, UK
[3] Department of Physics, University of Bath, Bath, BA2 7AY, UK

16.00-16.15: *Decreased spectral diffusion rate of a non-polar InGaN quantum dot*

C. C. Kocher[1], T. Zhu[2], J. C. Jarman[2], R. A. Oliver[2], R. A. Taylor[1]

[1] Department of Physics, University of Oxford, Parks Rd, Oxford OX1 3PJ, UK
[2] Department of Materials Science and Metallurgy, University of Cambridge, Cambridge CB3 0FS, UK

16.15-16.30: *Influence of MOVPE environment on the selective area thermal etching of GaN nanohole arrays*

Pierre-Marie Coulon[1], Peng Feng[2], Tao Wang[2], Philip A. Shields[1]

[1] Department of Electrical & Electronic Engineering, University of Bath, Bath, BA2 7AY, UK
[2] Department of Electronic and Electrical Engineering, University of Sheffield, S1 4DE, UK

16.30-16.45: *Room Temperature Quantum Light From Colour Centres in the Nitrides*

Sam Bishop[1], J.P. Hadden[2], Diana Huffaker[1,2], Anthony J. Bennett[1]

[1] School of Engineering, Cardiff University, Queen's Buildings, The Parade, Cardiff, CF24 3AA, UK
[2] School of Physics and Astronomy, Cardiff University, Queen's Buildings, The Parade, Cardiff, CF24 3AA, UK

16.45-17.30 The Foxon Lecture

Challenges for GaN to achieve its theoretical promise for power electronics

Mike Uren
HH Wills Physics Laboratory, University of Bristol, Tyndall Avenue, Bristol BS8 1TL

17.30-18.30 AGM

19.30-22.30 Conference dinner

Creation of an AlN topographical surface for the site-control of III-N quantum dots

Robert Armstrong[1], Pierre-Marie Coulon[1], Pavlos Bozinakis[2], Robert Martin[2], Daniel Wolverson[3], Philip Shields[1]

[1]Department of Electrical and Electronic Engineering, University of Bath, Bath, United Kingdom

[2]Department of Physics, University of Strathclyde, Glasgow, United Kingdom

[3]Department of Physics, University of Bath, Bath, United Kingdom

Quantum dots have a range of applications such as the improving of light emitting diode efficiencies [1], lowering laser diode thresholds [2], cancer detection [3] and quantum dot TVs [4]. These applications utilise either 'colloidal' or self-assembled quantum dots and generally display poor uniformity of size and shape along with random spatial locations. These characteristics are not suitable for applications in quantum information processing (QIP), such as quantum cryptography and quantum computing, where arrays of quantum dots with spatially determined locations and identical shapes and sizes are required to create dots with identical energy structures. For many QIP applications harnessing quantum dots, single photon emission is required. In many materials this has typically only been achieved at cryogenic temperatures [6], whereas due to the large band-gap offsets of the III-N's, this has been demonstrated up to 350 K [5], using AlGaN barriers with GaN quantum dots. Whilst the use of a pure AlN barrier for GaN quantum dots could lead to emission at even higher temperatures, so far this has largely been unrealised. One reason for this is the difficulty of creating uniform arrays of AlN nanostructures.

The best way to create GaN nanostructures is through the use of selective area growth. Here a dielectric mask is patterned with an array of apertures from which incident adatoms preferentially grow, resulting in the formation of nanostructures. Nanorods and nanopyramids have been demonstrated for GaN and are uniform and spatially predetermined [7-8] because of the large diffusion length of gallium adatoms. However, selective area growth of AlN is unsuccessful (see figure 1) since aluminium adatoms have a low diffusion length and a high sticking coefficient [9]. Hence, in order to achieve arrays of homogenous and spatially predetermined AlN nanostructures another route is necessary.

In this work, we combine top-down etching and bottom-up regrowth to create uniform topographical AlN surfaces. Metal-organic vapour-phase epitaxial (MOVPE) regrowth was performed on nanohole and nanorods geometries. The impact of the AlN regrowth conditions on the morphology and faceting of the nanostructures was investigated via scanning electron microscopy (see figure 2). Growth under low pressure and with hydrogen carrier gas was found to be favourable for well formed semipolar planes with small top c-plane truncation relative to growth under either high pressure or nitrogen carrier gas. The V/III ratio and growth temperature were found to impact the relative facet growth rates. By tuning the time of specific regrowth conditions, highly uniform faceted nanorods with very sharp tip apices were created. These apices, due to their nanometric dimensions, may be suitable for GaN quantum dot growth. Conversely, the creation of reverse pyramids from the etched nanohole structures was found to be more challenging to achieve. Finally, preliminary results on GaN site-controlled growth on sharp AlN features will be presented.

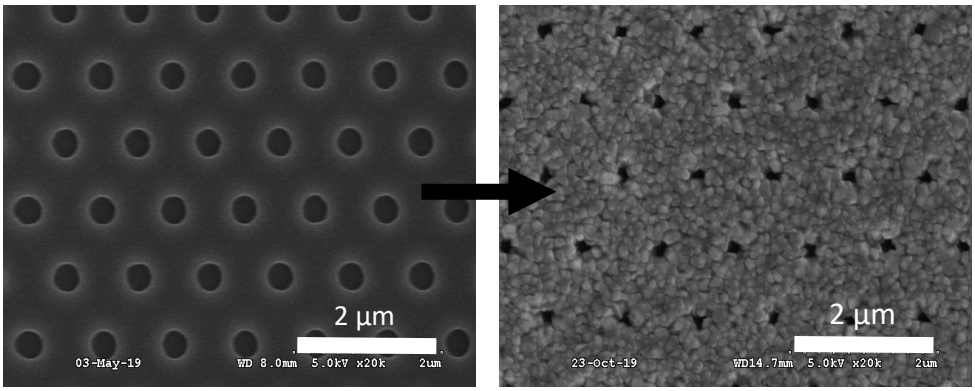

Figure 1: Demonstration that selective area growth with AlN does not work. On inspection of the image before (left) and after (right) growth one can see material just sticks to the mask and doesn't result in nanostructure growth.

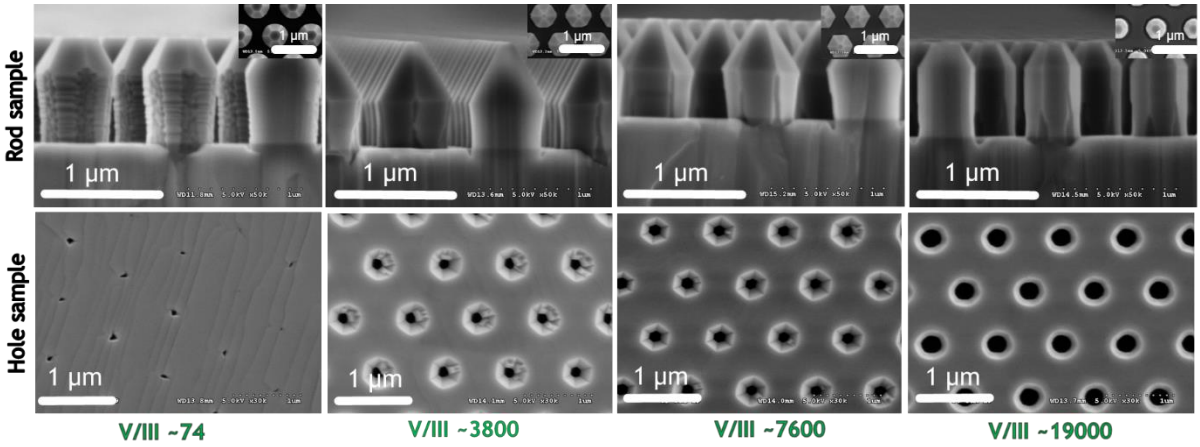

Figure2: Regrowth of AlN nanostructures as a function of the V/III ratio (displayed in green). All other parameters kept the same (H_2 carrier gas, reactor pressure 20 mbar, growth temperature 950 ^oC, growth time 60 minutes)

[1] Brault, J et al. (2013), AlGaN-Based Light Emitting Diodes Using Self-Assembled GaN Quantum Dots for Ultraviolet Emission, Japanese Journal of Applied Physics 52 (2013) 08JG01
[2] Zhang, M. et al (2011), A InGaN/GaN quantum dot green (λ = 524nm) laser, Appl. Phys. Lett. 98, 221104 (2011); doi: 10.1063/1.3596436
[3] Sharma, A et al. (2013), Quantum Dots Self Assembly Based Interface for Blood Cancer Detection, Langmuir 2013, 29, 8753−8762
[4] Luo, z et al. (2018), Television's Quantum dots will be the next darling of TV manufacturers, IEEE spectrum, Volume 55, Issue 3
[5] Holmes. M et al. (2016), Single Photons from a Hot Solid-State Emitter at 350 K, ACS Photonics 2016, 3, 543−546
[6] Zhang. L et al. (2016), Charge-tunable indium gallium nitride quantum dots, PHYSICAL REVIEW B 93, 085301 (2016)
[7] Kitamura. S et al. (1995), Fabrication of GaN hexagonal pyramids on dot-patterned GaN/Sapphire substrates via selective metal organic vapour phase epitaxy, Jpn. J. Appl. Phys. Vol. 34 Part 2. No. 9B
[8] Coulon. P-M et al. (2016), Dislocation filtering and polarity in the selective area growth of GaN nanowires by continuous-flow metal organic vapor phase epitaxy, Applied Physics Express 9, 015502
[9] Coulon. P-M et al. (2018), Hybrid Top-Down/Bottom-Up Fabrication of a Highly Uniform and Organized Faceted AlN Nanorod Scaffold, Materials 2018, 11, 1140; doi:10.3390/ma11071140

Decreased spectral diffusion rate of a non-polar InGaN quantum dot

C. C. Kocher[1], T. Zhu[2], J.C. Jarman[2], R.A. Oliver[2], and R.A. Taylor[1]

[1]University of Oxford, United Kingdom, [2]University of Cambridge, United Kingdom

Traditionally, nitride quantum dots suffer from strong spectral diffusion. This is partly due to their large in-built dipoles resulting from the polar nature of nitride materials. Another reason is the high dislocation density compared to the more mature arsenide material system, which gives carriers a multitude of opportunities to get trapped in the materials surrounding the dots. As a result, fast time scale spectral diffusion broadens linewidths of nitride dots up to more than 1 meV for integration times on the scale of seconds.

This presents a large obstacle for the generation of indistinguishable photons. However, recent publications reported a spectral diffusion time of ~22 ns for a polar GaN/AlGaN QD [1], and ~230 ns for a polar InGaN/GaN QD [2]. This puts an upper limit to the time scale in which indistinguishable photons could be generated; other mechanisms are likely to reduce the coherence further.

In contrast to these nitride dots conventionally grown along the polar direction, we studied a quantum dot grown on a non-polar plane. These have been shown to exhibit an increased oscillator strength by a factor of ~10 [3]. Furthermore, a theoretical analysis revealed for the special case of non-polar InGaN dots, that the second order piezoelectricity counteracts the first order [4], resulting in a further reduced dipole moment. However, along with the change of the growth plane comes an increased density of defects.

Here, we present a study of the fast time-scale spectral diffusion of a non-polar InGaN quantum dot grown by modified droplet epitaxy [3]. Its spectrum is shown in Fig. 1 (a). We conducted autocorrelation measurements for a range of different excitation powers. By restricting the signal to half of the emission peak width, bunching originating from fast spectral diffusion was observed. Its timescale varied approximately linearly with the excitation power, as shown in Fig. 1 (b). The longest spectral diffusion time obtained was ~900 ns for the lowest excitation power. This represents an increase by a factor of 2 to 3 compared to the polar case [2] and increases the chance of successful generation of indistinguishable photons.

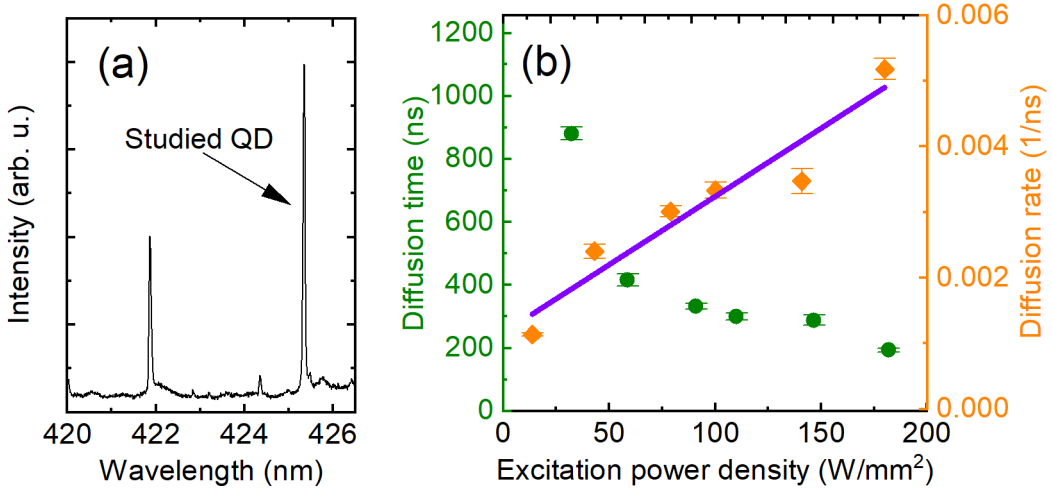

Fig. 1 (a) Spectrum of the QD. (b) Power dependence of the diffusion time/diffusion rate.

[1] K. Gao, *et al.*, AIP Advances. **7**, 125216 (2017).

[2] K. Gap, *et al.*, Appl. Phys. Lett. **114**, 112109 (2019).

[3] T. Zhu, *et al.*, Appl. Phys. Lett. **102**, 251905 (2013).

[4] S. Patra, S. Schulz, Phys. Rev. B **96**, 155307 (2017).

Influence of MOVPE environment on the selective area thermal etching of GaN nanohole arrays

Pierre-Marie Coulon[1], Peng Feng[2], Tao Wang[2] and Philip A. Shields[1]
[1] *Dept. Electrical & Electronic Engineering, University of Bath, Bath, BA2 7AY, UK*
[2] *Dept. of Electronic and Electrical Engineering, University of Sheffield, S1 4DE, UK*
P.Coulon@bath.ac.uk

Selective area thermal etching (SATE) is an original and simple top-down approach to form nanostructures that offers the possibility to create novel optoelectronic devices architectures and further improve the structural and optical quality of existing III-nitride based light emitting diodes. [1,2]

In this work, we report a parametric study to achieve SATE of highly uniform and organized GaN nanohole arrays within a MOVPE reactor from *c*-plane GaN-on-sapphire template. The morphology, etching anisotropy and etch depth of the nanoholes is investigated by scanning electron microcopy for a broad range of parameters such as the temperature, the pressure, the NH_3 flow rate and the carrier gas mixture. We found that the supply of NH_3 during SATE plays a crucial role in obtaining a highly anisotropic thermal etching process with the formation of hexagonally non-polar faceted nanoholes. Changing other parameters mainly impact on the formation, or not, of non-polar sidewalls, the uniformity of the nanohole diameter and the etch rate, which, in the best case, reaches 6 µm per hour. SATE of GaN nanohole is not only demonstrated on *c*-plane GaN for various filling factors but also on a (11-22) semi-polar GaN template. Finally, the etching mechanism behind the SATE of GaN nanohole arrays within a MOVPE environment will be discussed. We expect the process to be transferable to other features than circular SiN_x nano-opening, such as dots, rings or lines, along with other semi-polar orientations.

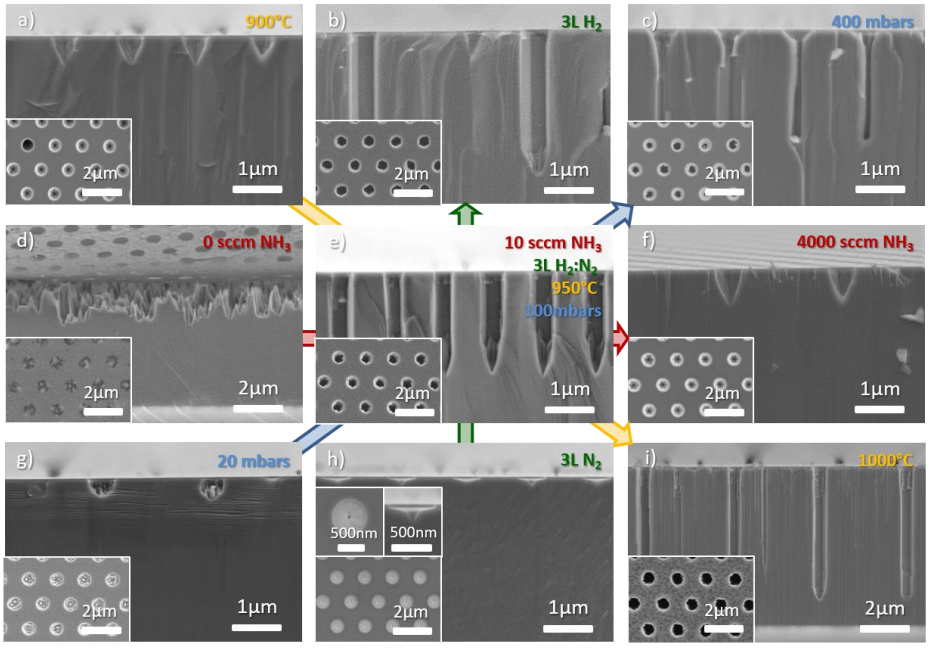

Figure 1. Cross-section and related plan view (in inset) SEM images of GaN nanoholes after 1h SATE for various annealing parameters.

[1] Damilano, B. *et al.* "Selective Area Sublimation: A Simple Top-down Route for GaN-Based Nanowire Fabrication," Nano Letters, 16(3), 1863–1868 (2016).
[2] Damilano, B. *et al.* Top-down fabrication of GaN nano-laser arrays by displacement Talbot lithography and selective area sublimation. Appl. Phys. Express 12, 045007 (2019).

Room Temperature Quantum Light from Colour Centres in the Nitrides

Sam Bishop[1], J. P. Hadden[2], Diana Huffaker[1,2], Anthony J. Bennett[1]

[1] *School of Engineering, Cardiff University, Queen's Buildings, The Parade, Cardiff, UK, CF24 3AA*
[2] *School of Physics and Astronomy, Cardiff University, Queen's Buildings, The Parade, Cardiff, UK, CF24 3AA*

Gallium Nitride has become a dominant force in high power electrical and UV-visible optical applications in the last few decades. This success is fuelling further research attention including into its use as ideal sources of single photons at elevated temperatures. The most widely studied solid state single photon sources such as quantum dots (QDs) and colour centres in Diamond and SiC all have significant disadvantages. QDs in the GaAs material system require the use of large cryogenic cooling equipment. Diamond vacancy centres are comparatively weak sources of light. However, diamond NV^- colour centres have been explored due to their emission of single photons as well as their spin-addressable ground state at room temperature.

III-Nitrides are a material family that promise the means to overcome issues associated with previous technologies [1]. Strong confinement can be achieved due to the large band gap difference between the binary

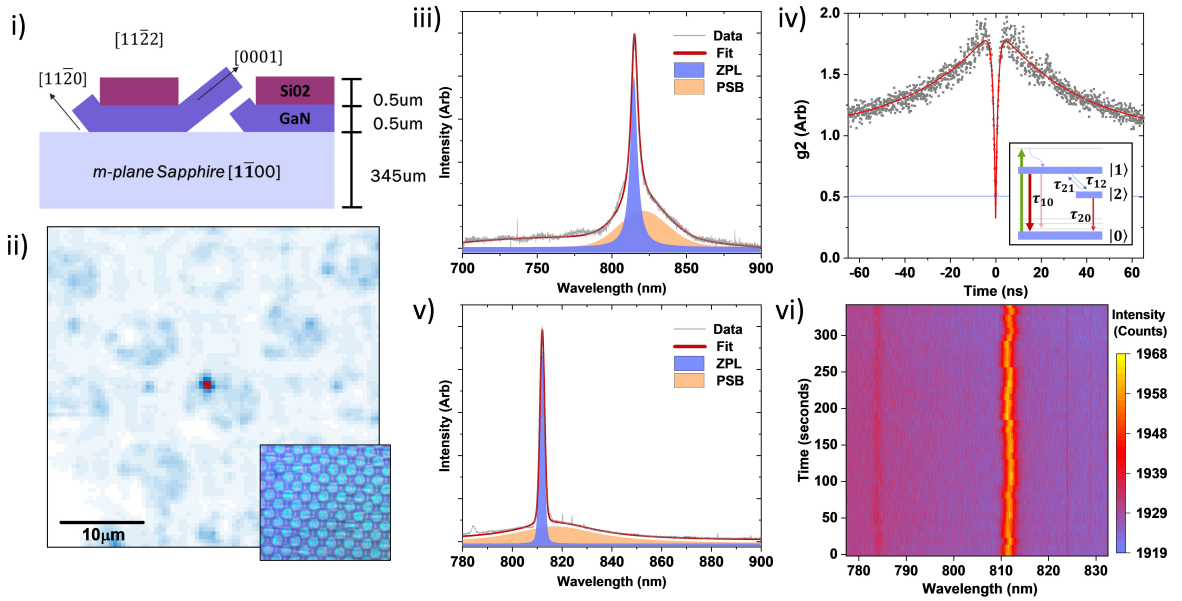

Figure 1: Spectroscopy of a colour centre in a Gallium Nitride semi-polar substrate. i) Illustration of the complicated growth of the substrate. ii) A room temperature confocal image showing a localised emitter. The insert is an optical image of the substrate. iii) Room temperature spectrum of the emitter under 532nm excitation. iv) Second order correlation measurement taken at high power, which clearly demonstrates photon anti-bunching as well as bunching. The insert shows a representation of the three level energy structure used to fit the data. v) and vi) Spectroscopy of the same emitter at 4K. Sharpening of the emission line and reduction in the coupling to phonons can be observed, as well as an instability in the spectra in vi) due to spectral diffusion.

alloys and optical tuning can be achieved with ternary alloys across the whole visible spectrum. Additionally GaN is an ideal candidate for near-infrared integrated quantum optics due to the lack of two-photon and inter-band absorption at these wavelengths. In the last couple of years quantum emission from point-like emitters has been reported in off-the-shelf GaN templates [2]. This discovery shows that GaN plays host to a number of colour centres that emit from the visible out to the telecommunication C-band [3]. Although once attributed to Cubic phase inclusions in the Wurtzite host matrix, a recent study has shown a more complex correlation between the density of emitters and density of growth dislocations [4].

Here we report on spectral, time-resolved, polarisation and autocorrelation measurements on near-infrared quantum emitters embedded deep within the band gap of an off-the-shelf semi-polar GaN template. We observe a continuous range of emissions energies for different emitters in the same sample suggesting that they are not formed due to a simple, single-site defect. Figure 1 gives a detailed analysis of a single emitter with a strong optical transition at 815nm. Second order autocorrelation measurements demonstrate antibunched emission with a single confined state with a recombination lifetime $\approx 1ns$ and a saturation brightness several times larger than unprocessed NV^- centers at 400kcps. Spectroscopy at 4K provides insight into significant sharpening of the emission line and additionally limitations of the linewidth due to slow spectral diffusion.

We acknowledge financial support provided by the Sêr Cymru National Research Network in Advanced Engineering and Materials, the European Union's Horizon 2020 research and innovation programme and the Royal Society for Research Grant RGS\R1\191251.

References

[1] M. J. Holmes, M. Arita, and Y. Arakawa, "III-nitride quantum dots as single photon emitters," *Semiconductor Science and Technology*, vol. 34, p. 033001, mar 2019.

[2] A. M. Berhane, K.-Y. Jeong, Z. Bodrog, S. Fiedler, T. Schröder, N. V. Triviño, T. Palacios, A. Gali, M. Toth, D. Englund, and I. Aharonovich, "Bright Room-Temperature Single-Photon Emission from Defects in Gallium Nitride," *Advanced Materials*, vol. 29, p. 1605092, mar 2017.

[3] Y. Zhou, Z. Wang, A. Rasmita, S. Kim, A. Berhane, Z. Bodrog, G. Adamo, A. Gali, I. Aharonovich, and W.-b. Gao, "Room temperature solid-state quantum emitters in the telecom range," *Science Advances*, vol. 4, p. eaar3580, mar 2018.

[4] M. Nguyen, T. Zhu, M. Kianinia, F. Massabuau, I. Aharonovich, M. Toth, R. Oliver, and C. Bradac, "Effects of microstructure and growth conditions on quantum emitters in gallium nitride," *APL Materials*, vol. 7, p. 081106, aug 2019.

Thursday 9th January

9.00-10.30: Session 4 – Electronic devices
Chairs: Rob Martin/Kean Boon Lee

9.00-9.45: *Towards the limits of GaN electronics*
Elison Matioli

Institute of Electrical Engineering, Ecole Polytechnique Federale de Lausanne (EPFL), Lausanne, Switzerland.

9.45-10.00: *A new method to achieve GaN power electronics approaching its intrinsic limits*
S. Jiang, Y. Cai, P. Feng, S. Shen, X. Zhao, P. Fletcher, V. Esendag, K. Lee, T. Wang

Department of Electronic and Electrical Engineering, University of Sheffield, UK

10.00-10.15: *Field Plate Design in ALGaN/GaN HEMTs for High Speed Monolithically Integrated DC-DC Converters*
Joseph Pinchbeck, Srikanth Devireddy, Sheng Jiang, Kean Boon Lee, Peter Houston

The University of Sheffield, Western Bank, Sheffield S10 2TN, UK

10.15-10.30: *High-temperature contact stability of 2DEG heater on GaN membrane for sensing applications*
Bogdan Spiridon[1], Andrea De Luca[2], Abdalla Eblabla[3], Saptarsi Ghosh[1], Simon Fairclough[1], Giorgia Longobardi[2], Khaled Elgaid[3], Florin Udrea[2], David Wallis[1,3], Rachel Oliver[1]

[1] Department of Materials Science and Metallurgy, University of Cambridge, Cambridge CB3 0FS, UK
[2] Department of Engineering, University of Cambridge, Trumpington St, Cambridge CB2 1PZ, UK
[3] Centre for High-Frequency Engineering, Cardiff University, UK

10.30-10.45: *Low Field Vertical Charge Transport in AlGaN/GaN – on – Si High Electron Mobility Transistors*
Filip Wach[1], Michael J Uren[1], Benoit Bakeroot[2], Steve Stoffels[2], Ming Zhao[2], Stefaan Decoutere[2], Martin Kuball[1]

[1] Centre for Device Thermography and Reliability (CDTR), H. H. Wills Physics Laboratory, University of Bristol, UK
[2] imec 3001 Leuven, Belgium

10.45-11.00: *Study of drain injected breakdown mechanisms in AlGaN/GaN-on-SiC HEMTs*

Feiyuan Yang[1], Manikant Singh[1], Michael J. Uren[1], Hassan Hirshy[2], Paul J. Tasker[2], Trevor Martin[3], Martin Kuball[1]

[1] Centre for Device Thermography and Reliability, School of Physics, University of Bristol, UK
[2] Centre for High Frequency Engineering, Cardiff University, UK
[3] IQE Europe, St Mellons, Cardiff, UK

11.00-11.30: Coffee

A new method to achieve GaN power electronics approaching its intrinsic limits

S. Jiang [#], Y. Cai [#], P. Feng, S. Shen, X. Zhao, P. Fletcher, V. Esendag, K. Lee, and T. Wang*
Department of Electronic and Electrical Engineering, University of Sheffield
[#]These authors contributed equally to the work; *Corresponding author: t.wang@sheffield.ac.uk;

It is well-known that c-plane GaN exhibit superior electrical properties to any other existing semiconductors, where the intrinsic polarisation leads to a high sheet carrier density of two-dimensional electron gas (2DEG) formed in an AlGaN/GaN heterostructure without using any modulation doping. It is also expected to have a high breakdown field (with the theoretical value of the critical electrical field of ~3MV/cm). GaN is supposed to be semi-insulating due to its wide bandgap intrinsic. However, the performance of GaN electronic devices reported so far is far from the limits of this material. Therefore, it is crucial to understand the fundamental issues from the perspective of epitaxial growth, and then to explore a new approach towards these theoretical limits. In this study, we reported our AlGaN/GaN HEMTs with a record breakdown field of 2.5 MV/cm and an extremely low off-state leakage current down to 1 nA/mm at up to 1000 V by means of using our high-temperature AlN buffer growth approach instead of the classic two-step growth method, where a 2D growth method is employed throughout our whole growth processes.

Our HEMT structures are grown on c-plane sapphire. A 500 nm high-temperature AlN buffer layer is initially grown, followed by a 1.5 µm GaN buffer layer, and then a 1 nm AlN spacer and finally a 25 nm $Al_{0.2}Ga_{0.8}N$ barrier. To maintain a 2D growth method and minimise auto carbon-doping in GaN, all the layers are grown at high temperatures. AlGaN/GaN depletion-mode (D-mode) devices with a gate width of 100 µm, a gate length of 1.5 µm, a gate-drain separation of 9 µm and a source-drain separation of 13 µm have been fabricated.

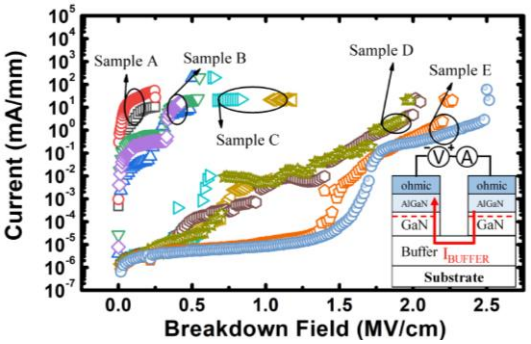

Fig. 1 Sample E exhibits an extremely high breakdown field of 2.5 MV/cm. Inset: Schematic of a test pattern used for buffer leakage measurements.

Fig. 1 shows our breakdown field measurements, where a buffer leakage test pattern consisting of two isolated ohmic contacts with a 3 µm gap spacing is used as shown in Inset of **Fig. 1**. Compared with Sample A, B and C (all below 1 MV/cm), Sample D and E demonstrate a high breakdown field over 2 MV/cm, in particular Sample E with an extremely high breakdown field of 2.5 MV/cm, approaching the theoretical limit.

Fig. 2 shows the characteristics of our AlGaN/GaN HEMTs fabricated on Sample E: an output current of 370 mA/mm (**Fig. 2a**); a specific on-resistance ($R_{on,sp}$) of 1.95 mΩ·cm^2 (**Fig. 2b**); an extremely low buffer (total) leakage below 1 nA/mm (100 nA/mm) at up to 1000 V (**Fig. 2c**) and an excellent figure-of-merit ($V_{br}^2/R_{on,sp}$) of 5.13 × 10^8 V^2/Ω·cm^2 (**Fig. 2d**).

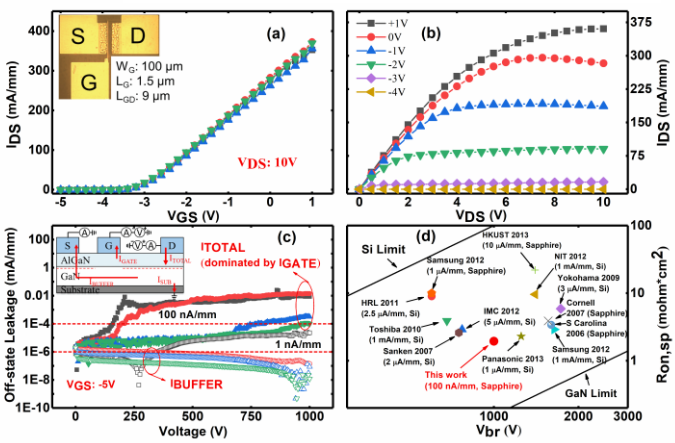

Fig. 2 (a-b-c) Characteristics of our HEMTs; (d) Benchmarking our devices against the state-of-the-art by comparing figure-of-merit ($V_{br}^2/R_{on,sp}$).

Sample D and E which benefits from our HT AlN buffers show typical layer-by-layer 2D growth mode of the GaN buffer with clear features of parallel and straight terraces in the AFM image in **Fig. 3b**, while GaN using classic two-step growth methods shows dark spots due to the termination of screw dislocations (**Fig. 3a**). The 2D growth method allows GaN to yield a narrow FWHM of <100 arcsec along (002) and broad FWHM along (102) GaN, leading to a highly resistive GaN buffer. Our PL spectrum of Sample E exhibits a negligible yellow band emission, ruling out auto carbon doping.

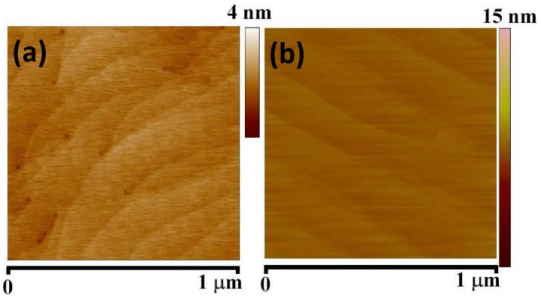

Fig.3 AFM image of the GaN layer grown (a) using the classic two-step growth method and (b) on our HT AlN buffer.

In conclusion, we have reported a record breakdown field of 2.5 MV/cm on our HEMTs, which approaches the theoretical limit of GaN and exhibits a negligible buffer leakage of 1 nA/mm at 1000 V with an excellent figure-of-merit ($V_{br}^2/R_{on,sp}$) of 5.13 × 10^8 V^2/Ω.cm^2. We believe that the 2D growth method as a result of employing our HT AlN buffer technology makes major contribution.

Field Plate Design in AlGaN/GaN HEMTs for High Speed Monolithically Integrated DC-DC Converters

Joseph Pinchbeck, Srikanth Devireddy, Sheng Jiang, Kean Boon Lee and Peter Houston
Department of Electronic and Electrical Engineering, The University of Sheffield

AlGaN/GaN high electron mobility transistors (HEMTs) are an attractive choice for use in high power converters due to their highly conductive 2DEG channel and large band gap (high critical breakdown field). These lead to low conduction loss for a given blocking voltage. In addition, low channel resistance also results in small gate width for a given output current rating and hence fast switching speed (and low switching losses) due to small intrinsic capacitances. Therefore, replacing conventional Si MOSFETs with AlGaN/GaN HEMTs in DC-DC converters will not only improve the efficiency, but also enable high switching frequency operation which reduces the size requirements of passive components in the converters. However, AlGaN/GaN HEMTs often suffer from dynamic *Ron* effects where *Ron* increases with drain voltage. Field plates (FPs) have been found to be effective in reducing the surface-trapping induced dynamic *Ron*. [1] However, the incorporation of FPs also affects the intrinsic capacitances of the transistors and hence the switching times. In this study, we investigate the effect of FP configurations on the dynamic *Ron* and intrinsic capacitances of the AlGaN/GaN HEMTs as well as the switching performance of 50V DC-DC converters.

Figure 1 shows the measured dynamic *Ron* from the AlGaN/GaN HEMTs without a FP, with a gate-connected FP (GFP) and a source-connected FP (SFP). Similar dynamic *Ron* is observed in devices with a GFP and a SFP, which is ~20% increase in the dynamic *Ron* at a drain voltage of 100V compared to low voltage. However, the dynamic *Ron* is more than 2x higher in the device without a FP compared to devices with FP at 100V, which indicates the effectiveness of the FP in suppressing this effect.

Figure 2(a) shows the comparison of Sentaurus T-CAD simulated gate-drain capacitance (*Cgd*) of the AlGaN/GaN HEMTs without FP, with a gate-connected FP (GFP) and a source-connected FP (SFP). While *Cgd* decreases gradually with increasing drain voltage for the device without a FP, a step drop in *Cgd* was observed at a drain voltage of ~15V in the devices with a GFP and SFP. The step drop behaviour is consistent with the experimental capacitance result, which is attributable to channel depletion under the FP and leads to a significant reduction in *Cgd*.

DC-DC converters with monolithically integrated gate drivers, power transistors and capacitors (Figure 3) were successfully demonstrated. SFP structures were used in the power transistors due to the T-CAD predicted low *Cgd* and an experimentally determined low dynamic *Ron*, compared to structures with a GFP and those with no FP. The power transistor voltage switching waveform of the DC-DC converter with an input voltage of 50V and output current of 50mA is shown in Figure 4(a). Turn on and turn off times (voltage) of 7ns and 6.3ns were measured, respectively. These higher-than-predicted values were due to non-optimised transistor threshold voltages and we expect subsequent iterations to approach the very competitive SPICE modelling results illustrated in Figure 4(b).

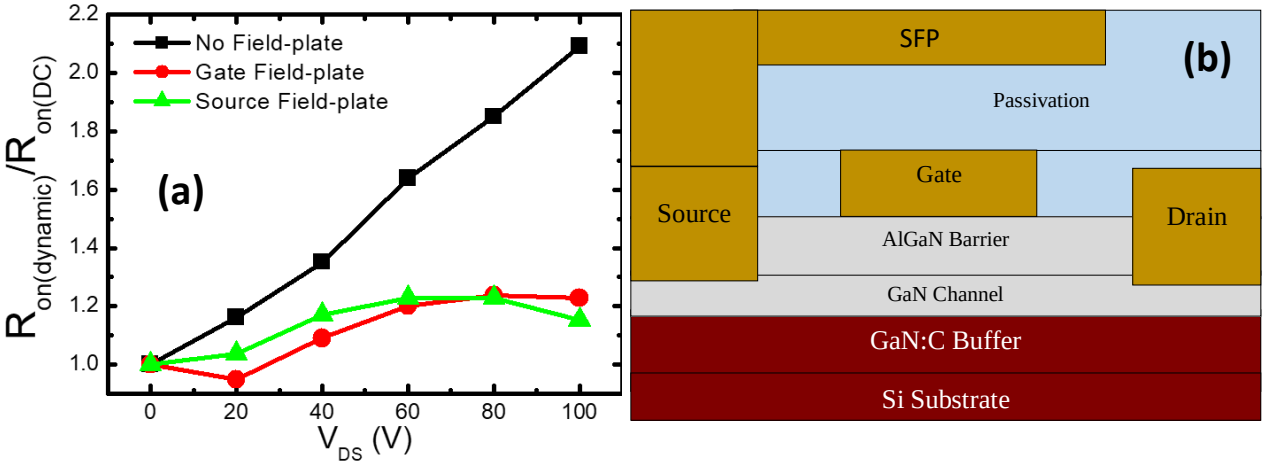

Figure 1: (a) Dynamic *Ron* of AlGaN/GaN HEMTs with different field plate configurations in a function of off-state V_{DS}. (b) Schematic diagram of AlGaN/GaN HEMTs with a SFP.

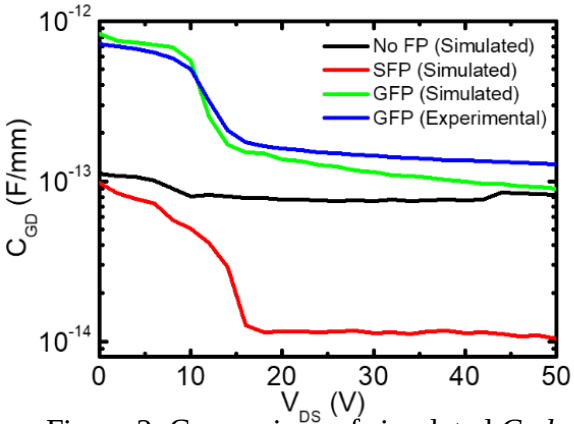

Figure 2: Comparison of simulated *Cgd* of AlGaN/GaN HEMTs with different FP configurations and experimental Cgd.

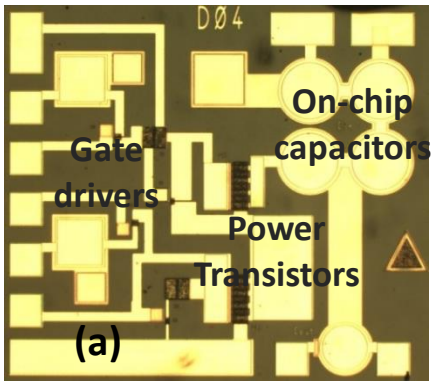

Figure 3: (a) A monolithically integrated DC-DC converter.

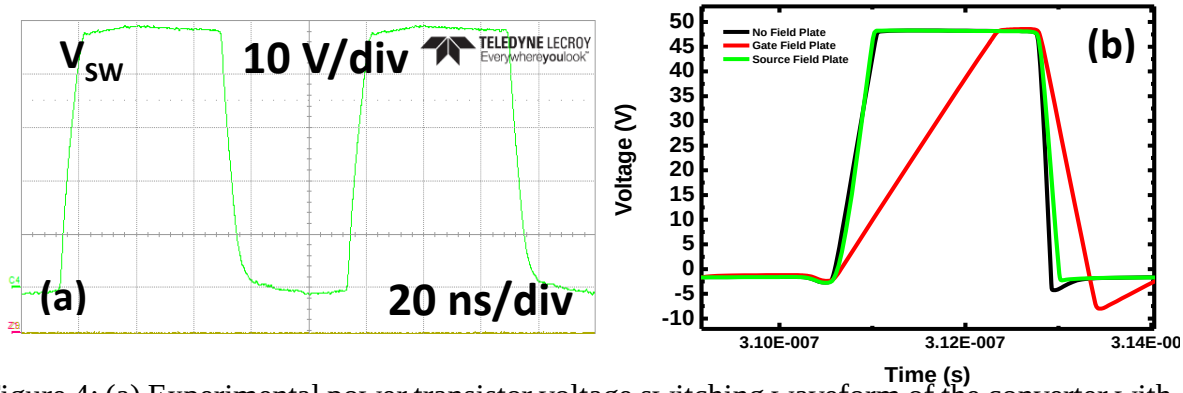

Figure 4: (a) Experimental power transistor voltage switching waveform of the converter with input voltage of 50V and output current of 50mA. (b) Simulated switching waveform of power transistors in the DC-DC converter with different field plate configurations using SPICE.

Reference:

[1] H. Xing, Y. Dora, A. Chini, S. Heikman, S. Keller, U. K. Mishra, IEEE Electron Device Letters, **25**, 161 (2004).

High-Temperature Contact Stability of 2DEG Heater on GaN Membrane for Sensing Applications

B.F. Spiridon[1], A. De Luca[2], A. Eblabla[3], S. Ghosh[1], S.M. Fairclough[1], G. Longobardi[2], K. Elgaid[3], F. Udrea[2], D.J. Wallis[1,3], R.A. Oliver[1]
1. Department of Materials Science and Metallurgy, University of Cambridge, Cambridge, UK
2. Department of Engineering, University of Cambridge, Cambridge, UK
3. Centre for High-Frequency Engineering, Cardiff University, Cardiff, UK

Summary

A custom GaN membrane 2D electron gas (2DEG) heater was designed, fabricated and tested to observe the stability of 2DEG ohmic contacts at elevated temperatures. The contact degradation mechanisms were investigated using electrical resistance monitoring, optical microscopy, scanning electron microscopy (SEM), and energy-dispersive X-ray (EDX) analysis. Asymmetrical heating concentrated at the drain contacts was observed, with contact degradation above 250°C average heater temperature and accelerated degradation and failure above 400°C. The GaN membrane design resulted in enhanced thermal insulation and survived repeated thermal cycling, indicating strong potential for GaN membrane heaters with alternative high-temperature contacts.

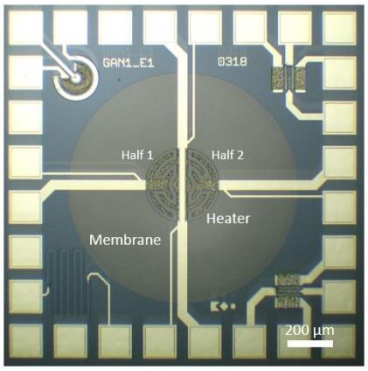

Figure 1. 2DEG membrane heater

Motivation

The rising interest around both GaN as a versatile and robust semiconductor [1] and thermal chemical and physical sensors [2,3] inspired this study of 2DEG heater contacts on a GaN membrane. For instance, GaN technology offers advantages for thermal gas sensors requiring high operating temperatures (for improved sensitivity and recovery time), on-chip driving circuitry and front-end signal amplification. Using a 2DEG resistor as the heater element also mitigates the risk of electromigration inside the heater channel and the use of membrane technology reduces power consumption and start-up times. In this context, the general objective of this study was to understand the feasibility of integrating a membrane heater architecture with GaN-on-Si technology with high electron mobility transistor (HEMT) material stack (AlGaN/GaN) and standard ohmic contact technology (Ti/Al/Ni/Au). These results are useful for informing future GaN heater designs, as well as understanding the range of sensing techniques compatible with standard HEMT contact technology.

Method and results

A custom thermo-electro-mechanical design (Fig. 1) was developed. Commercial GaN-on-Si material (Nexperia, NL) was fabricated into HEMTs using photolithography, followed by substrate thinning and DRIE Si etching to release GaN membranes in half of the samples. The devices were connected to support circuit boards and tested using Keithley instruments under standard laboratory conditions using increasing drive voltages (1h per step). After degradation and partial failure, optical, SEM and EDX analyses provided information regarding the degradation mechanisms. These observations were corroborated with previous Joule heating TCAD simulations.

The results include the temperature coefficient of resistivity of the track metal, the thermal resistance of the membrane setup compared with bulk substrate, observation of track electromigration in parallel-drive configuration, and the apparent concentration of heating at the drain contacts combined with localised passivation damage. Heater resistance was monitored throughout the drive-voltage ramps; slow electrical degradation was noticeable from approximately 250°C and a sudden change was recorded at over 400°C average heater temperature. Metal diffusion from the ohmic contacts along the tracks and into the semiconductor material, together with high-temperature electrical-discharge metal migration were observed and correlated with electrical degradation.

References

[1] H. Amano et al., “The 2018 GaN power electronics roadmap,” J. Phys. D: Appl. Phys., vol. 51, no. 16, p. 163001, 2018
[2] A. De Luca et al., “Diode-based CMOS MEMS thermal flow sensors,” in 2017 19th International Conference on Solid-State Sensors, Actuators and Microsystems (TRANSDUCERS), 2017, pp. 2211–2214.
[3] A. Ranjan et al., “AlGaN/GaN HEMT-based high-sensitive NO2 gas sensors,” Jpn. J. Appl. Phys., vol. 58, no. SC, p. SCCD23, 2019.

Low Field Vertical Charge Transport in AlGaN/GaN – on – Si High Electron Mobility Transistors

Filip Wach[1], Michael J Uren[1], Benoit Bakeroot[2], Steve Stoffels[2], Ming Zhao[2], Stefaan Decoutere[2], Martin Kuball[1]
[1] Centre for Device Thermography and Reliability (CDTR), H. H. Wills Physics Laboratory, University of Bristol, UK
[2] imec 3001 Leuven, Belgium

***Abstract* – Substrate ramps and stepped stress transient measurements are applied to study vertical charge transport mechanisms in GaN-on-Si power HEMTs. We present experimental evidence for 3D variable range hopping taking place in C – doped GaN and 1D hopping along the dislocations in UID GaN. We also observe for the first time a barrier from the dislocations to the 2DEG. Finally, we introduce a novel computational model for simulations of hopping conductivity across reverse biased pn – junction, which shows good agreement with the experiment.**

I. INTRODUCTION

GaN-on-Si power switching HEMTs offer dramatic improvements in efficiency and module volume, however they are vulnerable to buffer trapping related dynamic R_{ON} which limits the performance. It has been shown that suppression of dynamic R_{ON} requires controlled vertical leakage through the epitaxial stack [1], however there is remarkably little information available on the transport mechanism.

Here for the first time we report low-field vertical transport measurements in the regime relevant to dynamic R_{ON} undertaken in state-of-the-art HEMTs. We show that the transport is consistent with 3D variable range hopping in a defect band in the carbon doped layer, and 1D hopping along dislocations in the critical undoped channel layer, with a previously unrecognised barrier to the 2DEG. We model the transport and demonstrate how this can be implemented in a TCAD simulation.

Uren et al. proposed band-to-band leakage across UID GaN as potential mechanism for R_{ON} suppression [2] which was later identified as variable range hopping in pn – diodes by *Moroz et al* [3]. However, if the GaN buffer is doped with C exceeding 10^{19} cm^{-3}, it has been suggested the vertical transport occurs via the defect band and not by activation to the valence band as in case of lower C concentrations [4].

II. RESULTS AND DISSCUSION

This study was performed on ungated Ohmic structures consisting of a GaN–on–Si epitaxy architecture with AlGaN/GaN superlattice strain relief layer (SRL), C-doped GaN buffer (GaN:C), UID GaN channel and AlGaN barrier (Figure 1).

Substrate ramps were performed on the sample to investigate charge transport mechanisms in the buffer (Figure 2). In addition, substrate stress transient measurements were conducted, in which the substrate bias is switched rapidly (~10 µs) between two specific bias points (V_i, V_f), which allowed for clear separation of transport processes taking place in UID and GaN:C.

The transients measured for bidirectional voltage steps of constant potential difference ($V_i \leftrightarrow V_f$) show reversibility in case of C – doped GaN, suggesting constant resistivity of this layer (Figure 2b). The difference in the time constants between forward and reverse steps indicates a non-ohmic transport through the UID GaN. Comparison of (V_i, V_f) forward steps taken at increasing voltages reveals reduction in UID GaN resistivity with applied bias (Figure 3).

Temperature dependence of vertical leakage was evaluated using most likely theoretical models, demonstrating 1D hopping along dislocations as the mechanism responsible for charge transport through UID GaN (Figure 4a), whilst 3D variable range hopping through defect band best describes charge redistribution across GaN:C (Figure 4b). Evaluation of field dependence reveals an activation barrier for the charges entering 2DEG from the dislocations (Figure 5a), with the activation energy decreasing linearly with applied voltage.

Based on our analysis the 1D hopping model was implemented in a commercial TCAD simulator and applied to full transistor as seen in Figure 1.

IV. CONCLUSION

In summary, temperature and field dependent measurements of GaN-on-Si HEMT were performed to investigate transport mechanisms through the epitaxy at fields significantly below breakdown. 1D variable range hopping was identified as the dominant charge transport mechanism through UID GaN with activation barrier restricting charges from entering the 2DEG. Transport through GaN:C appears to involve 3D hopping conductivity likely via a defect band. Finally, a novel computational model for simulation of leakage across reverse biased pn – junction is presented, showing very good qualitative agreement with the experiment.

REFERENCES

[1] M. J. Uren, et al., *IEEE Transactions on Electron Devices*, vol. 64, pp. 2826-2834, 2017.
[2] M. J. Uren, et al. *IEEE Electron Device Letters* 35.3 (2014): 327-329.

[3] V. Moroz, et al. ECS *Journal of Solid State Science and Technology* 5.4 (2016): 3142-3148.
[4] Koller, Christian, et al. *IEEE Transactions on Electron Devices* 65.12 (2018): 5314-5321

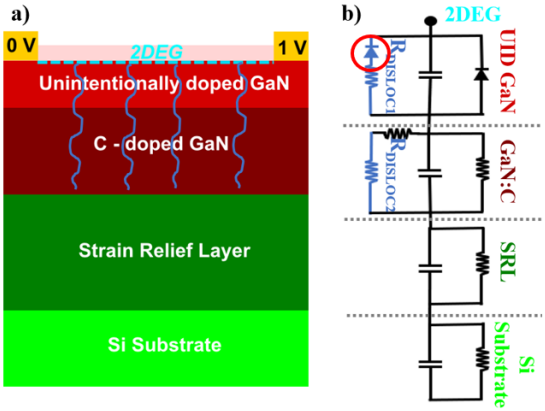

Figure 1: a) Diagram of the ungated HEMT used in this study. b) 1D lump element diagram of the epitaxial stack including dislocations (blue) across GaN layers; proposed new activation barrier circled red.

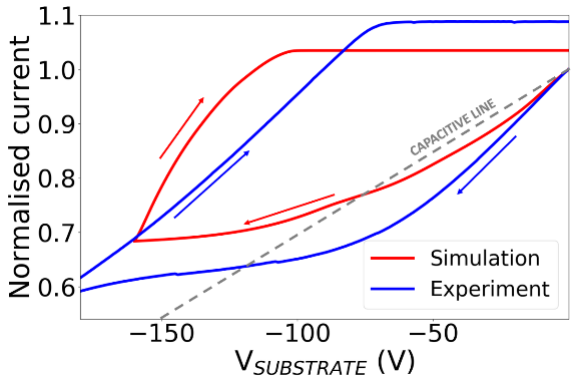

Figure 2: Normalized drain current as a function of applied substrate bias; experiment and simulation.

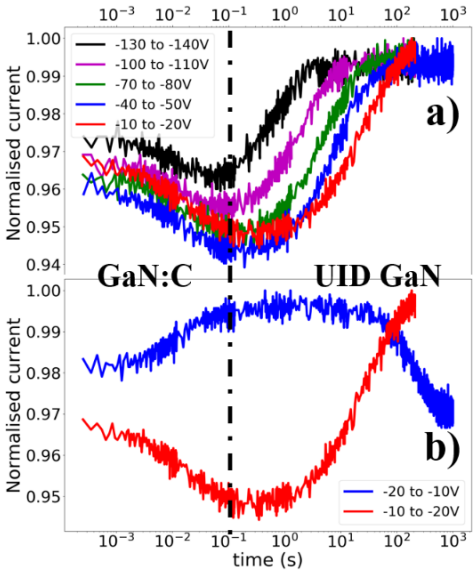

Figure 3: a) Normalized drain current as a function of time for a range of (V_i, V_f) bias points of constant potential difference. b) Transients for bidirectional step (V_i=-10↔V_f=-20).

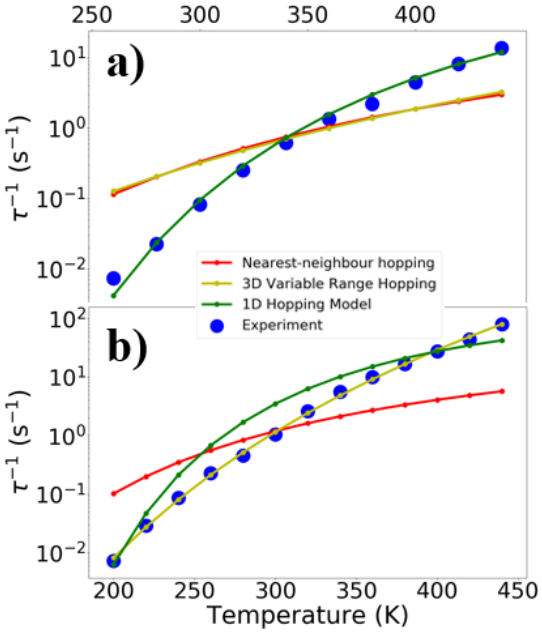

Figure 4: Inverse time constant as a function of temperature for a) UID GaN at -140 V, b) GaN:C at -10 V with different theoretical transport mechanisms fitted to data.

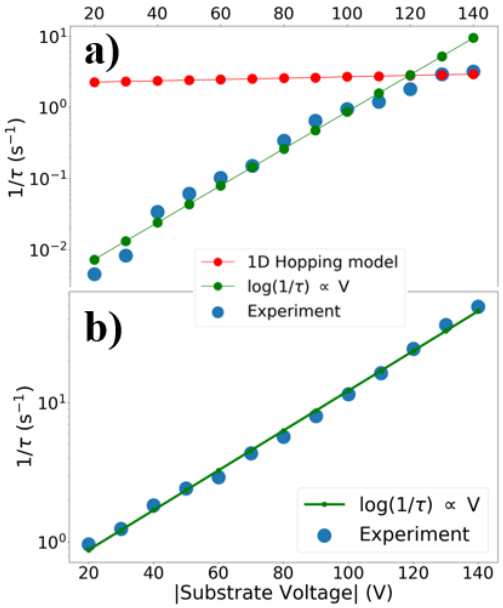

Figure 5: Inverse time constant as a function of temperature for a) UID GaN and b) GaN:C.

Study of drain injected breakdown mechanisms in AlGaN/GaN-on-SiC HEMTs

F. Yang[1], M. Singh[1], M. J. Uren[1], H. Hirshy[2], P. J. Tasker[2], T. Martin[3] and M. Kuball[1]
[1]Centre for Device Thermography and Reliability, School of Physics, University of Bristol, U.K.
[2]Centre for High Frequency Engineering, Cardiff University, U.K.
[3]IQE Europe, St Mellons, Cardiff, U.K.

In this study, we use the drain-current injection technique combined with simulation and electroluminescence (EL) measurements to investigate the breakdown mechanism in AlGaN/GaN-on-SiC HEMTs. We demonstrate that there are two steps in the breakdown process present in our devices. Through measurement and modelling we show that the first step is mainly due to punch-through within the buffer and the second step is due to localized strong impact ionization occurring near the gate edge, which eventually results in avalanche breakdown.

Several breakdown mechanisms have been reported for the different regions of HEMTs. Uren et al. [1] showed that an increase in drain current at high drain voltages during OFF-state can be ascribed to punch-through effects. By using drain-current injection technique, Wang et al. [2] suggested that the source/gate injection through the buffer can also induce impact ionization and cause a breakdown in AlGaN/GaN HEMTs. Shankar et al. [3] found that localized avalanche instability under high voltage stress can lead to localized thermally induced failure. In our work, we report a two-step breakdown with successively punch-through and then avalanche.

The device under test has a GaN-on-SiC structure with Fe doped buffer. The previous study has suggested that it suffered from the "kink" effect in static I-V characteristics due to buffer trapping [4]. In this work, we force a constant drain injection current and measure the drain voltage as we sweep the gate voltage from 0 V to -10 V. Fig. 1 shows the measured drain voltage as a function of gate bias for I_D changing from 1 nA to 500 µA. At low drain current (I_D < 1 µA), the drain voltage appears to be negligible since resistive leakage to the gate is sufficient to absorb the drain injection. At high drain current ($I_D \geq$ 100 µA), the results show there are two steps of drain voltage change. The first step appears when V_{GS} = -3 V and the second step appears when V_{GS} = -7 V. Electroluminescence measurements have been performed on the same devices as shown in Fig. 2. In the first step, when V_{GS} = -4 V and -6 V, we observe uniform EL intensity distribution along most of the gate finger. However, when V_{GS} < -7 V, localized bright spots appear in the middle of the gate finger.

2D-TCAD simulation has been implemented to help to interpret our measurement results. A structure with the same device dimension as well as the same doping profile has been constructed in Silvaco ATLAS. Impact ionization has been implemented in this simulation. As shown in Fig. 3 (a), when the channel under the gate is fully depleted, a punch-through current can be found within the UID GaN. Under this condition, only weak impact ionization is present near the gate edge where the electric field reaches its maximum value and it results in small gate leakage current, which corresponds to the uniform EL distribution we measured. In Fig. 3 (b), when V_{GS} = -10 V, the trace of punch-through current is pushed down further and the conducting hole current path to the gate becomes comparable to the punch-through current (labelled as "gate leakage" in Fig. (b)). This result is consistent with the gate leakage current we measured (not shown). However, the simulation does not show a clear second step. That is because we assume the device has uniform properties along the gate finger, whereas the EL results reveal that the origin of the second step is associated with localized current flow. It is known that a positive feedback process can result in current filamentation [5]; the observation of an increase in gate current together with the observation of EL hotspots is excellent evidence for the onset of impact ionization induced avalanche breakdown.

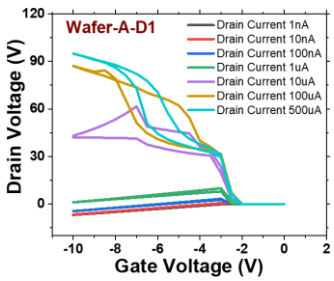

Fig. 1. Shows measured drain voltage for range of I_D bias changing from 1 nA up to 500 µA.

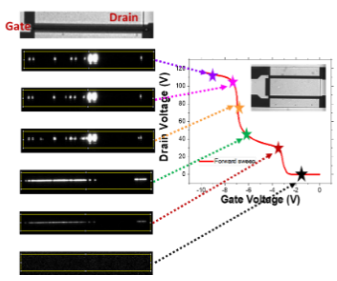

Fig. 2. Measured EL intensity for range of Vgs bias from 0 V down to -10 V. ID = 500 µA

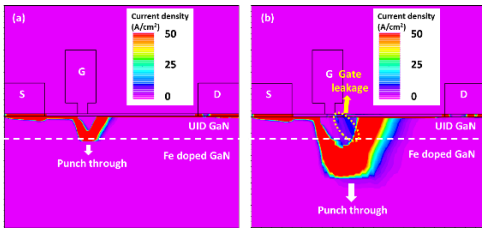

Fig. 3. Shows the simulated current density distribution under 2 different conditions. (a) V_{GS} = -3 V, I_D = 500 µA and (b) V_{GS} = -10 V, I_D = 500 µA.

References:

[1] M. J. Uren *et al.*, *IEEE Trans. Electron Devices*, vol. 53, no. 2, pp. 395–398, 2006.
[2] M. Wang *et al.*, *IEEE Trans. Electron Devices*, vol. 57, no. 7, pp. 1492–1496, 2010.
[3] B. Shankar *et al.*, *IEEE Trans. Electron Devices*, vol. 66, no. 8, pp. 3433–3440, 2019.
[4] M. Singh *et al.*, *IEEE Trans. Electron Devices*, vol. 65, no. 9, pp. 3746–3753, 2018.
[5] C. Koller *et al.*, *physica status solidi (b)*, vol. 1800527, pp. 1–8, 2019.

11.30-12.30: Session 5 – Systems and applications
Chairs: David Binks

11.30-11.45: *Gallium Nitride: a versatile compound semiconductor as novel piezoelectric film for acoustic tweezer in manipulation of cancer cells*

Chao Sun[1,2], Fangda Wu[2], David J. Wallis[2,3], Ming Hong Shen[4], Fan Yuan[5], Jian Yang[4], Jianzhong Wu[2], Zhihua Xie[6], Dongfang Liang[7], Hanlin Wang[2], Rowan Tickle[2], Roman Mikhaylov[2], Aled Clayton[8], You Zhou[9], Zhenlin Wu[10], Yongqing Fu[11], Wenpeng Xun[12], Xin Yang[2]

[1] School of Life Sciences, Northwestern Polytechnical University, 710072, P.R. China
[2] Department of Electrical and Electronic Engineering, School of Engineering, Cardiff University, CF24 3AA, UK
[3] Department of Materials Science and Metallurgy, University of Cambridge, Cambridge CB3 0FS, UK
[4] Preclinical Studies of Renal Tumours Group, Division of Cancer and Genetics, School of Medicine, Cardiff University, CF14 4XN, UK
[5] Department of Biomedical Engineering, School of Engineering, Duke University, NC 27708-0281, USA
[6] Department of Civil Engineering, School of Engineering, Cardiff University, CF24 3AA, UK
[7] Department of Engineering, University of Cambridge, Trumpington St, Cambridge CB2 1PZ, UK
[8] Tissue Microenvironment Group, Division of Cancer & Genetics, School of Medicine, Cardiff University, Cardiff, CF14 4XN, UK
[9] Systems Immunity University Research Institute and Division of Infection and Immunity, School of Medicine, Cardiff University, Cardiff, CF14 4XN, UK
[10] School of Optoelectronic Engineering and Instrumentation Science, Dalian University of Technology, 116023, P.R. China
[11] Faculty of Engineering and Environment, Northumbria University, Newcastle Upon Tyne, NE1 8ST, UK
[12] Department of Mechanical Engineering, Northwestern Polytechnical University, 710072, P.R. China

11.45-12.00: *Gb/s Underwater Wireless Optical Communications using micro-LEDs*

Georgios N. Arvanitakis[1], Jonathan J.D. McKendry[1], Rui Bian[2], Chen Cheng[2], Enyuan Xie[1], Xiangyu He[1], Gang Yang[3], Mohamed S. Islim[2], Ardimas A. Purwita[2], Erdan Gu[1], Harald Haas[2], Martin D. Dawson[1]

[1] Institute of Photonics, Department of Physics, SUPA, University of Strathclyde, Glasgow, G1 1RD, UK
[2] Li–Fi R&D Centre, Institute for Digital Communications, King's Buildings, University of Edinburgh, Edinburgh, EH9 3JL, UK
[3] Institute of Marine Optoelectronic Equipment, Harbin Institute of Technology at WeiHai, WeiHai 264209, China

12.00-12.15: *Hybrid GaN microLED platform for fluorescence sensing*
F. Farrell[1,2], N. Bruce[1,2], X. He[1], E. Xie[1], A.-M. Haughey[2], E. Gu[1], M. D. Dawson[1], N. Laurand[1]

[1] Institute of Photonics, Department of Physics, University of Strathclyde, Glasgow, G1 1RD, UK
[2] Fraunhofer Centre for Applied Photonics, 99 George St, Glasgow G1 1RD, UK

12.15-12.30: *Superior performance metal- semiconductor-metal photodiode on non-polar (11-20) GaN with patterned (110) silicon*
Y. Cai, S Shen, X. Zhao, C. Zhu, J. Bai, T. Wang

Department of Electronic and Electrical Engineering, University of Sheffield, Sheffield, S1 3JD

12.30-12.45 *Transfer printing integration of GaN micro-LEDs on CMOS*
Jose F. C. Carreira[1], Alexander D. Griffiths[1], Enyuan Xie[1], Benoit J. E. Guilhabert[1], Johannes Herrnsdorf[1], Robert K. Henderson[2], Erdan Gu[1], Michael J. Strain[1], Martin D. Dawson[1]

[1] Institute of Photonics, Department of Physics, University of Strathclyde, Glasgow, G1 1RD, UK
[2] Joint Research Institute for Integrated Systems University of Edinburgh, Edinburgh, UK

12.45-14.00: Lunch and Poster Session

Abstract
Gallium nitride (GaN) is a compound semiconductor lying at the crossroad where piezoelectric, pyroelectric, and piezo-resistive properties meet, which has its advantages to generate new functionalities and applications. Recently, surface acoustic wave (SAW) based acoustic tweezers were developed as an efficient and versatile tool to manipulate nano- and micro- particles aiming for patterning, separating and mixing biological and chemical components. Conventional materials to make SAW devices such as lithium niobate suffers from being brittle and incapable of highly integrating into multiphysical platform. This work piloted the development of a GaN-based Acoustic Tweezer (GaNAT) and the application in manipulating micro-particles and cells. For the first time, the GaN SAW device was integrated with a microfluidic channel to form an acoustofluidic functional chip for biological application. The GaNAT demonstrated the ability to work on high power (up to 10W) with minimal cooling while maintaining the device temperature below 33°C. The acoustofluidic modelling was successfully applied to numerically study and predict the acoustic pressure field and particle trajectories within the GaNAT. The model was tested by using polystyrene microspheres, fibroblast and renal tumour cells, which denoted a good agreement to actuate particles to aggregate at pressure nodes while maintaining high cell viabilities.

Gb/s Underwater Wireless Optical Communications using micro-LEDs

Georgios N. Arvanitakis[1], Jonathan J.D. McKendry[1], Rui Bian[2], Chen Cheng[2], Enyuan Xie[1], Xiangyu He[1], Gang Yang[3], Mohamed S. Islim[2], Ardimas A. Purwita[2], Erdan Gu[1], Harald Haas[2] and Martin D. Dawson[1]

[1] Institute of Photonics, Department of Physics, SUPA, University of Strathclyde, Glasgow, UK, G1 1RD
[2] Li–Fi R&D Centre, Institute for Digital Communications, King's Buildings, University of Edinburgh, Edinburgh, UK, EH9 3JL
[3] Institute of Marine Optoelectronic Equipment, Harbin Institute of Technology at WeiHai, WeiHai 264209, China

A large number of scientific, industrial and military activities in subsea environments increasingly require the transfer of large volumes of data. For example, the deployment of unmanned (UUVs), autonomous (AUVs) and remotely-operated vehicles (ROVs) for capturing high-resolution images or high-definition videos for oceanographic surveying, or the monitoring, control and maintenance of underwater oil and gas infrastructure, requires the establishment of high-speed underwater wireless links. These would be invaluable for subsea data transfer and communications from underwater vehicles to surface vessels as tethered links are often impractical and expensive due to the challenging underwater environment.

Visible light communications are an attractive complement to traditional acoustic and radio frequency (RF) methods. Underwater acoustic signals, despite their long range (tens of km [1]), suffer from high latency and low data rates (tens of kb/s). RF communications, although widely deployed in free-space, are limited underwater to sub-meter range for data rates up to Mb/s [2], as electromagnetic waves at these frequencies are strongly attenuated by seawater's conductivity. On the other hand, light sources operating at visible wavelengths, where water exhibits its lowest overall attenuation, enable high-speed transmission over tens of meters. For instance, Li *et al*. used vertical-cavity surface-emitting lasers (VCSEL) to demonstrate data rate of 25 Gb/s for 5 m [3]. Using light-emitting diodes (LEDs), Zhou *et al.* reported 15.17 Gb/s over 1.2 m of tap water [4], while 2.28 Mb/s were demonstrated by Doniec *et al.* over 50 m [5].

Here, we report recent advances in using bespoke high-bandwidth series-connected GaN micro-LEDs to demonstrate underwater communications at Gb/s rates. It has been established that as the active area of an LED reduces (< 100 µm, a "micro-LED"), the -3 dB modulation bandwidth increases up to hundreds of MHz [6] compared to a few tens of MHz for a typical off-the-shelf LED, as the device bandwidth is no longer limited by a large resistance-capacitance (RC) constant. These high bandwidths have allowed single micro-LEDs to optically transmit data at multi-Gb/s data over air [7]. Although visible wavelengths experience less attenuation in sea water than RF signals, strong attenuation can still take place due to scattering and absorption, especially in turbid waters. Therefore, for the establishment of an underwater communication channel in turbid waters, a single micro-LED may be insufficient due to its low output power (< 5 mW) and high channel loss. In order to mitigate this, a series-connected micro-LED array has been deployed in this work, consisting of 6 micro-LED pixels connected together in series and emitting with a peak wavelength of 450 nm. This configuration increases the available output power (> 20 mW) while retaining a high modulation bandwidth (> 330 MHz). Using the orthogonal frequency division multiplexing (OFDM) modulation scheme, a wireless data rate up to 4.92 Gb/s was obtained over 1.5 m and 3.4 Gb/s through 4.5 m of clear tap water. Furthermore, by adding a scattering agent to clear tap water, data rates ranging from 15 Mb/s over 5.33 attenuation lengths for 1.5 m to 170 Mb/s over 4.05 attenuation lengths for 4 m were achieved. These results demonstrate the potential of micro-LEDs to enable high-speed underwater wireless communications over meter ranges in clear and turbid water. They also highlight the importance of the specific LED format for optical performance.

[1] E. M. Sozer, M. Stojanovic, and J. G. Proakis, "Underwater Acoustic Networks," *IEEE J. Ocean. Eng.*, vol. 25, no. 1, pp. 72–83, 2000.
[2] P. Lacovara, "High-Bandwidth Underwater Communications," *Mar. Technol. Soc. J.*, vol. 42, no. 1, pp. 93–102, 2008.
[3] C. Y. Li *et al.*, "A 5 m/25 Gbps Underwater Wireless Optical Communication System," *IEEE Photonics J.*, vol. 10, no. 3, 2018.
[4] Y. Zhou *et al.*, "Common-anode LED on Si substrate for beyond 15 Gbit/s underwater visible light communication," *Photonics Res.*, vol. 7, no. 9, 2019.
[5] M. Doniec and D. Rus, "BiDirectional optical communication with AquaOptical II," *12th IEEE Int. Conf. Commun. Syst. 2010, ICCS 2010*, pp. 390–394, 2010.
[6] R. X. G. Ferreira *et al.*, "High Bandwidth GaN-Based Micro-LEDs for Multi-Gb/s Visible Light Communications," *IEEE Photonics Technol. Lett.*, vol. 28, no. 19, pp. 2023–2026, 2016.
[7] M. S. Islim *et al.*, "Towards 10 Gb/s orthogonal frequency division multiplexing-based visible light communication using a GaN violet micro-LED," *Photonics Res.*, vol. 5, no. 2, p. A35, 2017.

Hybrid GaN microLED platform for fluorescence sensing

F. Farrell,[1,2] N. Bruce,[1,2] X. He, E. Xie,[1] A.-M. Haughey,[2] E. Gu,[1] M. D. Dawson[1] and N. Laurand[1]

[1]*Institute of Photonics, Department of Physics, University of Strathclyde, Glasgow, G1 1RD, UK*

[2]*Fraunhofer Centre for Applied Photonics, 99 George St, Glasgow G1 1RD, UK*

Abstract - **A hybrid GaN µLED platform developed for wearable illumination is adapted here for fluorescence sensing. Proof-of-principle detection of colloidal quantum dots down to 80 pM using a mobile phone camera is demonstrated.**

Mechanically-flexible and wearable photonics have many applications including for novel forms of displays, illuminating safety clothing, and health technology [1, 2]. In this context, we have been working on a light emitting, mechanically flexible device for area illumination at wavelengths in the UV and visible [3]. Our device consists of an array of µLEDs combined with a polydimethylsiloxane (PDMS) slab waveguide structure (Fig. 1). PDMS is a biocompatible elastomer, often employed in microfluidics, and can be made mechanically flexible. Light from the µLED device is guided within the PDMS by total internal reflection, and by incorporating light diffracting and/or colour converting structures within the platform it is possible to obtain homogenous area illumination at different wavelengths as shown in Figs. 1a and 1b. Herein, we adapt this hybrid µLED device platform and demonstrate its capability for fluorescence sensing.

Fluorescence is a well-established biochemical sensing technique used for diagnostics. It is typically based on biomolecular processes whereby analytes are captured on a surface and coupled to fluorescent tags. The latter are then excited using a laser or LEDs and the resulting fluorescence is measured to assess the presence and amount of analytes. The approach taken here is based on total internal reflection fluorescence (TIRF) [4]. As light from the µLEDs is waveguided in the PDMS, an evanescent wave is formed near the PDMS interface. This evanescent wave probes the region very near (<100nm) the surface of the PDMS guide and therefore triggers fluorescence only if a label is in this region (Fig. 2a). In turn, TIRF sensing mitigates the issue of autofluorescence that can otherwise be a severe source of noise. The main advantage of the GaN microLED TIRF platform reported here compared to other implementation lies in its potential for small form, low-power instrumentation.

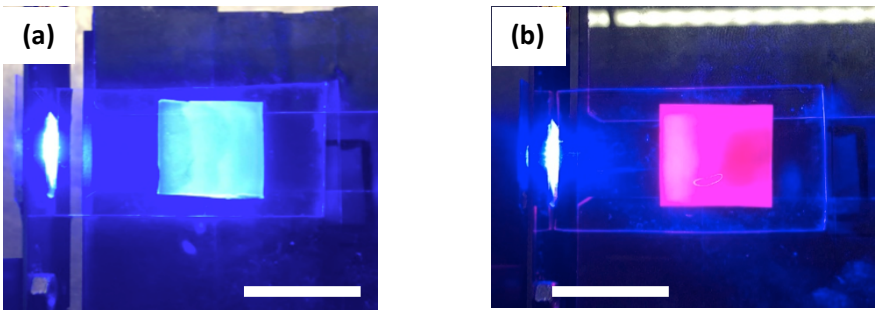

Fig. 1 Photographs of the top of the hybrid microLED/elastomeric platform showing homogeneous (a) blue illumination and (b) red illumination through colour conversion. The scale bars are 1.5 cm.

For the demonstration, the µLED consisted of 10 pixels in parallel, each 100 x 100 µm^2 and separated by 720 µm, as depicted in the inset of Fig. 2b, which otherwise summarizes the device optoelectronic characteristics. The device has a turn-on voltage of 2.6 V. For the fluorescence experiments it is ran at a current of 120 mA producing a total output optical power of 10 mW for a peak wavelength of 445 nm. The PDMS membrane (40 x 20 x 1 mm^3) was edge-coupled to the µLED and the imaging system consisted only of a long-pass filter and a phone camera. For the proof of principle experiment, we have used colloidal quantum dots (CQDs) as fluoresent labels (630nm-emitting CdSSe/ZnS, 6nm

mean diameter). Multiple concentrations were obtained by diluting the CQDs in toluene. 2 µL of these different CQD concentrations were drop-coated onto the PDMS waveguide slab. The toluene was then allowed to evaporate in air leaving on the PDMS surface CQD molar concentrations ranging from 770 nM down to picomolar level for reproducibility and limit of detection (LOD) experiments. The same experiments were also conducted with water-soluble CQDs and led to similar results.

Fig. 2c is an image of the PDMS surface with CQD labels taken (at an angle) with the phone camera. The camera settings for measurements were: ISO 800, exposure time 250 ms and 2x zoom. The corresponding pixel noise was 2.1+/-0.8 (relative intensity units). The pixel data from the phone camera was post-processed using Matlab to produce an intensity map (not shown) and a plot of fluoresence intensity versus concentration (Fig 2d). Based on results from the latter and from the noise floor of the system, the LOD of the CQDs is found to be below 80 pM. This is lower than the few nM LOD reported in [5] that used direct CQD excitation, and even lower LOD may be possible.

In summary, we have demonstrated the concept of a fluoresent sensor based on a hybrid µLED/PDMS platform. The detection uses a simple mobile phone (with the addition of a filter). The next steps include bioassay detection but these preliminary results shows the versatility of this GaN µLED platform and its potential for low-cost, low power and small format bio-instrumentation.

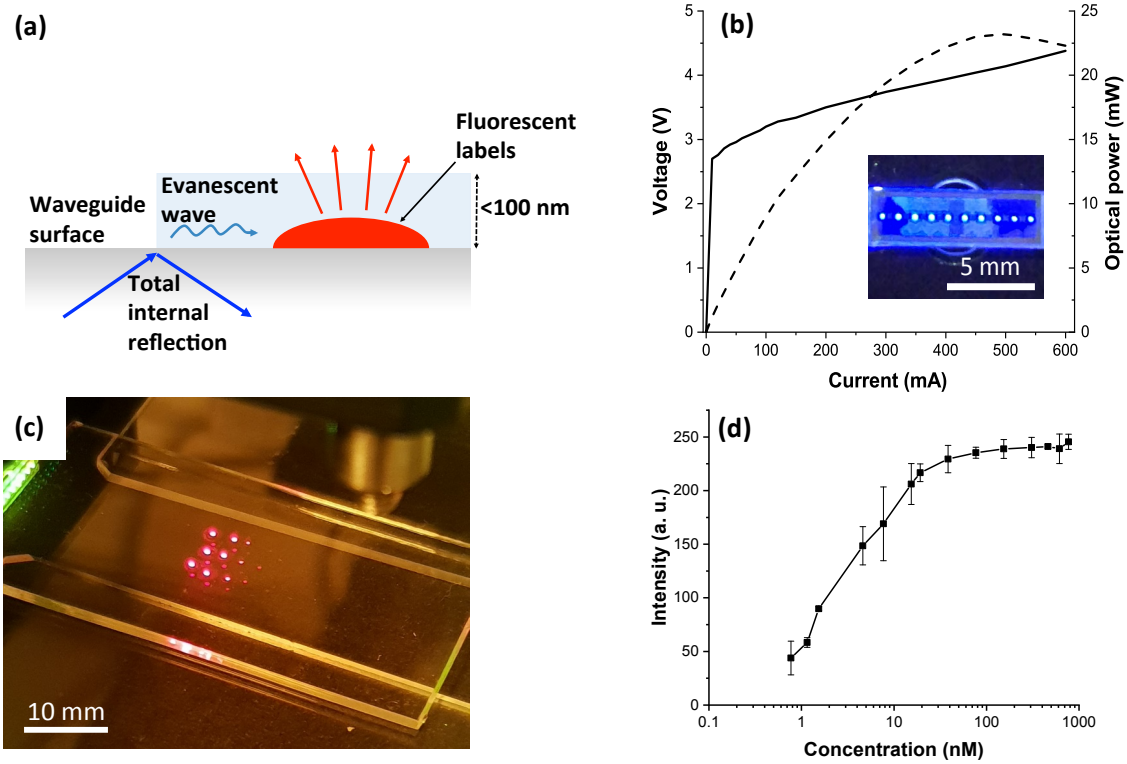

Fig. 2 (a) Schematic of TIRF sensing; (b) electrical and optical characteristics of the LED device, and (inset) photograph of the array; (c) mobile phone picture of the platform showing the red CQD fluorescence; (d) mean pixel intensity versus quantum dot concentration.

This work was partly supported by the EPSRC grant EP/L015595/1 and the MRC Confidence in Concept award (HTAF) MC_PC_17161.

[1] J. Hu et al, *Optical Materials Express*, 2013, 3, 1313-1331.
[2] B M Qaundt et al, *Biomedical Optics Express*, 2017, 8, 4316-4330.
[3] F. Farrell et al., *41st Annual International Conference of the IEEE Engineering in Medicine and Biology Society (EMBC)*, Berlin, Germany, 2019, pp. 67-70.
[4] C. Rowe Taitt et al., *Biosens. Bioelectron.*, vol. 15, no. 76, pp 103-112, 2016.
[5] E. Petryayeva and WR. Algar, Anal. Bioanal. Chem. 408 2913–25, 2016

Superior performance metal- semiconductor-metal photodiode on non-polar (11-20) GaN with patterned (110) silicon

Y Cai, S Shen, X Zhao, C Zhu, J Bai and T Wang *
Department of Electronic and Electrical Engineering, University of Sheffield, Sheffield, S1 3JD
* E-mail: t.wang@sheffield.ac.uk

There is an increasing demand of developing ultra-violet (UV) photodetectors, which can find a wide range of applications in space communications, flame sensors, atmospheric ozone detection, bio-photonics, etc. Given the direct bandgap structure of GaN with its bandgap (3.4 eV) in the ultraviolet spectral range, it is expected that GaN based UV photodetectors can exhibit superior performance to Si based photodetectors (with an indirect band structure and 1.1 eV bandgap) in the UV region. Unlike c-plane GaN based UV photodetectors which exhibit inherent polarisation, nonpolar GaN photodetectors without the inherent polarisation issue potentially exhibit much higher efficiency and much faster response than their c-plane counterparts, thus attracting intense intention in the recent years. However, a number of major challenges will have to be overcome in order to achieve nonpolar GaN with high crystal quality on silicon, the industry-compatible substrates, such as Ga melt-back, crystal quality, etc.

In this paper, we have demonstrated cracking-free and stripe arrayed non-polar (11-22) GaN with a step change in crystal quality on patterned (110) silicon. A two-step growth approach by metalorganic vapour-phase epitaxy (MOVPE) has been employed for the selective growth. Based on the high quality nonpolar GaN with the stripe configuration, which is particularly important for a photodetector, a metal-semiconductor-metal photodiode (MSM-PD) with interdigitated fingers, have been fabricated, demonstrating superior performance compared with the state-of-the-art.

Figure 1a shows a typical cross-sectional SEM image of our (11-20) GaN, exhibiting that the overgrowth initiates on the exposed (1-11) facet only, followed by the growth extending over the SiO_2 masks and then the formation of regualayly array stripes. There is no any Ga melting-back etching observed. Crystal quality of non-polar GaN has been characterized by X-ray diffraction (XRD). The full widths at half maximum (FWHM) of XRD rocking curves along the c and the m direction are 325 and 380 arcsec, respectively, as shown in **Figure 1b**, which are among the best reports. Low temperature photoluminescence (PL) measurements have been performed (not shown), indicating that the density of basal stacking faults (BSF) has been reduced to an almost invisible level. A MSM-PD with an active area of 284x393 μm^2 and a finger spacing of 30 µm has been fabricated on the high quality non-polar GaN. **Figure 1c** shows a responsivity of 484.53 A/W at 1V bias under 325 nm illumination, which is 5 order magnitude higher than its c-plane counterpart fabricated and measured under identical conditions. The response time has been measured with a modulated UV-LED light source at 1 kHz as shown in **Figure 1d**, exhibiting a fast response with a rise time of 58 µs and a fall time of 295 µs, which are much faster than those reported by any other GaN MSM-PDs. These record high MSM-PD performances can be attributed to the significantly improved crystal quality. It is worth highlight that nonpolar GaN is very promising candidate for UV detection applications.

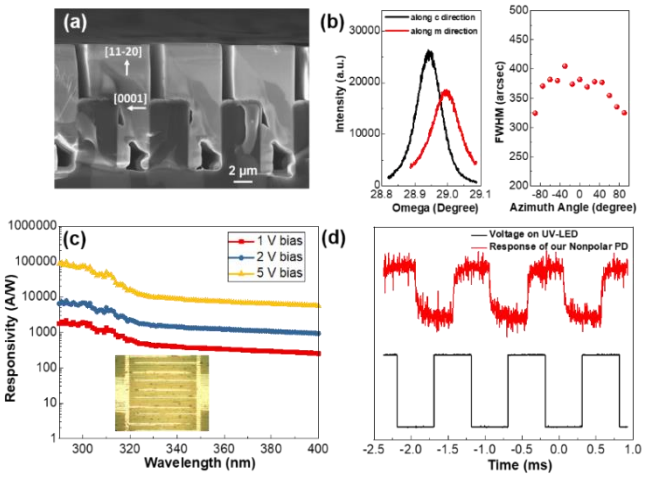

Fig. 1: (a) Cross-sectional SEM of (11-20) GaN on (110) Si; (b) XRD rocking curve and FWHM measured as a function of azimuth angle; (c) Responsivity of nonpolar Photodiode and Inset: Photodiode microscope image; (d) Response waveforms under a modulated UV-LED illumination.

Transfer printing integration of GaN micro-LEDs on CMOS

José F. C. Carreira[1*], Alexander D. Griffiths[1], Enyuan Xie[1], Benoit J. E. Guilhabert[1], Johannes Herrnsdorf[1], Robert K. Henderson[2], Erdan Gu[1], Michael J. Strain[1], and Martin D. Dawson[1]

[1] Institute of Photonics, Department of Physics, University of Strathclyde, Glasgow, G1 1RD, UK
[2] Joint Research Institute for Integrated Systems University of Edinburgh, Edinburgh, UK
*Corresponding author: *jose.correia-carreira@strath.ac.uk*

Arrays of GaN-based micron-sized light emitting diodes (micro-LEDs or µLEDs) on sapphire substrates can be directly integrated with their electronic drive chips using standard flip-chip bonding processes [1] producing individually addressable, high speed sources for visible light communications (VLC) [2] in compact, chip-scale systems. However, flip-chip integration can result in issues with uniformity in the emission from large arrays due to the bump bonding process, and multiple reflection paths within the substrate can lead to cross-talk between pixels. Furthermore, flip-chip bonding is not suitable in cases where the device emission, or detection, wavelength is absorbed by the flipped substrate.

In this work, we present the integration of GaN-based micro-LED devices directly onto silicon (Si)-CMOS drive chips by micro-transfer printing (µTP). This technique allows the population of the host substrate with devices only where required, removing issues associated with a flip-chipped substrate. For this purpose, top-emitting micro-LED platelets (100x100 µm^2 mesa size and 6.5x10^{-5} cm^2 active area) were fabricated from commercial InGaN epistructures, grown on a Si 111-oriented substrate, following previously reported microfabrication procedures [3]. The CMOS chip (Fig. 1(a)) was implemented in standard 0.35 µm CMOS technology and consists of a 16x16 array of individually-controllable 100x100 µm^2 p-MOS driver cells (highlighted by the red square) [2] and a single photon avalanche diode (SPAD - shown in detail in Fig. 1(b)). An 8x8 array of micro-LEDs was sequentially transfer printed directly, without any adhesion enhancement layer, onto the CMOS chip (Fig. 1(c)). Figure 1(d) shows, in further detail, the micro-LED p-GaN electrical contact through the adjacent p-MOS driver. A schematic cross-sectional drawing of a micro-LED directly printed onto to the CMOS is shown in Fig. 1(e).

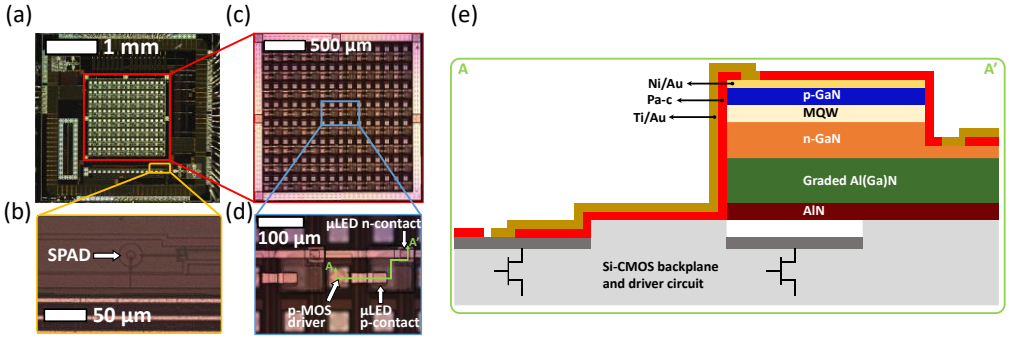

Figure 1: (a) Optical image of the CMOS chip with the micro-LED driving area and SPAD identified in red and yellow, respectively; (b) magnification showing in further detail the SPAD active area; (c) magnification of the CMOS chip showing the 8x8 array of transfer printed micro-LEDs; (d) shows, in further detail, the micro-LED p-GaN electrical contact through the adjacent p-MOS driver; (e) schematic cross-section drawing of a micro-LED directly printed onto to the CMOS.

The micro-LED array displayed excellent uniformity both in brightness and modulation performance across the full array. An optical camera communications (OCC) link is

demonstrated using spatio-temporal modulation of the array [4] and an ultrafast camera receiver (8000 fps). A 128 kbps link, below the 3.8×10^{-3} bit-error-ratio (BER) limit for forward error correction (FEC), is established at received power values larger than 0.02 µW (Fig. 2(a)). Figures 2(b1)-(b4) shows selected captured frames from the 8000 fps ultrafast camera video for all active micro-LEDs, alignment conditions, and two different pseudo-random patterns, respectively.

Using a single µTP micro-LED and the monolithic SPAD multifunctional capability of the hybrid device as an optical communication transceiver and time-of-flight ranging device has been demonstrated. As on-chip crosstalk between the micro-LED and the SPAD is insignificant, the light emitted by the micro-LED was lens collected, back reflected, and focused onto the on-chip SPAD. Using this setup 500 kbps and 1 Mbps VLC links, below the FEC threshold, were demonstrated (Fig. 2(c)). In addition, operating the micro-LED in a pulsed manner (20 ns wide electrical pulses at a repetition rate of 3.13 MHz) ranging capability up to 1.2 m with a root-minimum square deviation of 8.14 cm was demonstrated (Fig. 2(d)).

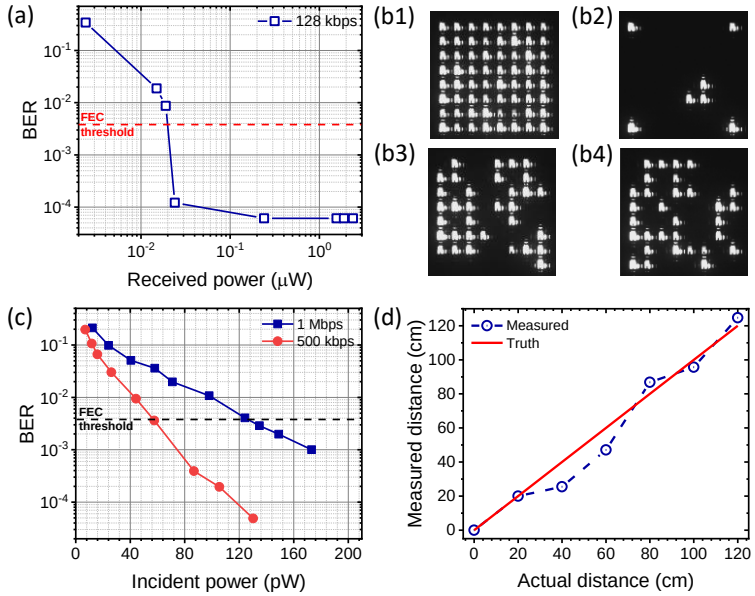

Figure 2: (a) Bit-error-ratio (BER) *vs* received power by ultrafast camera; (b1)-(b4) show the captured frames from the 8000 fps video for all active micro-LEDs, alignment conditions, and two different pseudo-random patterns, respectively; (c) BER as a function of the incident power on the SPAD; (d) measured distance plotted as a function of the actual distance in a ranging experiment.

Acknowledgements

This work is funded under the EPSRC Quantic (EP/T00097X/1) and EPSRC HeteroPrint (EP/R03480X/1) projects. Plessey Semiconductors Ltd. is acknowledged for providing the GaN-on-Si wafer.

References

[1] J. Day, J. Li, D. Y. C. Lie, C. Bradford, J. Y. Lin, and H. X. Jiang, "III-Nitride full-scale high-resolution microdisplays," *Appl. Phys. Lett.*, vol. 99, no. 3, p. 031116, Jul. 2011.

[2] S. Zhang *et al.*, "1.5 Gbit/s Multi-Channel Visible Light Communications Using CMOS-Controlled GaN-Based LEDs," *J. Light. Technol.*, vol. 31, no. 8, pp. 1211–1216, Apr. 2013.

[3] J. F. C. Carreira *et al.*, "On-chip GaN-based dual-color micro-LED arrays and their application in visible light communication," *Opt. Express*, vol. 27, no. 20, p. A1517, Sep. 2019.

[4] A. D. Griffiths, J. Herrnsdorf, M. J. Strain, and M. D. Dawson, "Scalable visible light communications with a micro-LED array projector and high-speed smartphone camera," *Opt. Express*, vol. 27, no. 11, p. 15585, May 2019.

14.00-15.00: Session 6 – Integration of GaN and Diamond
Chairs: Angela Dyson

14.00-14.15: *Development of a hybrid diamond-on-GaN photonic platform*
Jack Smith[1,2], Paul Hill[1,2,3], Charalambos Klitis[4], Erdan Gu[1], Martin D. Dawson[1], Michael J. Strain[1]

[1] Institute of Photonics, Dept. of Physics, 99 George St., Technology and Innovation Centre, University of Strathclyde, Glasgow, G1 1RD, UK
[2] Diamond Science and Technology, Centre for Doctoral Training, University of Warwick, Gibbet Hill Road, Coventry, CV4 7AL, UK
[3] Currently at: Biomedical Engineering, John Anderson Building, 107 Rottenrow E, University of Strathclyde, Glasgow, G4 0NG, UK
[4] School of Engineering, University of Glasgow, Glasgow, G12 8LT, UK

14.15-14.30: *Integrated GaN-Diamond Microwave Electronics (GaN-DaME): Plasma etching of III-nitrides for GaN-on-diamond substrate production*
Matthew D Smith[1], Jerome Cuenca[2], Daniel E Field[3], Simon Fairclough[4], James Pomeroy[3], Rachel Oliver[4], Oliver Williams[2], Iain Thayne[1], Martin Kuball[3]

[1] University of Glasgow, University Ave, Glasgow, G12 8QQ, UK
[2] Cardiff University, Cardiff, CF10 3AT, UK
[3] University of Bristol, Senate House, Tyndall Ave, Bristol, BS8 1TH, UK
[4] Department of Materials Science and Metallurgy, University of Cambridge, Cambridge CB3 0FS, UK

14.30-14.45: *Investigating the interfacial toughness and thermal resistance of GaN-on-diamond*
Daniel E. Field[1,2], Chao Yuan[1], Roland B. Simon[3], Daniel Twitchen[4], Daniel Francis[4], Firooz Faili[4], Dong Liu[1], Martin Kuball[1]

[1] Centre for Device Thermography and Reliability, H. H. Wills Physics Laboratory, University of Bristol, UK
[2] Centre for Diamond Science and Technology, UK
[3] ThermMap Solutions, Bristol, UK
[4] Element Six, 3901 Burton Drive, Santa Clara, California, USA

14.45-15.00: *Modelling Thermal Stress in CVD Diamond On GaN Using Membrane Structures*
Jerome A. Cuenca[1], Matthew Smith[2], Daniel Field[3], James Pomeroy[3], Fabien Massabuau[4], Soumen Mandal[1], Rachel A. Oliver[4], Iain Thayne[2], Martin Kuball[3], Oliver Williams[1]

[1] School of Physics and Astronomy, Cardiff University, Cardiff, UK
[2] School of Engineering, University of Glasgow G12 8LT, UK
[3] Centre for Device Thermography and Reliability, University of Bristol, Bristol, UK
[4] Department of Materials Science and Metallurgy, University of Cambridge, Cambridge, UK

15.00-15.30: **Tea**

Development of a hybrid diamond-on-GaN photonic platform

Jack Smith[1,2], Paul Hill[1,2,3], Charalambos Klitis[4], Erdan Gu[1], Martin D. Dawson[1], Michael J. Strain[1]

[1] *Institute of Photonics, Dept. of Physics, 99 George St., Technology and Innovation Centre, University of Strathclyde, Glasgow, G1 1RD*

[2] *Diamond Science and Technology, Centre for Doctoral Training, University of Warwick, Gibbet Hill Road, Coventry, CV4 7AL*

[3] *Currently at: Biomedical Engineering, John Anderson Building, 107 Rottenrow E, University of Strathclyde, Glasgow, G4 0NG*

[4] *School of Engineering, University of Glasgow, Glasgow G12 8LT*

The hybrid integration of diamond and III-V photonics is an attractive method for fluorescence enhancement and chip-scale routing of single photons emitted by diamond's colour centre defects. These defects, with emissions spanning the visible spectrum, are of great interest in chip-scale quantum information processing and nanoscale magnetometry [1]. However, without heterogeneous integration, taking a commercially available single-crystal diamond platelet and fabricating diamond photonic integrated circuits presents a significant challenge, due to the diamond's small area, large thickness, and extreme hardness.

Gallium nitride's (GaN) material properties make it highly suitable for heterogeneous integration with diamond emitters. Like diamond, it has a large bandgap (3.4 eV) and wide transparency window. It has relatively large optical nonlinearities [2, 3] which provide methods for active resonance tuning and switching. Further, unlike other receiver platforms, e.g. gallium phosphide [4], GaN benefits from a refractive index that matches that of diamond at visible wavelengths, which helps minimise scattering losses at GaN-diamond interfaces and eases the coupling of light from the GaN chip to the diamond and vice-versa.

We demonstrate the micro-assembly by transfer-printing of a diamond disk resonator with GaN waveguides and racetrack resonators (Fig. 1). After the concurrent fabrication of diamond donor and GaN receiver chips, the transfer-print method allows us to pick and place diamond components for integration with the GaN. Loaded quality factors of 8.8×10^4 and 3×10^4 are extracted for the diamond and GaN resonators respectively. We also thermally tune the resonance peaks of these devices; and over a 9 K temperature increase, measure a tuning range of 374 pm and 86 pm for the GaN and diamond, corresponding to thermo-optic coefficients of

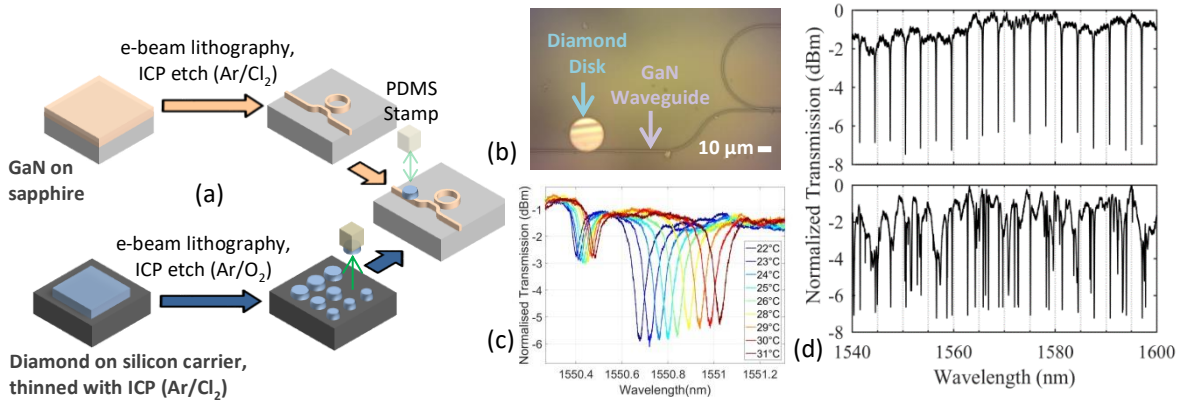

Fig.1 (a) Fabrication process flow. (b) Micrograph of device. (c) Thermal tuning of diamond *(left peak)* and GaN *(right peak)* resonances. (d) Transmission spectra before *(top)* and after *(bottom)* printing the disk.

$(5.95 \pm 1.25) \times 10^{-5}$ K^{-1} and $(1.35 \pm 0.37) \times 10^{-5}$ K^{-1} respectively, matching values found in literature for monolithic samples.

References

1. Aharonovich, I., et al. "Diamond-based single-photon emitters." Reports on progress in Physics 74.7 (2011): 076501.
2. Watanabe, et al. "Thermo-optic coefficients of 4H-SiC, GaN, and AlN for ultraviolet to infrared regions up to 500° C." Japanese Journal of Applied Physics 51.11R (2012): 112101.
3. Long, X-C., et al. "GaN linear electro-optic effect." Applied physics letters 67.10 (1995): 1349-1351.
4. Gould, M, et al. "Large-scale GaP-on-diamond integrated photonics platform for NV center-based quantum information." JOSA B 33.3 (2016): B35-B42.

Funding and Acknowledgements

This work was supported by the EPSRC [EP/P013597/1, EP/P013570/1, EP/L015315/1]. The authors acknowledge the efforts of the staff of the James Watt Nanofabrication Centre at the University of Glasgow.

Integrated GaN-Diamond Microwave Electronics (GaN-DaME): Plasma etching of III-nitrides for GaN-on-diamond substrate production

Matthew D Smith [1], Jerome Cuenca [2], Daniel E Field [3], Simon Fairclough [4] James Pomeroy [3], Rachel Oliver [4], Oliver Williams [2] Iain Thayne [1], Martin Kuball [3]

[1] University of Glasgow [2] Cardiff University [3] University of Bristol [4] University of Cambridge

matthew.smith@glasgow.ac.uk

Transistors fabricated on the GaN-on-diamond material platform have generated strong interest in recent years due to their improved power handling capability compared to commercially established GaN-on-SiC. The high thermal conductivity of diamond substrates enables ultra-efficient heat extraction from the active device layers at the surface, improving device performance, increasing on-chip power density and potentially mitigating heat-induced failure mechanisms. However, the existing GaN-on-diamond state-of-the-art relies on the inclusion of amorphous dielectric interlayers to initiate diamond growth on GaN buffer layers. Such intrinsically low thermal conductivity layers introduce significant thermal resistance between the GaN semiconductor and diamond substrate, acting as a thermal bottleneck and undermining the inclusion of high thermal conductivity diamond substrates.

In this work, epitaxially-integrated AlGaN interlayers were exploited to facilitate diamond growth without the need for dielectric growth initiation layers. First, GaN-on-Si wafers were bonded to a carrier wafer, and the original substrate removed. Plasma etch processes were then developed in order to successfully remove epitaxial growth nucleation and strain relief layers from the resulting N-polar III-nitride material, with in-situ interferometry used to monitor and control etch processes in real-time. A high etch rate, low roughness etch process was combined with a process that is highly selective in etch rate between the GaN buffer and AlGaN interlayer, and the resulting N-polar AlGaN surfaces were analysed using atomic force microscopy and scanning electron microscopy.

Diamond growth was subsequently achieved using microwave plasma chemical vapour deposition, and the thermal boundary resistance was characterized using transmission thermoreflectance measurements. The results represent a significant development in GaN-on-diamond electronics and are expected to enable to production of electrical devices and circuits with significant improvements in power handling capability for use in communications applications such as 5G and beyond.

Investigating the interfacial toughness and thermal resistance of GaN-on-diamond

*Daniel E. Field[1,2], Chao Yuan[1], Roland B. Simon[3], Daniel Twitchen[4], Daniel Francis[4], Firooz Faili[4], Dong Liu[1], Martin Kuball[1]

[1]Centre for Device Thermography and Reliability, H. H. Wills Physics Laboratory, University of Bristol, UK

[2]Centre for Diamond Science and Technology, UK

[3]ThermMap Solutions, Bristol, UK

[4]Element Six, 3901 Burton Drive, Santa Clara, California

*df13461@bristol.ac.uk, Tel: +44 (0) 117 928 8734

***Abstract* - The mode I energy release rate (G_{IC}) between diamond and GaN has been quantified using a nanoindentation induced blistering method. These has been carried out on three GaN-on-diamond samples with varying SiN_x interlayer thicknesses. The thermal boundary resistance (TBR) between the GaN and the diamond has also been investigated using transient thermoreflectance. It has been found that a thin SiN_x layer (17 nm) resulted in a low TBR of 14±1 m^2 K GW^{-1} whilst maintaining a relatively strong interface (G_{IC} = 1.4±0.5 J m^{-2}). For the other two samples, with SiN_x thicknesses of approximately 35 nm, the sample with a higher interfacial toughness had a significantly decreased TBR. This is indicative that the intrinsic properties which enhance the interfacial toughness also play a role in improving the TBR.**

I. INTRODUCTION

In order to increase the power density and long-term device reliability of GaN based high electron mobility transistors (HEMT), thermal management must be improved [1]. The exceptionally high thermal conductivity of diamond, approaching 2000 W m^{-1} K^{-1}, makes it a highly attractive material for integrating with GaN HEMTs [2]. This has been achieved by growing polycrystalline diamond by chemical vapour deposition onto a thin SiN_x seeding layer deposited onto the GaN [3], [4]. When fabricating GaN-on-diamond, there are two main issues to be considered. First, to fully exploit the diamond's thermal properties, the thermal boundary resistance (TBR) between the GaN and diamond needs to be small. Second, the GaN/diamond interface needs to be mechanically robust in order to survive the significant stresses which result from the thermal expansion mismatch between the two materials [5].

This study aims to investigate the correlation between interfacial fracture toughness (adhesion energy) and the TBR for different GaN-on-diamond materials. Nanoindentation induced blisters have been used to assess the interfacial fracture toughness and transient thermoreflectance (TTR) to probe the TBR [3], [5].

II. EXPERIMENTAL METHODS

The details of the three samples investigated are shown in table 1. Nanoindentation was carried out using a Berkovich tip at a range of depths to cause blistering of the GaN film. Indents were separated by 100 µm to ensure no interaction between them. The resulting blisters were analysed using atomic for microscopy (AFM) to extract the blister radii, a, and the maximum buckle height, δ, along the principal directions of the indenter (Fig. 1).

Means of the radii and the buckle heights were then used to calculate G_{IC} for each blister using the Hutchinson-Suo method [6]. This models the blister as a clamped plate undergoing Eulerian buckling. It is possible to calculate the mode I fracture toughness for circular blisters with brittle interfaces using the equation

$$G_{IC} = \frac{G_{ic}(\psi)}{\left[1 + \tan^2\left((1-\lambda)\psi\right)\right]}. \qquad (1)$$

The mixed mode interfacial toughness $G_{ic}(\psi)$ can be derived from a, δ, the film thickness (h), and the Young's modulus (E) and Poisson's ratio (ν) of the film. In this work, E was taken as 296 GPa, ν as 0.25 [5], and λ, the shear contribution to the fracture toughness, as 0.3. The asymptotic solution for the phase angle of a circular blister was used to calculate ψ [6].

Table 1: Detail of the structure of the samples. Samples had a ~50 nm SiN_x protective layer, a GaN layer, a SiN_x adhesion interlayer, followed by a diamond substrate.

Sample	GaN / nm	SiN_x Interlayer / nm
1	375	17
2	742	33
3	752	35

Thermoreflectance measurements were made using a 355-nm pulsed laser to heat the GaN surface while a 488-nm continuous wave laser was used to monitor the reflectance change as a function of time. There is a linear relationship between the surface temperature and its reflectivity meaning that the normalised reflectivity change is equivalent to the normalised temperature change. These traces were fitted by solving the heat diffusion equation through a multilayer stack to extract the TBR between the GaN and the diamond [7].

II. RESULTS AND DISCUSSION

A fitted TTR trace is shown in Fig. 1 whilst Fig. 2 shows a micrograph of a blister. The measured TBR and G_{IC} are shown in Fig 3. as a function of the SiN_x thickness. Sample 1 was found to have the lowest TBR as a result of its thin SiN_x layer. The amorphous SiN_x used here has a very low thermal conductivity and reducing its thickness will greatly reduce the measured TBR. An adhesion energy of 1.4±0.5 J m^{-2} was determined which compares favourably to values in the literature (0.5-1 J

m^{-2}). However, it is still much lower than for GaN-on-Si (G_{IC}>2.96 J m^{-2}) [5].

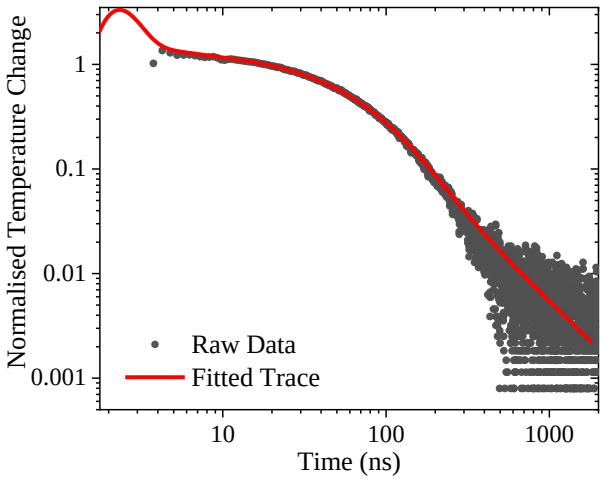

Fig 1: TTR trace for sample 2 with a fitted TBR of 20 m^2K GW^{-1}. Temperature rise is normalised from 20 ns.

Samples 2 and 3 have similar interlayer thicknesses but, as a result of different growth conditions, the TBR of sample 2 is significantly lower (Fig. 3). Sample 2 also appears to have a greater interfacial toughness, 2.4±0.9 J m^{-2} compared to 1.2±0.3 J m^{-2}. The increased adhesion could provide an explanation for the decreased TBR as the stronger bonds associated with a higher interfacial toughness would be expected to aid heat transfer across it. Hence, there is evidence that increasing the mechanical strength of the interface could help in reducing TBR.

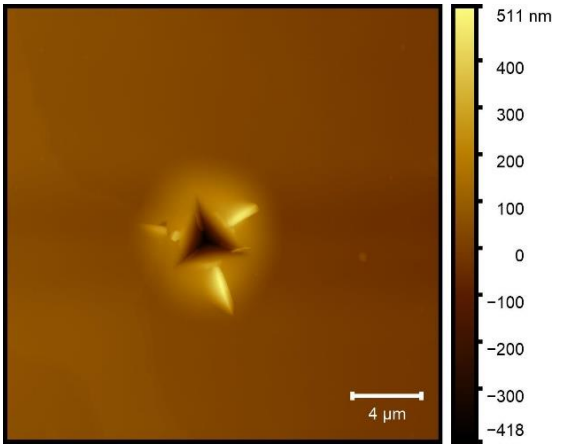

Fig 2: Atomic force micrograph of a 700 nm deep indent on sample 1. Line profiles were taken long the three principal directions of the indent to extract the buckle height and blister radius.

Currently, the thickness of the SiN_x interlayer is the dominant factor in determining the TBR. This work has shown that thinning the SiN_x does not have detrimental effects on the strength of the interface, indicating that it is a viable option for maximising the benefits of diamond/GaN integration. Moving forward, replacing the SiN_x interlayer with a material with high thermal conductivity, such as single crystalline AlN [8], will reduce the impact of the interlayer thickness on the TBR. Hence, there is potential that the strength of the interfacial bonding between GaN and diamond could play a bigger role in decreasing the TBR when attempting to manufacture a viable technology for RF applications.

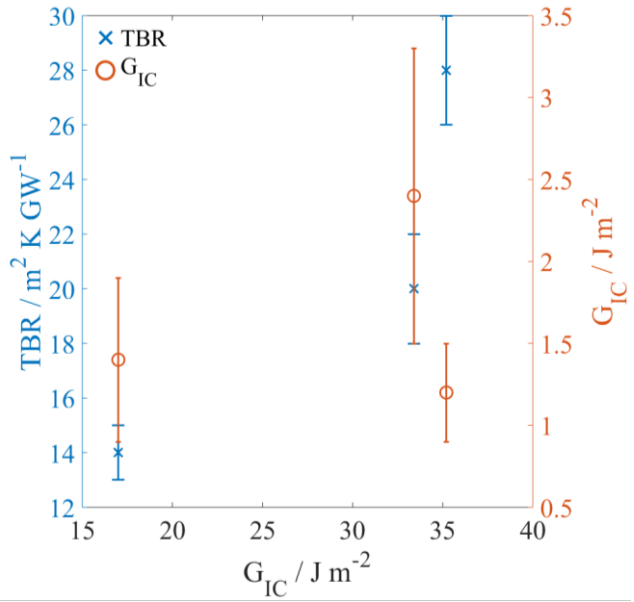

Fig 3: The combined graph of SiN_x interlayer thickness against TBR and G_{IC} for the three samples. Note, the TBR point for sample 2 is underneath the G_{IC} point.

III. CONCLUSION

The biggest factor in reducing TBR is the thickness of SiN_x and this work has shown that a thin SiN_x interlayer can still result in a strong interface. It has also been shown that there is some correlation between the TBR and the interfacial toughness.

Acknowledgements **- The authors would like to acknowledge financial support of the Engineering and Physical Sciences Research Council under the program Grant GaN-DaME (EP/P00945X/1). Thanks also go to the Engineering and Physical Sciences Research council, the centre for doctoral training in diamond science and technology, and Element 6 for funding.**

REFERENCES

[1] S. Lee *et al.*, *IEEE Int. Reliab. Phys. Symp. Proc.*, pp. 446–449, 2008.

[2] C. J. H. Wort *et al.*, *Diam. Relat. Mater.*, vol. 3, no. 9, pp. 1158–1167, Aug. 1994.

[3] J. W. Pomeroy *et al.*, *IEEE Electron Device Lett.*, vol. 35, no. 10, pp. 1007–1009, 2014.

[4] D. Francis *et al.*, *Diam. Relat. Mater.*, vol. 19, no. 2–3, pp. 229–233, 2010.

[5] D. Liu *et al.*, *ACS Appl. Electron. Mater.*, vol. 1, pp. 354–369, 2019.

[6] J. W. Hutchinson and Z. Suo, *Adv. Appl. Mech.*, vol. 29, pp. 63–191, 1991.

[7] Y. Zhou *et al.*, *ACS Appl. Mater. Interfaces*, vol. 9, no. 39, pp. 34416–34422, 2017.

[8] S. Mandal *et al.*, *ACS Appl. Mater. Interfaces*, 2019.

Modelling Thermal Stress in CVD Diamond On GaN Using Membrane Structures

Jerome A. Cuenca[1*], Matthew Smith[2*], Daniel Field[3], James Pomeroy[3], Fabien Massabuau[4], Soumen Mandal[1], Rachel A. Oliver[4], Iain Thayne[2], Martin Kuball[3] and Oliver Williams[1]

[1]*School of Physics and Astronomy, Cardiff University, Cardiff, UK*
[2]*School of Engineering, University of Glasgow G12 8LT, UK*
[3]*Centre for Device Thermography and Reliability, University of Bristol, Bristol, UK*
[4]*Department of Materials Science and Metallurgy, University of Cambridge, Cambridge, UK*
cuencaj@cardiff.ac.uk

Increasing demand for high power microwave devices has driven research into Gallium Nitride (GaN), in particular, high electron mobility transistors (HEMTs). Current device technologies either have impressive high power handling (e.g. Si LDMOS) or high frequency potential (e.g. GaAs), though not both. GaN is a possible candidate although, despite significant progress, the thermal conductivity of GaN limits its power handling capability. This can be overcome with sufficient heat extraction; for example, integration with SiC which has a thermal conductivity ~4 times that of GaN. However, better heat spreader materials exist, such as diamond, enhancing the potential of GaN devices.

Single crystal diamond is known to form at extreme temperatures and pressures. Poly-crystalline diamond (PCD), can be grown using microwave plasma chemical vapour deposition (MPCVD) at slightly more favourable conditions for GaN (800 to 1000 °C) though is still a significant challenge. In particular, the thermal expansion coefficient of diamond differs from GaN, the III-N stack and its substrate (e.g. Si or Sapphire). A firm understanding of the induced thermal stress and deformation is needed before integration of these materials becomes commercially viable. Additionally, the device layer is often at the top of the stack and so a wafer bonding approach to a temporary carrier is required. Hence, producing test samples to simply study the stress becomes a lengthy process.

In this work we demonstrate a means to study thermal stress in GaN/III-N stacks using inductively coupled plasma etched membranes followed by direct MPCVD diamond growth. This method circumvents the temporary wafer bonding step. This is achieved with a modified diamond seeding process and low power growth in a H_2/CH_4 plasma. We have designed and modelled various membrane structures to understand the thermal stresses induced during MPCVD and demonstrate structures that will not yield. Experimentally, we have successfully grown tens of micron thick PCD films onto membranes from 1 to 5 mm in diameter.

We acknowledge funding from the EPSRC Programme Grant GaN-DaME (EP/P00945X/1).

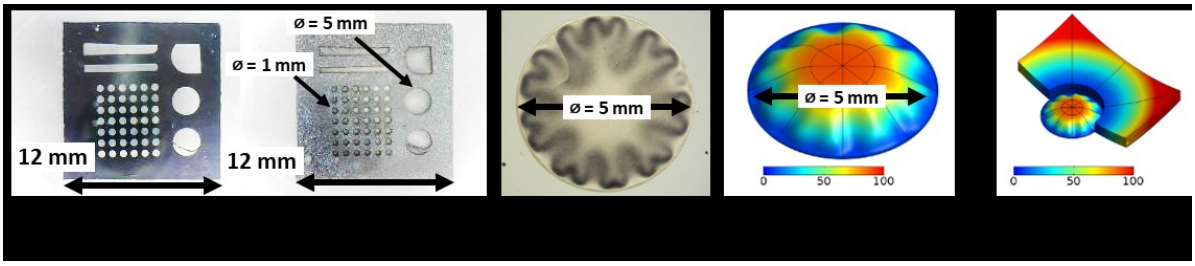

Figure 1. Exposed III-V membranes structures (a) before CVD diamond growth (b) after CVD diamond growth (c) wrinkled III-V membrane before growth and (d,e) thermal stress simulation of III-V membrane during CVD diamond growth (colour bar shows displacement in μm).

15.30–16.30: Session 7 – LEDs and LED-related materials
Chairs: Trevor Martin

15.30-15.45: *Carrier localization in polar InGaN QWs: Consequences for the temperature dependence of the radiative recombination*
Joshua M. McMahon[1,2], Daniel S. P. Tanner[1], Emmanouil Kioupakis[3], Stefan Schulz[1]

[1] Tyndall National Institute, University College Cork, Lee Maltings, Dyke Parade, Cork, Ireland
[2] Department of Physics, University College Cork, Cork City, Cork, Ireland
[3] Materials Science and Engineering Department, University of Michigan, 2300 Hayward St., Ann Arbor, Michigan 48109, USA

15.45-16.00: *Semi-polar InGaN-based green LEDs with super-lattice on patterned silicon*
X. Zhaol, K. Huang[1], J. Bruckbauer[2], S. Shen[1], C. Zhu[1], P. Fletcher[1], F. Peng[1], Y. Cai[1], J. Bai[1], C. Trager-Cowan[2], R. Martin[2], T. Wang[1*]

[1] Department of Electronic and Electrical Engineering, University of Sheffield, Sheffield, S1 3JD, UK
[2] Department of Physics, SUPA, University of Strathclyde, Glasgow, G4 0NG, UK

16.00-16.15: *From the electronic structure to transport properties of III-N based quantum well systems: Connecting atomistic and continuum-based models*
Debapriya Chaudhuri[1], M. O'Donovan[1,2], S. K. Patra[1], T. Streckenbach[3], O. Marquardt[3], P. Farrell[3], T. Koprucki[3], Stefan Schulz[1]

[1] Tyndall National Institute, University College Cork, Cork T12 R5CP, Ireland
[2] Department of Physics, University College Cork, Cork T12 YN60, Ireland
[3] Weierstrass Institute (WIAS), Mohrenstr. 39, 10117 Berlin, Germany

16.15-16.30: *Polarised room temperature photoluminescence from zincblende InGaN/GaN quantum wells grown using MOVPE on 3C-SiC/Si (001) substrates*
S. A. Church[1], B. Ding[2], P. W. Mitchell[1], M. J. Kappers[2], S. Fairclough[2], G. Kusch[2], M. Frentrup[2], D. J. Wallis[2,3,4], R. A. Oliver[2], D. J. Binks[1], P. Dawson[1]

[1] Photon Science Institute & Department of Physics and Astronomy, University of Manchester, UK
[2] Department of Materials Science and Metallurgy, University of Cambridge, Cambridge CB3 0FS, UK
[3] Kubos Semiconductors Ltd, Future Business Centre, King's Hedges Road, Cambridge, UK
[4] Centre for High Frequency Engineering, University of Cardiff, UK

16.30-16.35: Concluding remarks and prize-giving

Carrier localization in polar InGaN QWs: Consequences for the temperature dependence of the radiative recombination

Joshua M. McMahon[1,2], Daniel S. P. Tanner[1], Emmanouil Kioupakis[3], and Stefan Schulz[1]

[1]Tyndall National Institute, University College Cork, Lee Maltings, Dyke Parade, Cork, Ireland
[2]Department of Physics, University College Cork, Cork, Ireland
[3]Materials Science and Engineering Department, University of Michigan, 2300 Hayward St., Ann Arbor, Michigan 48109, USA

Polar InGaN quantum wells (QWs) have found widespread application as the active region of light emitting diodes (LEDs) operating in the short-wavelength part of the visible (violet to green) spectral range [1]. To further improve the efficiency of these devices it is essential to understand their fundamental properties, such as the radiative recombination rate. Recent experimental studies have investigated the evolution of the radiative recombination rate with temperature (T) [2]. To do so, in Ref. [2] the T dependence of the radiative recombination rate is studied in terms of the widely used radiative recombination coefficient B. It is found that B reflects a rather unusual behavior, namely that it increases with T. This is in stark contrast to the usual behavior found in semiconductor QWs, for instance those based on GaAs, which reflect an inverse (1/T) dependence of B on T. Recent theoretical studies of polar InGaN/GaN QWs, which calculate B as a function of T reveal a decrease of B with T [4] or that B is independent of T [5]. A very recent atomistic theoretical study finds the experimentally observed increase of B with T but only if significant In atom clustering is present in InGaN QWs. However, inclusion of In clustering is not consistent with experimental studies on the structural properties of polar InGaN/GaN QWs [6]. Overall, it is important to note that for predicting the T dependence of the radiative recombination it is crucial to understand the density of (localized) states. Here, without using the density of states (DOS) as a free fitting parameter, our atomistic theoretical studies predict an increase of B with T *without* the assumption of In atom clustering.

In this study, we use a fully atomistic nearest neighbor sp^3 tight-binding model [7] to calculate the electronic structure of InGaN/GaN QWs with In contents varying between 5% and 25%. Given the atomistic nature of this theoretical framework, the In atom distribution in the active region is required. Here, consistent with experimental studies, we assume a random distribution of In atoms in the well region. To treat (i) DOS, (ii) increasing carrier densities, and (iii) temperature effects accurately, we calculate 100 electron and 100 hole wavefunctions for 125 different microscopic configurations of In

atoms. Using the electron and hole wave functions, we evaluate the spontaneous emission rate for the here studied $In_xGa_{1-x}N$ wells [8]. Building on the spontaneous emission rate, the B coefficient for varying temperatures and free carrier densities is obtained.

In a first step we present results for the DOS and, in particular, the energetic distribution of localized hole states. This is done by means of an Urbach-like description of DOS tail energies [9]. Our calculations show that these "Urbach" tail energies strongly increase with increasing In content. Here, an approximately quadratic dependence of the tail energy on In content is found, resulting in values between 20 meV to 100 meV for the In content range studied. The energy and spatial distribution of localized states affects the wavefunction overlap and ultimately the radiative recombination rate. By populating energetically higher and spatially more extended states, the wave function overlap increases and as a consequence so does the radiative recombination rate.

Equipped with this knowledge, we calculate the spontaneous emission rate from our fully atomistic model as a function of temperature T. We show that when assuming similar settings (carrier densities, well width, In content, temperature range) as in the experiment in Ref. [2], our model reproduces the experimentally observed trend of an increasing B with T. We find this result without the assumption of In atom clustering. We also show that by increasing the carrier density, and thus saturating the localized states, our model shows that B is independent of T, similar to previous studies. Overall, this highlights that in order to describe the electronic and optical properties of polar InGaN/GaN QWs, an accurate description of the energetic distribution of localized states, and thus DOS, is key.

References

1. C. J. Humphreys, MRS Bulletin, **33**(4), pp. 459 – 470 (2008)
2. F. Nippert *et al*., Appl. Phys. Lett. **109**, 161103 (2016)
3. M. A. Hopkins *et al*., J. Appl. Phys. **122**, 234505 (2017)
4. A. Di Vito *et al*., Phys. Rev. Appl. **12**, 014055 (2019)
5. C. M. Jones *et al*., Appl. Phys. Lett. **111**, 113501 (2017)
6. T. M. Smeeton *et al*., Appl. Phys. Lett. **83**, 5419 (2003)
7. S. Schulz *et al*., Phys. Rev. B **91**, 035439 (2015)
8. F. Tang *et al*., J. Appl. Phys. **125**, 225794 (2019)
9. M. Piccardo *et al*., Phys. Rev. B **95**, 144205 (2017)

Semi-polar InGaN-based green LEDs with supper-lattice on patterned silicon

X. Zhao[1], K. Huang[1], J. Bruckbauer[2], S. Shen[1], C. Zhu[1], P. Fletcher[1], F. Peng[1], Y. Cai[1], J. Bai[1], C. Trager-Cowan[2], R. Martin[2] and T. Wang[1]*

[1]Department of Electronic and Electrical Engineering, University of Sheffield, Sheffield, S1 3JD

[2]Department of Physics, SUPA, University of Strathclyde, Glasgow, G4 0NG

III-nitride semiconductors on silicon have drawn increasing attention recently due to the requirements of the integration of III-V semiconductors and silicon technologies. The last decade has seen significant progress on developing III-nitride optoelectronics on Si, but they are mainly limited to c-plane GaN which suffers from quantum confined Stark effects (QCSE) and thus exhibits reduced quantum efficiency, in particular for longer wavelength emitter such as green and yellow emitters. The growth of InGaN based LEDs on semi-polar GaN, in particular (11-22) GaN, is expected to be a very promising approach to achieving longer wavelength emitters with enhanced quantum efficiency. Furthermore, the growth of InGaN on (11-22) GaN tends to have an enhanced indium incorporation rate compared with its c-plane counterparts. Our group have established a reliable approach to growing semi-polar (11-22) GaN with high quality on patterned (113) Si. A combination of a stripe-patterning process and anisotropic chemical etching is used to form parallel grooves on (113) Si with a designed depth, on which selective growth on the (111) sidewall facet of the silicon is performed. A GaN footprint on the bottom of grooves has been avoided. As a result, an InGaN based green light-emitting diode (LED) has been achieved.[1] However, the quantum efficiency is still lower than its c-plane counterpart. Therefore, it is necessary to further develop a new growth approach. In this study, we have borrowed an idea from the well-established c-plane LEDs, where a super-lattice (SL) structure has been widely applied in c-plane GaN devices as an important method. By introducing a SL structure, a further improvement in optical efficiency has been achieved on our semi-polar green LEDs. In this work, a (11-22) semi-polar green InGaN based LED structure with 15 pairs of InGaN/GaN SLs has been grown. This is similar to a standard c-plane LED structure. A similar LED structure but without using any SL has been also grown for comparison.

Fig. 1a shows the temperature dependent photoluminescence (PL) spectra of the green LED with SLs, exhibiting strong green emissions at 554 nm at room temperature and 544 nm at 18.2K. Fig. 1b indicates integrated PL intensity as a function of temperature, by which an internal quantum efficiency (IQE) of approximately 23% has been estimated. In contrast, under identical conditions, the green LEDs without SLs exhibits an IQE of 13.5%.

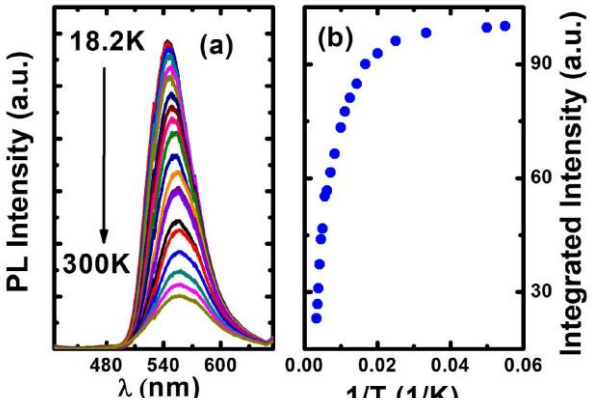

Fig.1: (a) Temperature dependent PL; (b) Integrated PL intensity as a function of temperature

Fig. 2a shows the electroluminescence (EL) spectra as a function of injection current. A slight blue shift with increasing current has been observed, indicating reduced QCSE. Fig.2b shows normalised external quantum efficiencies (EQEs) a function of injection current, also demonstrating an enhanced EQE for the LED with SL compared with the LED without SL, although detailed cathodoluminescence (CL) measurements indicate that SL can introduce extra misfit dislocations (MDs).

In conclusion, we have demonstrated high efficiency green LEDs with a SL structure on semi-polar (11-22) GaN, although extra MDs have been introduced. It is worth highlighting that the improvement in performance as a result of the SL structure for semi-polar LEDs is not so significant as those for c-plane LEDs.

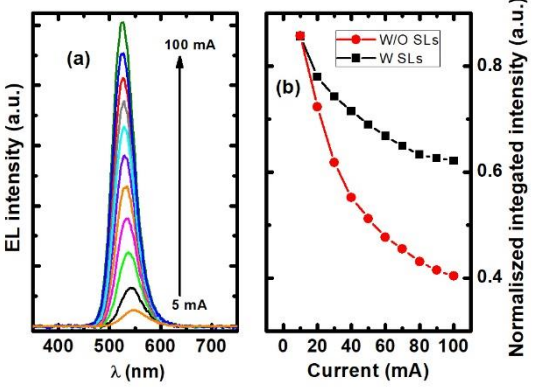

Fig.2: (a) EL spectra of the LED with SL as a function of current; (b) Normalised EQE as function of current for both LEDs with and without SL

1. S. Shen, X. Zhao, X. Yu, C. Zhu, J. Bai and T. Wang, Phys. Stat. Sol. (A) 1900654 (2019);
2. 2 Y. Zhang, R. M. Smith, L. Jiu, J. Bai and T. Wang, Scientific Reports 9, 9735 (2019).

From the electronic structure to transport properties of III-N based quantum well systems: Connecting atomistic and continuum-based models

Debapriya Chaudhuri[1], M. O'Donovan [1,2], S. K. Patra [1], T. Streckenbach[3] , O. Marquardt [3], P. Farrell [3], T. Koprucki[3], Stefan Schulz[1]

[1]Tyndall National Institute, University College Cork, Cork T12 R5CP, Ireland
[2] Department of Physics, University College Cork, Cork T12 YN60, Ireland
[3] Weierstrass Institute (WIAS), Mohrenstr. 39, 10117 Berlin, Germany

III-nitride based heterostructures form the heart of modern light emitting diodes (LEDs) operating in the blue spectral range. Despite the widespread application of these LED structures, to further improve their efficiencies, a detailed understanding of their fundamental properties is required. Theoretical studies can help here to guide the design of structures with improved and new capabilities. However, such a modelling procedure is inherently a multi-scale problem, meaning that one needs to bridge the gap between atomistic and continuum-based models. This is particularly important for InGaN-based systems since random alloy fluctuations lead to strong carrier localization effects in these systems which strongly affects their electronic and optical properties [1,2,3,4]. This problem is ideally addressed in an atomistic theoretical framework [4]. On the other hand, such a microscopic treatment is numerically too demanding for simulating a full device. Therefore, recently modified continuum-based calculations have been discussed and applied in the literature [3,5]. While these calculations indicate the capture of carrier localization effects, so far they have not been compared in detail to atomistic calculations. Furthermore, a significant challenge for these continuum-based calculations is always the generation of the potential energy landscape, which basically defines the carrier localization centres. In this work, we present a new framework that allows us to generate local band edges from atomistic tight-binding calculations, which then form the basis of modified continuum-based calculations. The benefit of this is manifold, including that the outcome of the continuum-based calculations can directly be compared to the atomistic results.

The starting point for our multiscale approach is an atomistic tight-binding model that accounts for strain and built-in field fluctuations arising from (random) alloy fluctuations in $In_xGa_{1-x}N$/GaN Quantum Wells (QWs). To study the impact of the In content on the results, calculations have been performed for structures with In contents ranging from 5% up to 25%. For each In content, several different random microscopic configurations have been generated, allowing us to test the impact of the alloy microstructure on the results. Local conduction and valence band edges that have strain and built-in potential effects readily included are directly calculated from the tight-binding model. Subsequently, to establish a bridge between the continuum and the atomistic picture, finite element and volume meshes are generated which have as many nodes as the atomistic lattice. At these nodes, the atomistic local band edge energies are defined. This transfer is achieved by WIAS-pdelib tool [6]. We highlight here that this procedure, in contrast to literature modified continuum-based calculations, is free of averaging local In contents to obtain, for instance local elastic or piezoelectric constants in a continuum-based picture. This sets our approach clearly apart from previous studies.

Equipped with this mesh and similar to previous studies, the electronic states of the above InGaN QWs are calculated in the framework of a single-band effective mass approximation (EMA). In principle, the only free adjustable parameter in our EMA is the effective electron/hole mass; the potential energy landscape is determined directly from tight-binding. Our calculations reveal that the first 10 electron energies in the modified continuum-based model are shifted to higher values when compared to the tight-binding results. Adjusting the effective mass may allow for achieving a better agreement in terms

of the ground state energy, however, this comes at the cost of poorly described excited states. Thus the density of states, important for instance for transport aspects, is poorly described. We will discuss here different approaches how an improved agreement between tight-binding and continuum-based results may be achieved, including adjusting band offsets and/or mesh sizes. Given that not only the energy eigenvalues but also charge densities are important, we present also a comparison of charge densities obtained from the two models. This analysis will be extended to hole states.

Finally, we briefly discuss how the here established multiscale approach can then be used as a starting point for transport calculations. We present general aspects and first initial results of our atomistically motivated and benchmarked modified continuum-based model for drift-diffusion calculations.

References

1. W. Bao, Z. Su, C. Zheng, J. Ning and S. Xu Sci. Rep **6,** 34545 (2016).
2. S. Hammersley, D. Watson-Parris, P. Dawson, M. J. Godfrey, T. J. Badcock, M. J. Kappers, C. McAleese, R. A. Oliver, and C. J. Humphreys, J. Appl. Phys. **111**, 083512 (2012).
3. D. Watson-Parris, M. J. Godfrey, P. Dawson, R. A. Oliver, M.J. Galtrey, M. J. Kappers, C.J. Humphreys, Phys. Rev. B **83**, 115321 (2011).
4. S. Schulz, M. A. Caro, C. Coughlan, E. P. O'Reilly, Phys. Rev B **91**, 035439 (2015).
5. D. Bayerl, S. M. Islam, C. M. Jones, V. Protasenko, D. Jena, E. Kioupakis, Appl. Phys. Lett. **109** (24), 241102.
6. H. Si, "TetGen, a Delaunay-Based Quality Tetrahedral Mesh Generator", ACM Trans. on Mathematical Software, vol. **41**, article 11, 2015.

Polarised room temperature photoluminescence from zincblende InGaN/GaN quantum wells grown using MOVPE on 3C-SiC/Si (001) substrates

S. A. Church[1], B. Ding[2], P. W. Mitchell[1], M. J. Kappers[2], S. Fairclough[2], G. Kusch[2], M. Frentrup[2], D. J. Wallis[2,3,4], R. A. Oliver[2], D. J. Binks[1] and P. Dawson[1]

1 - Photon Science Institute & Department of Physics and Astronomy, University of Manchester.
2 - Department of Materials Science & Metallurgy, University of Cambridge.
3 - Kubos Semiconductors Ltd, Future Business Centre, King's Hedges Road, Cambridge.
4 - Centre for High Frequency Engineering, University of Cardiff.

The internal quantum efficiency (IQE) of c-plane wurtzite (wz) InGaN/GaN quantum wells (QWs) reduces as the indium content in the QWs is increased and the emission wavelength moves towards the green [1]. This effect has been has been attributed to a number of factors associated with higher indium content, such as the greater incorporation of defects at the lower growth temperatures required [2] and increased polarisation fields transverse to the QWs, which act to separate electrons and holes and reduce the radiative recombination rate [3].

The polarisation fields can be significantly reduced by using the zincblende (zb) crystal phase which has no piezoelectric polarisation for biaxial strain in QWs grown along the [001] direction [4], thereby facilitating a faster radiative recombination rate [5]. Additionally, the bandgap of zb-GaN is smaller by 200 meV [6], therefore a reduced indium content may be required to achieve green emission, offering the potential for lower point defect densities. However, zb-GaN is metastable during growth, and tends to contain a large number of defects, such as stacking faults (SFs). These defects have been reported to act as centres of non-radiative recombination in zb-GaN/AlN QWs, which may negatively affect the IQE [7].

We study zb-InGaN/GaN QWs grown by MOVPE on 3C-SiC/Si (001) substrates. Cross-sectional STEM/EDX measurements show that indium atoms segregate adjacent to SFs within the QWs, which results in carrier confinement in two-dimensions rather than just one. Photoluminescence (PL) spectroscopy of these regions reveals an emission band which has a high degree of linear polarisation (DOLP) (up to 80%) at room temperature. The FWHM of the emission is large (400 meV), likely caused by varying levels of In segregation and the impact of local polarisation fields induced by the SFs [8]. PL-excitation spectra show that these states capture carriers from the rest of the QW. At a temperature of 10K, a higher energy emission is present which has a reduced DOLP when compared with the other emission. The low temperature recombination curves for this second peak are monoexponential, with a lifetime of around 400 ps. Similar results have been obtained on non-polar wz m-plane InGaN/GaN QWs [9,10], and therefore such behaviour may be indicative of there being no intrinsic fields: suggesting this is due to recombination in the zb-QWs away from the InN rich regions around the SFs.

[1] Auf der Maur, M., et. al. Phys. Rev. Lett. 116 (2016) 27401.
[2] Hammersley, S. et al. Appl. Phys. Lett. 107 (2015) 132106.
[3] Humphreys, C. J. et. al. Ultramicroscopy 0 (2017) 1.
[4] Park, S.-H., & Chuang, S. L. J. Appl. Phys. 87 (2000) 353.
[5] Elsaesser, D. R., et al. J. Appl. Phys. 122 (2017) 115703.
[6] Vurgaftman, I., & Meyer, J. R.J. Appl. Phys. 94 (2003) 3675.
[7] Kemper, R. M. et al. Phys. Status Solidi C 12 (2015) 469.
[8] Church, S. A. et. al. J. Appl. Phys. 123 (2018) 185705.
[9] Marcinkevičius, S. et al. Appl. Phys. Lett. 103 (2013) 111107.
[10] Dawson, P. et al. J. Appl. Phys. 119 (2016) 181505.

List of Posters

Comparison of Micron-scale Spatial Variation of Photoluminesence between Blue- and Green-emitting InGaN/GaN Multiple Quantum Wells

R. Barrett[1], R. Ahumada-Lazo[1], J.A. Alanis[1], P. Parkinson[1], S. A. Church[1], M. J. Kappers[2], R. A. Oliver[2], D. J. Binks[1]

[1] Photon Science Institute & Department of Physics and Astronomy, University of Manchester, UK
[2] Department of Materials Science and Metallurgy, University of Cambridge, Cambridge, UK

Displacement Talbot Lithography for nano-engineering of III-nitride materials

Pierre-Marie Coulon[1], Benjamin Damilano[2], Blandine Alloing[2], Pierre Chausse[1], Sebastian Walde[3], Johannes Enslin[4], Robert Armstrong[1], Stéphane Vézian[2], Sylvia Hagedorn[3], Tim Wernicke[4], Jean Massies[2], Jesus Zúñiga-Pérez[2], Markus Weyers[3], Michael Kneissl[3,4], Philip A. Shields[1]

[1] Dept. Electrical & Electronic Engineering, University of Bath, Bath, BA2 7AY, UK
[2] Université Côte d'Azur, CNRS, CRHEA, rue B. Gregory, 06560 Valbonne, France
[3] Ferdinand-Braun-Institut, Leibniz-Institut für Höchstfrequenztechnik, 12489 Berlin, Germany
[4] Technische Universität Berlin, Institute of Solid State Physics, 10623 Berlin, Germany

Effect of Mg concentration on the optical properties of Mg doped zinc-blende GaN epilayers

Daniel Dyer[1], Stephen A. Church[1], Peter W. Mitchell[1], Menno J. Kappers[2], David J. Wallis[2,3,4], Rachel A. Oliver[2], David J. Binks[1]

[1] Department of Physics and Astronomy, Photon Science Institute, University of Manchester, M13 9PL, UK
[2] Department of Materials Science and Metallurgy, University of Cambridge, CB3 0FS, UK
[3] Centre for High Frequency Engineering, University of Cardiff, CF24 3AA, UK
[4] Kubos Semiconductors Ltd., Future Business Centre, Cambridge, CB4 2HY, UK

Excited State Deep Level Transient Spectroscopy

Simon Hammersley, Xiaoyan Tang, Vladimir Markevich, Ian Hawkins, Iain Crowe, Tony Peaker, Matthew Halsall

Photon Science Institute and Department of ELectrical and Electronic Engineering, University of Manchester, Manchester, M13 9PL, UK

Modified localization landscape theory for studying the electronic structure of III-nitride quantum wells

Debapriya Chaudhuri[1], John C. Kelleher[2], Megan R. O'Brien[3], Eoin P. O'Reilly[4], Stefan Schulz[5]

[1] Tyndall National Institute, University College Cork, T12 R5CP, Ireland
[2] Department of Physics, University College Cork, T12 YN60, Ireland
[3] Tyndall National Institute, University College Cork, T12 R5CP, Ireland, Department of Physics, University College Cork, T12 YN60, Ireland
[4] Tyndall National Institute, University College Cork, T12 R5CP, Ireland, Department of Physics, University College Cork, T12 YN60, Ireland
[5] Tyndall National Institute, University College Cork, T12 R5CP, Ireland

Surface Morphologies of Cubic GaN

Thomas J. Wade[1], Abhiram Gundimeda[1], Martin Frentrup[1], Gunnar Kusch[1], Menno J. Kappers[1], David J. Wallis[1,2], Rachel A. Oliver[1]

[1] Department of Materials Science and Metallurgy, University of Cambridge, 27 Charles Babbage Rd, Cambridge, CB3 0FS, UK
[2] Centre for High Frequency Engineering, University of Cardiff, 5 The Parade, Newport Road, CF24 3AA, Cardiff, UK

Thermal management of GaN power devices with 3D printed polymeric micro-jet impingement channel

G. Zhang[1], H. Cao[1], M. E. Navarro[1], J.W. Pomeroy[2], M. Kuball[2], Y. Ding[1*]

[1] Birmingham Centre for Energy Storage, School of Chemical Engineering, University of Birmingham, UK
[2] Centre for Device Thermography and Reliability, H.H. Wills Physics Laboratory, University of Bristol, UK

Variation of the Emission Properties of Blue and Green emitting InGaN/GaN Multiple Quantum Wells with Growth Temperature

R. Ahumada-Lazo[1], R. Barrett[1], J.A. Alanis[1], S. Skalsky[1], P. Parkinson[1], S. A. Church[1], M. J. Kappers[2], R. A. Oliver[2], D. J. Binks[1]

[1] Photon Science Institute & Department of Physics and Astronomy, University of Manchester, UK
[2] Department of Materials Science and Metallurgy, University of Cambridge, 27 Charles Babbage Rd, Cambridge, CB3 0FS, UK

Photoluminescence of zincblende InGaN/GaN quantum wells with different thicknesses

K. Cooley-Greene[1], M. Quinn[1], S. A. Church[1], M. J. Kappers[2], D. J. Wallis[2,3,4], R. A. Oliver[2], D. J. Binks[1]

[1] Photon Science Institute & Department of Physics and Astronomy, University of Manchester, UK

[2] Department of Materials Science and Metallurgy, University of Cambridge, 27 Charles Babbage Rd, Cambridge, CB3 0FS, UK

[3] Kubos Semiconductors Ltd, Future Business Centre, King's Hedges Road, Cambridge, UK

[4] Centre for High Frequency Engineering, University of Cardiff, UK

Comparison of Micron-scale Spatial Variation of Photoluminesence between Blue- and Green-emitting InGaN/GaN Multiple Quantum Wells.

R. Barrett[1], R. Ahumada-Lazo[1], J.A. Alanis[1], P. Parkinson[1], S. A. Church[1], M. J. Kappers[2], R. A. Oliver[2], and D. J. Binks[1]

1 - Photon Science Institute & Department of Physics and Astronomy, University of Manchester.
2 - Department of Materials Science & Metallurgy, University of Cambridge.

InGaN/GaN quantum well (QW) based LEDs emitting blue light can be made with very high room temperature external quantum efficiencies (EQEs) of ~90% [1]. However, similar devices that emit in the green part of the spectrum are significantly less efficient, with EQEs of 30-55% depending on wavelength [1]. There are a number of factors that could contribute to the lower IQE of green QWs, including: an increased polarisation field, a greater defect density, and fewer gross well width fluctuations (GWWFs). The fractional In content in the QWs required to produce green emission is greater than that for blue. This increases the strength of the polarisation field across the QW [2], reducing the overlap of the electron and hole wave functions in the active region. This reduced overlap decreases the rate of radiative recombination [2] and is a possible contribution to the reduction in IQE. A lower growth temperature is required to produce QWs with higher In content (in order to avoid In desorption) and this has been shown to increase the density of structural defects, including point defects which act as non-radiative recombination centres, which also may reduce efficiency [3]. Lastly, GWWFs have been reported to prevent carrier diffusion to defect sites, reducing non-radiative recombination and increasing emission efficiency [4].

Recently, cathodoluminescence (CL) mapping of InGaN/GaN QWs combined with TEM has shown that there is significant micron-scale variation in the density of both defects and GWWFs, and that this is associated with differences in CL intensity, peak energy and FWHM [5]. In this work, we further investigate this spatial variation of emission by comparing micron-scale photoluminescence (PL) maps of two series of QW samples. Each sample in the blue-emitting first series has the same In content, and therefore polarisation field, but was grown at a different temperatures, resulting in a different defect density [3]. The second series contains samples with a higher In content (and thus polarisation field) so that they emit in the green part of the spectrum. These samples too were grown at different temperatures, again resulting in range of defect densities [3]; moreover GWWF density for this sample series has also been measured and shown to increase with growth temperature [5]. All of the samples show significant micron-scale variation in PL intensity, peak energy and peak width. Notably, the blue-emitting QWs show a strong negative correlation between PL intensity and peak energy whilst the green-emitting QWs show a correlation that is both weaker and positive. This difference in behaviour indicates that different spatial variation mechanisms are dominant in the blue and green QW structures. CL mapping has also shown that a positive correlation is associated with the effects of GWWFs [5], suggesting that this is the dominant spatial variation mechanism for the green QW structures.

[1] M. Auf der Maur *et al*. Physical Review Letters **116**, 2 (2016), 027401
[2] T. Takeuchi *et al*. Japanese Journal of Applied Physics **36** (1997), L382.
[3] S. Hammersley *et al.* Applied Physics Letters **107** (2015), 132106.
[4] R. A. Oliver *et al.* Applied Physics Letters **103** (2013), 141114
[5] B. Ding *et al.* 13th International Conference on Nitride Semiconductors (2019).

Displacement Talbot Lithography for nano-engineering of III-nitride materials

Pierre-Marie Coulon[1], Benjamin Damilano[2], Blandine Alloing[2], Pierre Chausse[1], Sebastian Walde[3], Johannes Enslin[4], Robert Armstrong[1], Stéphane Vézian[2], Sylvia Hagedorn[3], Tim Wernicke[4], Jean Massies[2], Jesus Zúñiga-Pérez[2], Markus Weyers[3], Michael Kneissl[3,4], Philip A. Shields[1]

[1]*Dept. Electrical & Electronic Engineering, University of Bath, Bath, BA2 7AY, UK*
[2]*Université Côte d'Azur, CNRS, CRHEA, rue B. Gregory, 06560 Valbonne, France*
[3]*Ferdinand-Braun-Institut, Leibniz-Institut für Höchstfrequenztechnik, 12489 Berlin, Germany*
[4]*Technische Universität Berlin, Institute of Solid State Physics, 10623 Berlin, Germany*
P.Coulon@bath.ac.uk

Nano-structuring III-nitride semiconductor materials offers a route for controlling their material and optoelectronic properties, enabling novel functionalities and applications. Although various lithography techniques can be used to pattern these materials at the nanoscale, including electron beam lithography, scalability and cost can be an obstacle for manufacturing processes. Displacement Talbot lithography (DTL) is a fast and robust novel patterning technique that can pattern rough and bowed wafers with features down to 100 nm on large areas, e.g. 100 mm wafers. As a wafer-scale nanofabrication process, it competes with nanoimprint lithography and laser interference lithography. However, it has advantages over both these processes (sensitivity to surface defects of substrate, lifetime of master, system stability etc.) for the manufacturing of periodic nano-engineered semiconductors.

So far, the few existing reports on DTL mainly focus on resist patterning rather than its use to nano-engineer materials. Therefore, in this work we report the use of DTL to successfully nano-engineer III-nitride materials. The concept and principle of DTL and our nano-patterning capabilities will be presented with the fabrication of nanoholes, nanodots, nanorings and nanolines in positive and/or negative resist. We demonstrate the fabrication of dielectric masks by transferring the resist pattern via etching into a SiN_x/SiO_2 layer, and metal dot masks by using a lift-off process. The masks are then used to create III-nitride nanostructures via bottom-up growth, top-down etching or via a combination of both.

Examples of such nano-engineering applied to III-nitride materials will be given, such as: the bottom-up selective area growth of GaN nanorods, the sublimation of GaN high aspect ratio nanoholes and nanorods, the top down etching of various III-nitride materials such as AlGaN UVB nanorod LEDs and InGaN/GaN visible nanotubes LEDs, and the hybrid top-down/bottom-up fabrication of AlGaN/AlN core-shell structures. The fabrication of nano-patterned sapphire substrates and successful overgrowth and coalescence of an AlN layer will also be presented. Compared to the planar approach, these 3D nanostructures enable the reduction of defects and/or the enhancement of light extraction, therefore improving the efficiency of the final device.

Finally, the concept of 'Double' Displacement Talbot D^2TL lithography will be presented. By introducing an additional x-y lateral nano-displacement, either during or between exposures, a broad range of patterns, e.g. holes, dots, rings, and lines, having various configurations, e.g. dimension and pitch, can be obtained from one mask. This concept extends the flexibility of DTL and will enable further research into nano-engineering. Most importantly, it could potentially unlock the manufacturing of nano-engineered III-nitride materials not achievable yet via other lithography techniques.

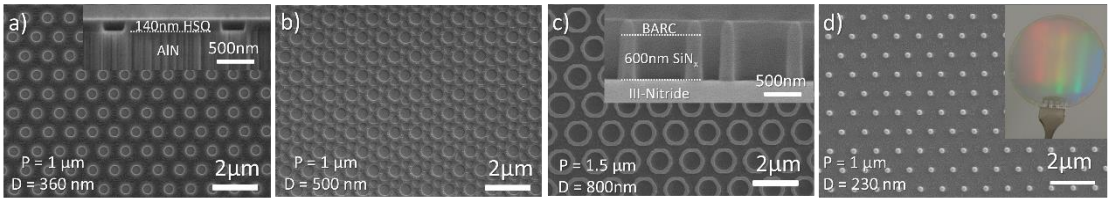

Figure 1. (a) 1 µm pitch holes in 140 nm HSQ. (b) Double periodicity of holes in 30 nm HSQ, with a primary pattern of 1µm pitch. (c) 1.5 µm pitch rings in 600 nm SiNx. (d) Hexagonal array of metal dot after lift-off and associated photograph of 2inch GaN template with metal dot array on its surface.

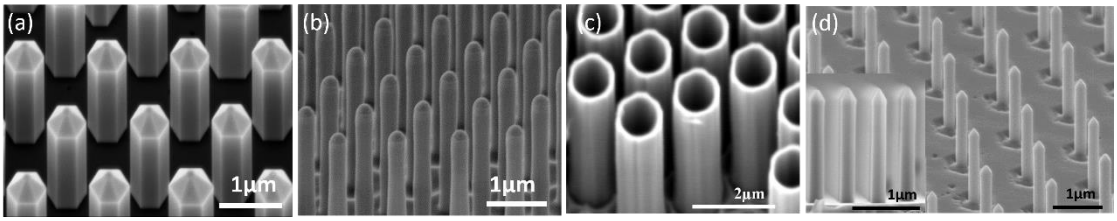

Figure 2. (a) Bottom-up selective-area-grown GaN nanorods (b) Top-down etched axial AlGaN UVB nanorods. (c) Top-down etched InGaN/GaN axial nanotubes. (d) Hybrid top-down, bottom-up fabricated AlGaN core-shell structures.

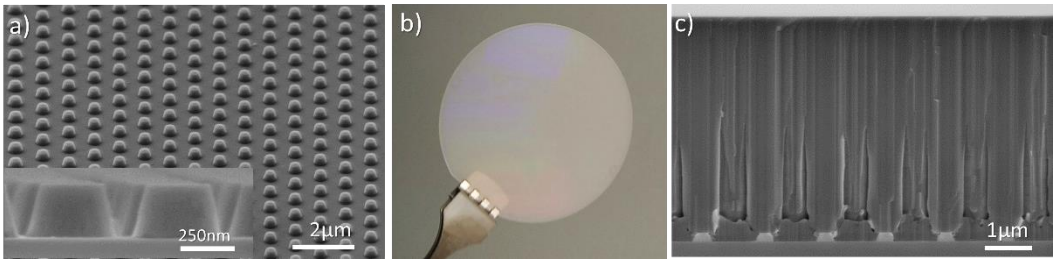

Figure 3. (a) SEM image of nano patterned sapphire substrate and (b) associated photograph of 2inch nano-PSS. (c) 6 µm thick AlN layer grown on nano-PSS.

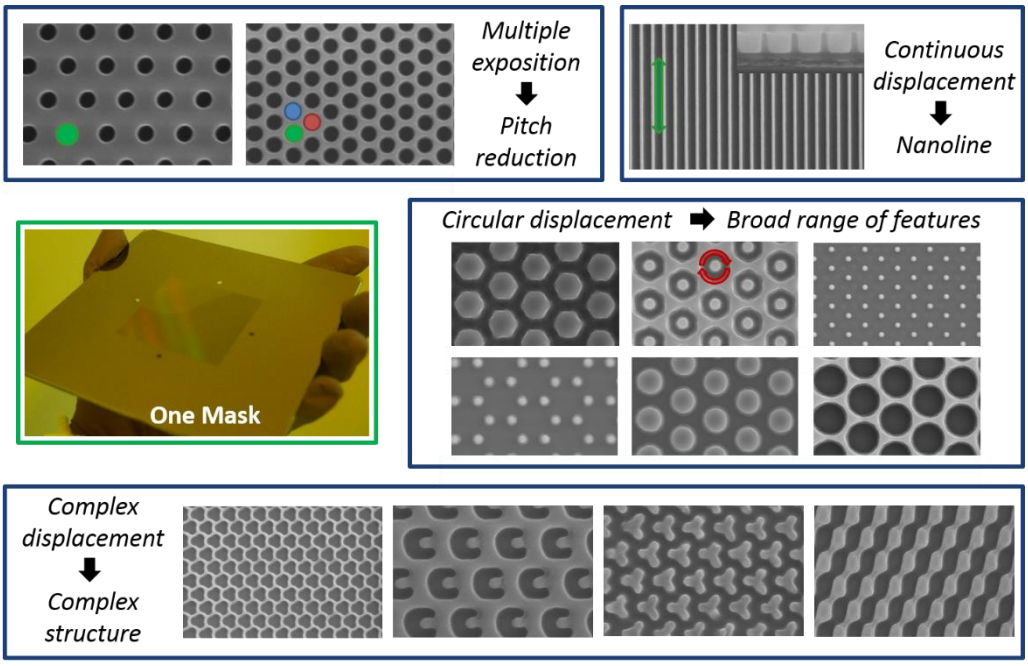

Figure 4. Double Displacement Talbot Lithography capabilities.

Effect of Mg concentration on the optical properties of Mg doped zinc-blende GaN epilayers

Daniel Dyer[†], Stephen A. Church [†], Peter W. Mitchell [†], Menno J. Kappers [‡], David J. Wallis [‡, §, #], Rachel A. Oliver [‡] and David J. Binks [†]

[†] Department of Physics and Astronomy, Photon Science Institute, University of Manchester, M13 9PL
‡ Department of Materials Science and Metallurgy, University of Cambridge, CB3 0FS
§ Centre for High Frequency Engineering, University of Cardiff, CF24 3AA
# Kubos Semiconductors Ltd., Future Business Centre, Cambridge, CB4 2HY

Light generation in commercial white LEDs utilises blue emission from InGaN/GaN quantum wells (QWs) combined with a yellow phosphor. This method of white light generation has inherent losses due to the absorption and re-emission process in the phosphor. A more efficient approach would be to combine separate red, green and blue emitting LEDs [1]. Efficient blue emission is already obtained using InGaN/GaN QWs as the active layer and efficient red emission can be obtained from AlGaInP based LEDs [2]. However, efficient green LEDs are yet to be realised. This is known as the "*green-gap"* problem and is a major hurdle to overcome in order to achieve more efficient white light emission.

Achieving green emission from InGaN/GaN QWs involves increasing the In content to reduce the bandgap of the QW; however, the internal quantum efficiency of InGaN/GaN QWs drops as the wavelength is extended towards the green [3]. A contributing factor towards this are the strong polarisation fields across the QW due to the wurtzite (wz) crystal phase of the GaN typically used for LEDs; these fields act to separate electrons and holes in the QW, resulting in a reduction of the rate of radiative recombination and thus making it less competitive with non-radiative processes [4]. This effect can be mitigated by using instead the zincblende (zb) phase, which lacks these fields [5] due to its higher symmetry. Another advantage of the zb phase is its intrinsically lower bandgap, reducing the In content required in order to access the green spectral region. This will result in reduced lattice mismatch between the InGaN and the GaN and therefore potentially a lower density of non-radiative defects [6].

LEDs require a p-type layer and in GaN this is achieved by using Mg as a dopant [7]. As a step toward producing a zb-GaN LED, we have therefore investigated Mg-doped zb-GaN epilayers. The epilayers were grown by metalorganic vapor phase epitaxy (MOVPE) on SiC/Si substrates. The flow rate of Mg was altered to allow samples with Mg concentrations of 8.6×10^{18} cm^{-3} and 1.9×10^{19} cm^{-3} to be produced, as confirmed by secondary ion mass spectrometry (SIMS) measurements. Photoluminescence (PL) measurements at a temperature of 10 K show that the emission from these samples is dominated by a blue band (BB), which has been associated with donor-acceptor pair (DAP) recombination involving the Mg acceptor in wz-GaN [8]. An Initial investigation by Powell et al. have also attributed the BB in Mg doped zb-GaN, grown by molecular beam epitaxy on GaAs substrates, to DAP recombination with Mg as the acceptor [9]. As the excitation power density was increased, the BB progressively saturated, with the saturation effect greater in the sample with the lowest Mg concentration. Increasing the sample temperature caused the BB to quench; however, this occurred at a lower temperature for the sample with the higher Mg concentration. These results suggest that the recombination dynamics of the BB depend sensitively on the Mg concentration, as will be discussed.

References:

[1] M Crawford, IEEE J. Sel. Top. Quant. **15**, 4 (2009).
[2] G. Wang, X. Yi, T. Zhan and Y. Huang, Chapter 5, in Solid State Lighting Technology and Application Series: Light-Emitting Diodes Materials, Processes, Devices and Applications edited by J. Li and G. Q. Zhang, Springer (2019).
[3] M. Auf der Maur et al. Phys. Rev. Lett. **116**, 027401 (2016).
[4] V. Fiorentini and F. Bernardini, Phys. Rev. B, **60**, 12 (1999).
[5] D. As, Microelectron. J. **40**, 204-209 (2009).
[6] S. Nakamura, Science, **281,** 5379, 956-961 (1998).
[7] S. Nakamura, N. Iwasa, M. Senoh and T. Mukai, Jpn. J. Appl. Phys. **31**, 1258-1266 (1992).
[8] M. Reshchikov, P. Ghimire and D. Demchenko, Phys. Rev. B, **97**, 205204 (2018)
[9] R. Powell et al. Phys. Status Solidi C. **11**, 385-388 (2014).

Excited State Deep Level Transient Spectroscopy

Simon Hammersley[1], Xiaoyan Tang[1], Vladimir Markevich[1], Ian Hawkins[1], Iain Crowe[1], Tony Peaker[1], Matthew Halsall[1]

[1] Photon Science Institute and Department of Electrical and Electronic Engineering, School of Engineering, University of Manchester, Manchester, M13 9PL, UK.
Corresponding author: simon.hammersley@manchester.ac.uk

While group III-Ns are already commercially important, able to produce high efficiency optical and electrical devices, there are still several unanswered questions. One of the most important of these unanswered questions is the so-called green gap, in which the emission wavelength of InGaN-GaN quantum wells is pushed to lower emission energies there is a corresponding reduction in the internal quantum efficiency. The role of defects in this reduction in efficiency has been recently highlighted [1]. In narrower band gap semiconductors, a powerful technique for investigating defects is deep level transient spectroscopy (DLTS). Because this technique relies on the thermal emission of carriers from traps, this puts a practical limitation to the maximum depth of traps that can be measured of ~1 eV from the conduction/valence bands for electron/hole traps. In addition to this, features observed in DLTS of GaN are often significantly broadened, making discrimination between defects with similar energies is more difficult.

The deep states of defects in GaN have been shown to have excited states between the ground state and the conduction/valence bands [2], if these excited states can be populated by use of a tunable laser excitation source then we can thermally excite carriers from these excited states to the conduction/valence band. In addition to the reduction in the thermal energy requirements, the spacing of the excited states would also act as a fingerprint of the specific defect center, helping to identify its origin.

In order to test this approach, we have started with a Pt doped Si sample, as the excited states of hole transitions at the Pt acceptor state are already know [3]. Pt forms a deep acceptor 250 meV from the conduction band in Si [4], and excited states have been observed when exciting with photon energies of between 910-930 meV [3].

Our sample was placed onto the cold finger of a closed cycle helium cryostat, and electrical connection to both the n and p+ sides of the diode, and an optical fiber connected to a tunable laser diode was then edge connected in order to provide sub gap illumination. In order to test that the excited states were in fact observable in this system, the diode was placed under a constant DC bias and the excitation laser was slowly tuned while monitoring the resulting current. When the laser energy coincided with one of the excited states a small increase in the measured current was observed. This change in current was found to dramatically increase as the temperature was increased from 20 K to 85 K, showing that carriers excited into these excited states can then be subsequently excited to the valence band.

Once the presence of these excited states was confirmed in our sample, we continued to look at the emission rate of these carriers from the excited state to the valence band. To do this, the ground state of the Pt acceptor was filled using a bias pulse, and the resulting current transient was recorded after the fill pulse was removed. This transient was then recorded as a function of excitation photon energy. In the energy range of interest, two features were observed and the lifetime of these features was extracted.

Excited state DLTS has shown some promising results on the excited states of the Pt acceptor in Si and should enable the characterization of deep trap states close to the mid-gap in wide band gap semiconductors such as GaN.

[1] S. Hammersley *et al.*, Appl. Phys. Lett. 107, 132106, (2015)
[2] D. Wickramaratne *et al.*, Appl. Phys. Lett. 109, 162107 (2016)
[3] M. Kleverman *et al.*, Phys Rev B 37, 2613, (1988)
[4] H. Carchano and C. Jund, Solid State Electronics, 13, 83-90, (1970)

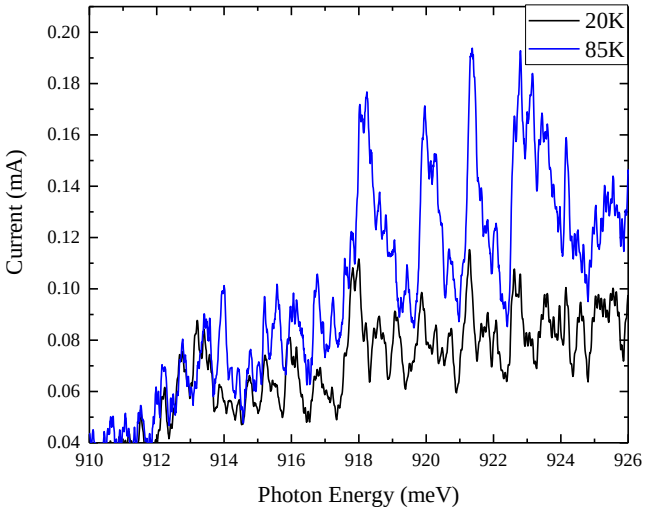

Measured Current as a function of excitation photon energy. Black line shows the excited current at 20K, blue line shows the recorded current at 85K.

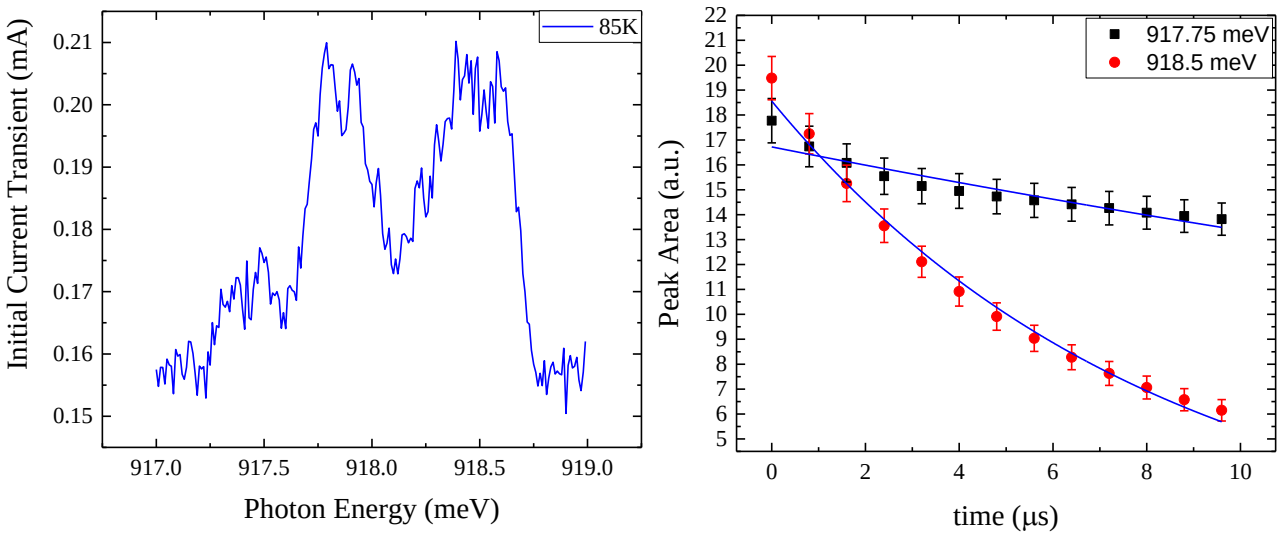

(left), Initial transient intensity of as a function of excitation photon energy. (right) the measured transient intensity as a function of time after the end of the applied fill pulse. The 918.5 and 917.75 meV peaks decay with lifetimes of 8.1±0.2 and 45 ±5 $\times 10^{-6}$ s respectively

Modified localization landscape theory for studying the electronic structure of III-nitride quantum wells

Debapriya Chaudhuri[1], John C. Kelleher[2], Megan R. O'Brien[1,2], Eoin P. O'Reilly [1,2] and Stefan Schulz[1]

[1]Tyndall National Institute, University College Cork, Cork T12 R5CP, Ireland

[2]Department of Physics, University College Cork, Cork T12 YN60, Ireland

With the recent developments of III-nitride semiconductors, these materials have found widespread use in modern light-emitting diodes (LEDs) [1]. To further improve the efficiencies of these devices, understanding their fundamental properties is key. From a modelling perspective this is challenging since it requires on the one hand understanding properties on an atomistic level and how these effects, e.g. carrier localization, affect the device properties [2]. On the other hand modelling of transport properties relies mainly on continuum-based simulations since they are computationally relatively cheap and can treat large structures easily. However, this comes at the cost of overlooking atomistic features and often carrier localization effects. Recently, a new method has been introduced, the so-called localization landscape theory (LLT) which in principle allows for a numerically efficient way of calculating carrier localization effects and transport properties in the same frame [3].

In this work, we present a modified version of LLT, which keeps all the advantages of LLT for solving the Schrödinger equation (SE) while at the same time adding benefits such as (i) improving the overall convergence for calculating the ground state energies, (ii) a "robust" behaviour of the method against changes in the integration region, (iii) better agreement with results from SE, especially for higher In contents and (iv) extracting an effective confining potential comparable to that of LLT [4].

More specifically, we discuss the electronic properties of III-N quantum wells (QW) by means of this modified localization landscape theory (MLLT) where $H^2u=1$ is solved instead of $Hu=1$ as in LLT. This formalism enables us to calculate the ground-state wave function and eigen-energies of InGaN QWs with different In contents. We find here that u obtained from MLLT provides a very good description of the ground state wave function, and it also provides an improved estimate of the ground state energy when compared to the solution of the SE. We also highlight that MLLT, specially for higher In contents provides a better approximation of the ground state energy when compared to the LLT result. Overall, both LLT and MLLT circumvent the task of solving a (large) eigenvalue problem; this feature is one reason why these methods are highly attractive for 3D transport calculations where a Schrödinger-Poisson treatment is computationally very expensive. The second feature that makes LLT attractive for transport calculations is that it allows to extract an effective potential from u, which in a drift-diffusion solver can mimic for instance quantum mechanical tunnelling effects. Here, we discuss an efficient way to extract such an effective potential W_{MLLT} from MLLT, which is in good agreement with the effective potential W_{LLT} extracted from LLT. Therefore, and as discussed above the here proposed MLLT approach keeps the advantages of LLT but improves LLT in certain aspects for instance leading to a better agreement between MLLT and SE results when compared to the same analysis carried out in LLT.

References

1. J. Piprek, ed., Handbook of Optoelectronic Device Modeling & Simulation, CRC Press, Taylor & Francis Group, Boca Raton, 2017.
2. S. Schulz, M. A. Caro, C. Coughlan, and E. P. O'Reilly, Phys. Rev. B 91, 035439 (2015).

3. M. Filoche, M. Piccardo, Y.-R.Wu, C.-K. Li, C.Weisbuch, and S. Mayboroda, Phys. Rev. B 95, 144204 (2017).
4. D. Chaudhuri, J. C. Kelleher, M. R. O'Brien, E P. O'Reilly, and S. Schulz, arXiv : 1910.07261v1 (2019).

Surface Morphologies of Cubic GaN

Thomas J. Wade[1,*], Abhiram Gundimeda[1], Martin Frentrup[1], Gunnar Kusch[1], Menno J. Kappers[1], David J. Wallis[1, 2], Rachel A. Oliver[1]

[1] *Department of Materials Science and Metallurgy, University of Cambridge, 27 Charles Babbage Rd, Cambridge, CB3 0FS, United Kingdom*

[2] *Centre for High Frequency Engineering, University of Cardiff, 5 The Parade, Newport*

**E-mail: tjw84@cam.ac.uk*

Using current technologies, the efficiency of green LEDs is approximately half of that of blue LEDs [1] - this problem is known as the 'green gap'. A major contributor to this is the spontaneous polarisation along the c-axis of hexagonal (wurtzite) GaN that is traditionally used, leading to the so-known quantum-confined Stark effect [2]. Due to its inherent symmetry, zb-GaN does not experience this effect, potentially minimizing non-radiative recombination rates and making it a very promising material for higher efficiency green LEDs. In addition, the smaller bandgap of zb-GaN relative to its hexagonal counterpart reduces the amount of indium alloying required to reach the ~530 nm wavelength of green light. For such LEDs smooth layers with low interface roughness and waviness are required as both can potentially impair the internal recombination efficiency in the quantum wells of the LED. In this study we investigate the surface morphologies of cubic GaN grown by metal-organic vapour phase epitaxy (MOVPE) under various gas-phase V/III-ratios and growth temperatures at a higher than previously used reactor pressure using atomic force microscopy (AFM), complemented by cathodoluminescence (CL) and X-ray diffraction (XRD) data.

Initial results show that compared to sample series grown at lower pressures and studied previously [3], the present samples show similar elongated surface features, which become more square-like as the growth temperature is increased and the V/III ratio is decreased separately. The observed trends can be explained by the diffusion of Ga adatoms on the two-fold symmetric (001) zb-GaN surface. The barrier energy difference between diffusional jumps in the [110] and [1-10] directions was determined as (5.6 ± 0.3) eV, which is slightly above the value reported in [3]. These data suggest that a higher reactor pressure during growth could produce (slightly) smoother interfaces at the cost of a slightly lower phase purity of the zb-GaN layers.

References:

[1] Lee LY et al., J. Mat. Sci. Tech. 33, 14, 1570 (2017)
[2] Miller DAB et al., Phys. Rev. Lett. 53, 22, 2173 (1984)
[3] Lee LY et al., J. Appl. Phys. 124, 10, 105302 (2018)

Thermal management of GaN power devices with 3D printed polymeric micro-jet impingement channel

G. Zhang[1], H. Cao[1], M. E. Navarro[1], J.W. Pomeroy[2], M. Kuball[2], Y. Ding[1] *

[1]Birmingham Centre for Energy Storage, School of Chemical Engineering, University of Birmingham, UK

[2]Centre for Device Thermography and Reliability, H.H. Wills Physics Laboratory, University of Bristol, UK.

*Corresponding author: y.ding@bham.ac.uk

Abstract

This study demonstrates a new method of the thermal management of the microelectronic with 3D printed polymeric micro-jet impingement channel. The micro-jet impingement channel was used as the cooling channel due to high local heat transfer coefficient. The 3D printed polymeric micro-jet impingement channel was designed and fabricated. The integration of the micro-jet impingement channel with the microelectronic device was successfully accomplished by following the proposed thermal packaging procedure. Subsequently, the performance of the integrated microelectronic device was assessed with an IR camera. The experimental results were used to validate previous numerical simulation studies. The results showed that 18.35 W applied on the microchip, resulted in a maximum temperature of the cooling channel 13.5 °C higher than the inlet water temperature, with a flow rate of 0.2 L/min. The results also showed that a higher flow rate, 0.25 L/min, allowed a maximum heat transfer coefficient of 158.5 kW/(m^2·K).

Graphical Abstract

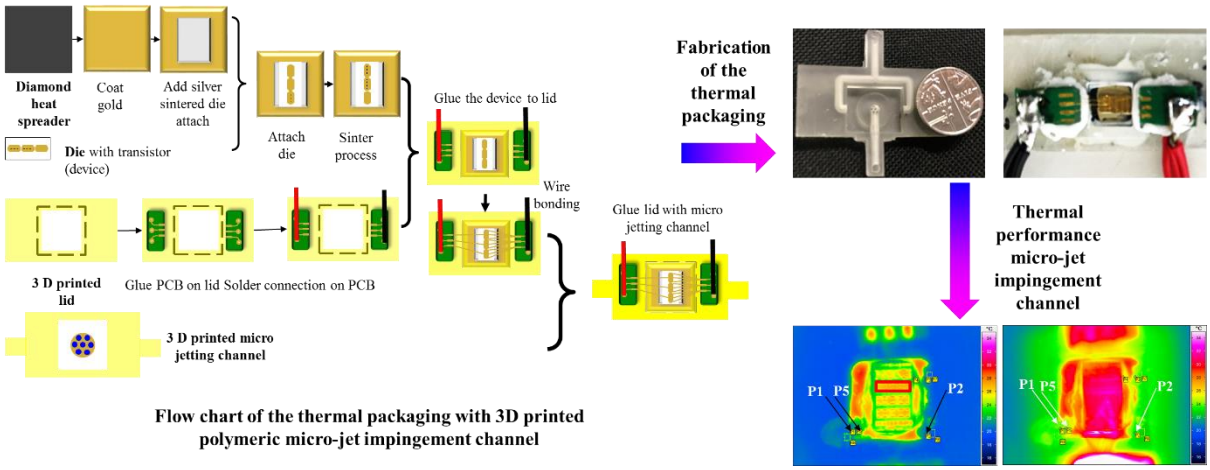

Flow chart of the thermal packaging with 3D printed polymeric micro-jet impingement channel

Variation of the Emission Properties of Blue and Green emitting InGaN/GaN Multiple Quantum Wells with Growth Temperature

R. Ahumada-Lazo[1], R. Barrett[1], J.A. Alanis[1], S. Skalsky[1], P. Parkinson[1], S. A. Church[1], M. J. Kappers[2], R. A. Oliver[2] and D. J. Binks[1]

1 - Photon Science Institute & Department of Physics and Astronomy, University of Manchester.
2 - Department of Materials Science & Metallurgy, University of Cambridge.

InGaN/GaN quantum well (QW) LEDs can be highly efficient, achieving room temperature internal quantum efficiencies (IQEs) in excess of 90% when emitting in the blue [1]. However, peak IQE is typically obtained for drive current densities of a few $A.cm^{-2}$ and drops significantly as the current density is increased, a phenomenon known as 'droop'. A number of possible explanations for droop have been proposed, including: Auger recombination [2], defect assisted Auger recombination [3], carrier escape [4], and the saturation of carrier localisation sites [5]. In the latter case, these sites reduce the likelihood of carriers encountering defects, and thus undergoing non-radiative recombination, at low carrier density; however, at higher carrier densities they saturate so that defect-related non-radiative recombination becomes increasingly significant.

In this study, room temperature fluence-dependent photoluminescence (PL) is used to study the defect-dependence of droop. Two sample series are investigated, one emitting in the blue spectral region and one in the green. The samples in each series have the same structure and composition but were produced using MOCVD with different growth temperatures. This results in PL dynamics at low initial carrier densities consistent with a point defect density that increases as the growth temperature is reduced [6]. Each sample was excited at a wavelength of 400 nm so that carriers are produced directly in the QW, rather than being captured from the GaN substrate or barrier region. Sub-ps pulses are used for this excitation, so that the initial carrier density produced depends only on the laser fluence and is independent of the carrier recombination lifetime, which may differ between samples. Finally, PL is collected only from a region with a diameter five times smaller than the excitation spot, and concentric with it, to ensure that the measurements are only sensitive to regions of the highest initial carrier densities. We find that, although the normalised PL efficiency (i.e. spectrally integrated PL /carrier density) of the samples differs at low excitation, at the level of excitation corresponding to droop, we find no difference in the normalised PL efficiency between the samples. Moreover, the PL decay transients for high initial excitation were also measured. We find that they are very similar for times after excitation when the carrier density remains at levels corresponding to the observation of droop, and only deviate from one another at later times when the carrier concentration has further decreased. These results suggest that efficiency droop is unaffected by the density of point defects in the QWs.

[1] T. Sano *et al*. Japanese Journal of Applied Physics **52** (2013), 08JK09.
[2] Iveland, J. *et al.* Physical Review Letters **110** (2013), 177406.
[3] David, A. *et al.* Physical Review Applied **11** (2019), 31001.
[4] Schubert, M. F. *et al.* Applied Physics Letters **94** (2009), 23.
[5] Verzellesi, G. *et al.* Journal of Applied Physics **114** (2013), 071101.
[6] S. Hammersley *et al.* Applied Physics Letters **107** (2015), 132106.

Photoluminescence of zinc blende InGaN/GaN quantum wells with different thicknesses

K. Cooley-Greene[1], M. Quinn[1], S. A. Church[1], M. J. Kappers[2], D. J. Wallis[2,3,4], R. A. Oliver[2] and D. J. Binks[1]

1 - Photon Science Institute & Department of Physics and Astronomy, University of Manchester.
2 - Department of Materials Science & Metallurgy, University of Cambridge.
3 - Kubos Semiconductors Ltd, Future Business Centre, King's Hedges Road, Cambridge.
4 - Centre for High Frequency Engineering, University of Cardiff.

The InGaN/GaN quantum wells (QWs) used as the active region in LEDs are typically grown in the wurtzite (wz) crystal phase, and consequently have strong spontaneous and piezoelectric polarisation fields across them. These fields separate charge carriers transverse to the QW [1], reducing the efficiency as the QW width is increased. This prevents the use of wider QWs as a means to obtain longer emission wavelengths, which is instead achieved by increasing the In content. However, a higher fraction of In results in an increase in the polarisation fields, and also requires lower growth temperatures which increases defect incorporation [2]. In contrast, QWs grown in the zinc blende (zb) crystal phase have been shown to have effectively zero spontaneous and piezoelectric fields [3] so that increasing the emission wavelength by increasing QW width rather than increasing In content becomes a more viable option. Wider QWs will also result in reduced carrier densities for a given drive current, delaying the onset of efficiency 'droop', i.e. the reduction of efficiency at high carrier densities, and thus potentially enabling efficient, high luminosity LEDs.

In this study we examine the photoluminescence spectra of zb-InGaN/GaN QWs with different QW-widths, grown using MOCVD on 3C-SiC/Si (001) substrates. The samples were excited with a photon energy above the bandgap of GaN. Carriers generated in the GaN barriers are subsequently captured by the QWs, where they recombine. The temperature and excitation power were varied to study how the recombination efficiency is affected by the thickness of the QW. The efficiency at 300K was estimated by assuming the recombination is radiative at 10K. The 300K efficiency increases with increasing QW width, a result which is distinct from typical observations of wz-InGaN/GaN QWs [4], and may be partially due to the lack of internal fields. This result is complemented by PL-time decays which illustrate that the radiative recombination rate does not significantly change with QW-width. Preliminary results at high excitation powers are also shown.

References

[1] Fiorentini, V. et al , "Effects of macroscopic polarization in III-V nitride multi-quantum-wells". *Phys. Rev. B* 60(12), (1999)

[2] Hammersley, S. et al "Effects of quantum well growth temperature on the recombination efficiency of InGaN/GaN multiple quantum wells that emit in the green and blue spectral regions". *Appl. Phys. Lett.* 107(13), (2015).

[3] As, D., J., "Cubic group-III nitride-based nanostructures—basics and applications in optoelectronics". *Microelectronics Journal* 40(2), (2009).

[4] Liu, W., eta al, "Temperature dependence of photoluminescence spectra for green light emission from InGaN/GaN multiple wells". *Optics Express* 23(12). (2015).